Title

The BCKDK inhibitor BT2 is a chemical uncoupler that lowers mitochondrial ROS production and de novo lipogenesis

Author

Acevedo, Aracely

Publication Date

2023

Peer reviewed|Thesis/dissertation

UNIVERSITY OF CALIFORNIA

Los Angeles

The BCKDK inhibitor BT2 is a chemical uncoupler that lowers mitochondrial ROS production and *de novo* lipogenesis

A dissertation submitted in partial satisfaction of the requirements for the degree

Doctor of Philosophy in Molecular, Cellular, and Integrative Physiology

by

Aracely Acevedo

2023

ABSTRACT OF THE DISSERTATION

The BCKDK inhibitor BT2 is a chemical uncoupler that lowers mitochondrial ROS production and *de novo* lipogenesis

by

Aracely Acevedo

Doctor of Philosophy in Molecular, Cellular, and Integrative Physiology

University of California, Los Angeles, 2023

Professor Ajit S. Divakaruni, Chair

Elevated levels of BCAAs have been associated with heart failure and metabolic disease. The branched-chain ketoacid dehydrogenase kinase (BCKDK) inhibitor BT2 (3,6-dichlorobenzo[b]thiophene-2-carboxylic acid) was designed to induce branched-chain amino acid (BCAA) oxidation to restore levels of BCAAs. BT2 treatment confers cardioprotection and protects from metabolic disease in preclinical models including mice subjected to trans-aortic constriction or LAD ligation, db/db mice, ob/ob mice, and Zucker fatty rats. However, mice with the BCKDK knocked out specifically in the heart or skeletal muscle does not protect from heart failure, suggesting an alternative molecular mechanism by which BT2 is conferring its protective effects. In this study, we provide evidence characterizing BT2 as a mitochondrial uncoupler. Using reductionist systems including respirometry, mitochondrial membrane potential, and patch-clamp electrophysiology, we demonstrate that BT2 is indeed uncoupling mitochondria and is approximately five-fold milder than the well-known chemical uncoupler DNP. Functional assays expose BT2's protective effects originate from diminishing ROS production and reducing *de novo* lipogenesis. The evidence provided here more likely solves the long-standing question on BT2's mechanism by which it is conferring therapeutic effects. Furthermore, these studies establish mild uncouplers of mitochondria as promising pharmacological agents for the treatment of cardiovascular and metabolic disease.

The dissertation of Aracely Acevedo is approved.

Yibin Wang

Ambre M. Bertholet

Karen Reue

Orian Shirihai

Ajit S. Divakaruni, Committee Chair

University of California, Los Angeles

2023

DEDICATION

I, Aracely Acevedo, dedicate my PhD dissertation to my mother, Celia Acevedo, and my father, José Elías Acevedo, for they were the reason I decided to pursue science. I am grateful for the emotional support my beloved cats, Light and Shadow, gifted me. I thank God for the divine, unconditional love that held me in my darkest hours and for lighting my path throughout this journey.

TABLE OF CONTENTS

LIST OF FIGURES

LIST OF TABLES

ACKNOWLEDGEMENTS

The work for this dissertation was performed under the direction of Dr. Ajit S. Divakaruni.

VITA

EDUCATION

University of California, Los Angeles, Los Angeles, CA
Ph.D. (Expected, September 2023), Molecular, Cellular, & Integrative Physiology

California State University, Los Angeles, Los Angeles, CA
M.S. (2016), Chemistry with an option in Biochemistry

University of California, Santa Cruz, Santa Cruz, CA
B.S. (2013), Molecular, Cell, & Developmental Biology

Pasadena City College, Pasadena, CA
A.A. (2011) Natural Sciences
A.A. (2011) Social Behavioral Sciences
A.A. (2011) Humanities

RESEARCH EXPERIENCE

University of California, Los Angeles (2019-2023)
Dept. of Molecular and Medical Pharmacology
Doctoral Dissertation: *"The BCKDK inhibitor BT2 is a mitochondrial uncoupler that lowers mitochondrial ROS production and de novo lipogenesis"*
Advisor: Ajit Divakaruni, Ph.D.

California State University, Los Angeles. (2014-2016)
Dept. of Chemistry and Biochemistry
M.S. Thesis: "*Determining if Truncated Dopamine and cAMP-Regulated Phosphoprotein (t-Darpp) has Oncogenic Potential in Breast Cells"*
Advisor: Jamil Momand, Ph.D.

University of California, Santa Cruz (Fall 2012-Fall 2013)
Dept. of Chemistry and Biochemistry
Project: "*The Effects of Cu^{2+} Binding on the Global Structure of the Prion Protein*"
Advisor: Glenn L. Millhauser, Ph.D.

PUBLICATIONS

Acevedo A, Jones AE, Danna BT, Turner R, Montales KP, Beninca C, Reue K, Shirihai OS, Wang Y, Stiles L, Wallace M, Wang Y, Bertholet AM, Wallace M, Divakaruni AS. (2023) The BCKDK inhibitor BT2 is a chemical uncoupler that lowers mitochondrial ROS production and *de novo* lipogenesis. Manuscript in review at *Journal of Biological Chemistry*.

Jones AE, Arias NJ, **Acevedo A**, Reddy ST, Divakaruni AS, Meriwether D. (2021) A Single LC-MS/MS Analysis to Quantify CoA Biosynthetic Intermediates and Short-Chain Acyl CoAs. *Metabolites*.11(8):468. PMID: 34436409.

Jones AE, Sheng L, **Acevedo A**, Veliova M, Shirihai OS, Stiles L and Divakaruni AS (2020) Forces, fluxes, and fuels: tracking mitochondrial metabolism by integrating

measurements of membrane potential, respiration, and metabolites. *Am J Physiol: Cell Physiol*. 320(1): C80-C91. PMID: 33147057.

TEACHING EXPERIENCE

Instructor in the EduExplora Honors Academies Program, Human Nutrition & Metabolism Course, at Albert Einstein Instituto Israelita De Ensino E Pesquisa, São Paulo, Brazil, January 2023
Instructor in the EduExplora Program, Human Metabolism Course, UCLA, July 2022
Instructor in the EduExplora Program, Mitochondrial Metabolism Course, UCLA, July 2022
Teaching Assistant for MCD BIO 165A Discussion: Biology of Cells, UCLA, Spring 2020

\

CHAPTER 1: INTRODUCTION

CARDIAC PHYSIOLOGY AND METABOLISM IN HEALTH & DISEASE

Healthy Heart Physiology

The major structural components of the healthy heart include the left ventricle (LV), a chamber that is filled with arterial blood arriving from the lungs. This arterial blood is oxygenated and pumped by the LV to the body for oxygen and nutrient distribution to the tissues and organs of the body. The right ventricle (RV) is a chamber that is filled with venous, deoxygenated blood carrying carbon dioxide that is exchanged for oxygen upon arrival to the bronchioles of the lungs. These two chambers are separated by a common wall dividing them, called the muscular interventricular septum. Above the LV and RV resides the left atrium (LA) and right atrium (RA), respectively (**Scheme 1**). The RA assists in transporting deoxygenated blood from the body to the RV. The LA helps the oxygenated blood from the lungs get to the LV. The walls that compose the LV and RV are made up of cells called ventricular cardiomyocytes. The structure and function of ventricular cardiomyocytes allow them to contract and relax during systole and diastole, respectively, during a heartbeat. This contraction and relaxation of the chambers allow the heart to respond to the physiological pressure and volume of the blood. In this manner, the heart can pump oxygen and nutrient rich blood throughout the body.

The contraction and relaxation of the heart depends on the intracellular concentration of Ca^{2+} (calcium) and the excitation-contraction (E-C) coupling of each ventricular cardiomyocyte. During the plateau phase of an action potential in a ventricular cardiomyocyte, the slow calcium L-type channels get activated and Ca^{2+} enters the cell very slowly, while K^{+} (potassium) is reduced my exiting the cell. The increase in intracellular cytosolic Ca^{2+} cause calcium-induced calcium release, which is when Ca^{2+} is released from the sarcoplasmic reticulum (SR) through the Ryanodine Receptor (RyR). The role of increased Ca^{2+} concentrations in ventricular cardiomyocyte contractility is crucial in enabling sarcomeres to shorten during contraction (troponin complex, myosin, myofilaments). During the rapid falling phase after the plateau phase

of an action potential, Ca^{2+} channels get inactivated and K^+ exits the cell quickly through voltage-gated K^+ channels, leading to a resting membrane potential. The decrease in Ca^{2+} at this last phase is not only due to inactivation of calcium channels, but also due to the sodium-calcium exchanger (NCX) and the ATPase, SERCA (SR Calcium ATPase), which is a pump that removes cytosolic Ca^{2+} by importing Ca^{2+} back into the SR. Therefore, concentrations of Ca^{2+} and ATP are crucial factors the heart relies for relaxation and contraction of the heart.

Heart Failure (HF) Pathology and Etiology

The heart may undergo physiological cardiac hypertrophy in response to exercise, where the cardiomyocytes change in morphology and become hypertrophied (cell growth) to adapt their contractility to the increased in wall pressure and blood volume. However, during pathological cardiac hypertrophy, cardiomyocytes fail to adapt to pressure and volume overload in response to stress which leads to contractile dysfunction and reduced cardiac output.[12] Heart failure (HF) then ensues from pathological cardiac hypertrophy (**Scheme 1**). Heart failure is a cardiovascular disease that is afflicting approximately 6 million human beings in the United States and # in the world as of 2023. Other causes of HF include arterial hypertension, cardiomyopathy, acute myocardial infarction (AMI), and valvular diseases.

HF with Preserved Ejection Fraction (HFpEF) or Reduced Ejection Fraction (HFrEF)

The contractility of the heart can be measured by the ejection fraction (EF), which is a percentage measurement of how much blood the left ventricle of the heart pumps in each contraction to the rest of the body. Heart failure with preserved ejection fraction (HFpEF) occurs when a person has HF due to high filling pressure in the LV even though the EF of the heart is normal (50% or more). Heart failure with reduced ejection fraction (HFrEF) presents itself when the EF is 40% or less and the LV cannot pump the blood required to meet the demands of the body. The failing heart becomes less efficient, producing less work per O_2 consumed.

Healthy Myocardial Energy Metabolism

The heart is the organ with the most metabolic demands in the body, as its function in contractility to deliver oxygen and nutrient rich blood throughout the body requires a surmountable amount of ATP production. In the healthy heart, carbohydrates (glucose and lactate) and fatty acids (FAs) are the major contributors to ATP production required for myocardial contractility and heart function. About 40-60% of ATP production comes from the oxidation of FAs. Mitochondrial oxidation of glucose contributes 20-40% to ATP production in the heart. Lactate contributes 10-15% to cardiac ATP and glycolysis 2-8%. Branched-chain amino acids (BCAAs) contribute to overall myocardial ATP production very minimally, about 1-2%. An estimated 10-15% of ATP production comes from ketone oxidation.[3] These fuels are obtained from the blood since cardiomyocytes are not well able to store fuels.

In general, glycolysis produces less ATP (2 ATP) than the amount of ATP (31 ATP) produced from complete, mitochondrial oxidation of glucose. Glucose produces more ATP per O_2 consumed in comparison to other fuels. However, FAs produce more ATP per two carbons but are less efficient in producing ATP per O_2 consumed compared to glucose. Mitochondrial oxidative phosphorylation contributes about 95% to ATP in the heart and approximately 5% of ATP comes from glycolysis.[4,5]

The oxidation of glucose can yield ATP either through glycolysis or through complete oxidation of glucose in the mitochondria through the import of pyruvate. The cardiomyocyte uptakes glucose via the glucose transporter 1 (GLUT1) and the insulin dependent GLUT4 transporter. GLUT4 is the primary transporter for glucose uptake and is also controlled by the contraction of the cardiomyocyte. Upon uptake, glucose can be diverted through several metabolic pathways including glycolysis, mitochondrial oxidation through pyruvate, glycogen synthesis, the hexosamine biosynthetic pathway, or the pentose phosphate pathway. Glucose-derived pyruvate can also be broken down to lactate and vice versa, lactate can be imported through the monocarboxylic anion transporter (MCT4) and can be converted to pyruvate by lactate dehydrogenase (LDH). In this manner, lactate can be used as a fuel in the heart.

FA oxidation (FAO) is the major fuel source of the healthy heart. FAs are delivered via the blood to the heart by binding to albumin or as triacylglycerols (TAGs) bound to very low-density lipoproteins (VLDLs). After FA uptake and transport into the mitochondria through carnitine and CPT-1 (carnitine palmitoyl transferase 1), FAs are broken down through **β**- oxidation which gives rise to acetyl-CoA.[6] Acetyl-CoA is then fed into the TCA cycle (**Scheme 2**), where NADH and $FADH_2$ are produced and completely oxidized at the electron transport chain (ETC) complexes (**Scheme 3**). FAO in the heart is tightly regulated by several factors, including FA supply and uptake, CPT-1 inhibition by malonyl CoA, ratios of FAD/$FADH_2$ and NAD^+/NADH, mitochondrial acetyl-CoA/CoA ratios, and transcriptional and translational regulation of enzymes involved in FA oxidation.[7]

Ketone bodies are derived from the oxidation of FAs in the liver. These species are more efficient than FAs when producing ATP per O_2 consumed, however, less efficient than glucose. **β**-hydroxybutyrate (**β**-OHB) is the main ketone body used by the heart as a fuel source and is imported into the cell via the monocarboxylate ketone transporter SLC16A1. It then undergoes oxidation by several enzymes, one in which it includes the **β**-hydroxybutyrate dehydrogenase 1 (BDH1). If levels of ketones elevate in circulation, then they can potentially become the major fuel source of the heart.[8]

BCAAs are the main amino acids used by the heart as fuel and are oxidized by the enzymes mentioned in the BCAA oxidation section below. Although only a small percentage of their oxidation contributes to ATP in the heart, BCAAs play a role in cardiomyocyte signaling processes involved in ventricular function. Additionally, BCAAs play a role in insulin signaling and the mTOR pathway, which will be further discussed in the BCAA oxidation section.

Overall, the heart is metabolically flexible to be able to meet its ATP demand. The substrate preference of the heart for ATP production is FAs, followed by lactate, then ketone bodies, glucose, and finally BCAAs. The well-known Randle's glucose and FA cycle also applies

to the heart of humans and rodents, where the oxidation of FAs and glucose are inversely correlated.

Changes in Energy Substrate Metabolism in HF

Pathological alterations that occur in HF can be explained by convoluted metabolic shifts in substrate preference and energy metabolism (**Scheme 1**) and are further obscured by the severity and type of HF as well as the co-existence of comorbidities, which include obesity and diabetes. Additionally, HFpEF and HFrEF can co-exist with or without ischemic heart disease or with hypertension (HTN).[9]

The failing heart has a deficit in ATP that results from decreased mitochondrial oxidative capacity. It is estimated that ATP is about 30% lower in the failing heart. The failing heart then tries to compensate its deficit by producing ATP from an increase in glycolysis. However, mitochondrial glucose oxidation, oxidation of amino acids, and ketone oxidation is attenuated. The failing heart may either increase or decrease oxidation of FAs. A decrease in FAO has been observed during co-existence of HF and myocardial infarction (MI) or HTN. Therefore, decreased mitochondrial oxidative capacity, switch in substrate preference, and attenuated cardiac efficiency all contribute to HF in an orchestrated manner.

Earlier studies on the metabolism of the failing heart suggested that during HF, the heart's energy substrate preference switches to a fetal-like state, where glycolysis is increased, and FA oxidation decreased.[10] During the fetal phase of life, the hemodynamic load in the fetus's heart is supported by the mother's circulatory system and its dependence on the mother's circulatory oxygen place the cardiac mitochondria in preference for glycolysis to meet its energetic demands (anaerobic). It may be that during the transition from a fetus to a neonate, the shift in hemodynamic load onto the neonate heart and the increase in oxygen levels allow the mitochondria to switch to mitochondrial oxidation of glucose FAs to meet the ATP demand of the heart. Earlier research suggested then that in the failing heart, the decreased access to oxygen,

due to lower ejection fraction (EF), led to the transition from an adult to a fetal metabolic state in the heart.

However, recent studies in the past couple of decades do not show changes in FAO or show an increase or decrease in FAO. HF co-existing with diabetes or obesity show an increase in FAO. Again, in HF associated with MI or HTN, FAO decreases. It is possible that during early-stage HF when there is cardiac hypertrophy but changes in blood flow and cardiac energy expenditure have not yet arise, FA uptake and oxidation is increased to meet the increase in energy demand. However, because FAO cannot satisfy the ATP required to meet the demand as efficient as glucose, the structural and function of cardiomyocytes worsens, thus pushing the cardiomyocytes toward glycolysis to quickly meet the ATP demand of the heart. Potentially by this point, the heart has now progress to end-stage HF (or HFrEF), where there is a large decrease in FAO and increase in glycolysis. It is possible that at this stage and severity of HF, the failing heart has indeed undergone the transition from an adult-like to a fetal-like metabolic state as earlier studies had indicated.

In general, ketone body levels are raised in the body upon fasting. In patients with HF, this increase is further elevated. More specifically, during HFrEF, a dramatic enhancement of ketone body oxidation is observed and furthermore, it is accompanied by reduced FA oxidation.[11] These results have been observed in patients with HFrEF and animal models of TAC.[12] Mouse models of MI-induced HFrEF show induced expression of enzymes that play a role in ketone oxidation and attenuation of expression of enzymes involved in FA oxidation.[11] The role of ketone oxidation in HFpEF is not completely understood.

Additionally, BCAA levels accumulate in the failing heart due to damaged BCAA oxidation pathways. Mice with the knock out of the protein phosphatase 2Cm (PP2Cm), an activator of BCAA oxidation, were more prone to developing HFrEF after trans-aortic constriction (TAC) surgery, due to the inability to oxidize the elevated levels of BCAAs and BCKAs.[13] Furthermore, although BCAAs contribute to only a small fraction for ATP production, BCAAs play a major role

in cellular signaling in the development of HF. Elevated levels of BCAAs activate the mTOR signaling pathway in the heart, which promotes the pathological hypertrophy of cardiomyocytes. Impaired oxidation of BCAAs has also been implicated in insulin resistance, diabetes, and obesity. BCAA oxidation in HF and other metabolic diseases will be further explored in depth in a later section.

It is currently unknown whether changes in substrate utilization during HF are adaptive or maladaptive. Meaning, if adaptive, these changes in energy substrate metabolism is a mechanism that the failing heart adapts to protect itself from progressive irreversible structural and functional damage. During these changes, it is hypothesized that the decreased in blood flow and therefore oxygen to the heart require the mitochondria to switch to a glycolytic state. If these changes are maladaptive, then the metabolic shift in the heart potentially causes it to fail to maintain its healthy, physiological function.

PREVIOUS EFFORTS IN TARGETING METABOLISM & MITOCHONDRIA TO TREAT CVD

The question remains, would the failing heart benefit from reversing increase in glycolysis back to FAO, or is the answer to this question vary depending on the stage of HF the patient is in? Researchers have developed therapeutics to target cardiac metabolism in HF in the past. They have aimed to stimulate oxidation of glucose, ketones, BCAAs, and have intended to modulate oxidation of FAs.

Since the oxidation of FAs in the failing heart is very complicated and targeting FAO is not black or white, researchers have attempted to stimulate or inhibit FAO. Studies show that the CPT-1 inhibitors Etomoxir and Perhexiline in addition to the anti-ischemic agents Trimetazidine and Ranolazine can inhibit myocardial FAO and activate glucose oxidation. Treatment with these drugs show improved function and efficiency in the failing heart.[14,15,16,17]. Malonyl CoA is a metabolite that is known to endogenously inhibit mitochondrial FA uptake and therefore FAO. Malonyl CoA is synthesized by acetyl CoA carboxylase (ACC) and degraded by malonyl CoA decarboxylase (MCD). There are several conflicting studies showing inhibition of ACC or MCD,

thus increasing or decreasing FAO respectively, can prevent the development of HF and be cardioprotective.[18,19,20] Inhibition of ACC or MCD leads to stimulation of mitochondrial glucose oxidation. Furthermore, ACC inhibition is correlated with improved mitochondrial function.[20]

As previously mentioned, impaired glucose oxidation is observed in the failing heart, which has been linked to insulin resistance. Therefore, stimulating oxidation of glucose in the failing heart by treatment with dichloroacetate, an inhibitor of the PDH kinase, has resulted in improved glucose oxidation and therefore improved cardiac function and recovery post ischemic injury in patients and rodents.[21] This process allows for glucose to be diverted from glycolysis to mitochondrial glucose oxidation. The human monoclonal antibody (mAb A) has been used to target the glucagon receptor (GCGR) and has resulted in enhanced insulin signaling and glucose oxidation , which led to improved cardiac function post-myocardial infarction.[22] However, inhibitors of the sodium-glucose transporter (SGLT) have been used to inhibit reuptake of glucose and are primarily used to treat diabetic failing hearts. In addition, SGLT inhibitors increase ketone bodies in circulation, which are made readily available to the heart for fuel. Indeed, SGLT inhibitors have been shown to have cardioprotective effects and improve cardiac function.

Many studies indicate that enhanced ketone oxidation in the failing heart is adaptive. Therefore, researchers have aimed to increase circulating ketone levels and enhance ketone oxidation by the infusion of ketones or ketone esters and by administration of a ketogenic diet. In addition to increasing circulating ketone levels with SGLT inhibitors, infusion of **β**-OHB or R-3-hydroxybutyral-(R)-3-hydroxybutyrate, which leads to increased **β**-OHB, showed improved cardiac contractile function in patients with HFrEF.[23] The drug Empagliflozin has been shown to increase **β**-OHB, thereby increasing ketone body oxidation and improving cardiac function in the failing heart. Lastly, weight loss, a ketogenic diet, and nutrient intake modulation have been shown to improve oxidation of fuels in the heart and therefore heart function during HF.

Elevated levels of BCAAs and impaired BCAA oxidation has been associated with cardiovascular and metabolic disease. In human dilated cardiomyopathy, low expression of BCAA

catabolic enzymes has been observed.[13] However, the heart contributes about 4% to whole-body level BCAA oxidation, indicating that increasing BCAA oxidation would not significantly improve cardiac ATP production and therefore improve contractile function in the heart.[24] Surprisingly, increasing oxidation of BCAAs with BT2 (3,6-dichlorobenzo[b]thiophene-2-carboxylic acid) has been shown to be cardioprotective. In the next sections, I will discuss the role of BCAA oxidation in HF and metabolic diseases, the BCAA oxidation pathway, and the evidence for and against enhancing BCAA oxidation to treat HF.

BCAA OXIDATION IN HEART FAILURE AND METABOLIC DISEASE

Association of BCAA Oxidation in HF

Increased levels of BCAAs are associated with HF in humans and preclinical animal models of this disease. A study demonstrated that intramyocardial levels of branched-chain α-ketoacids (BCKAs) in humans were significantly increased in cardiomyopathy hearts compared to healthy, control human hearts.[13] In addition, there is evidence showing a significant association of elevated levels of plasma BCAAs levels with coronary artery disease (CAD). In parallel, there are several other studies illustrating a similar pattern in preclinical models of cardiovascular disease. Mice subjected to trans-aortic constriction (TAC) surgery, a model for pressure-overload-induced heart failure, showed increased levels of BCKAs in heart tissue compared to sham mice. These studies suggest an association of elevated levels of BCAAs/BCKAs in heart failure. Furthermore, elevated levels of BCAAs are associated with metabolic disease including insulin resistance, diabetes, and obesity in both humans and mouse models of metabolic disease.

BCAA Oxidation in Diabetes and Obesity

From the Framingham Offspring Study, evidence arose showing a strong relationship between high concentrations of plasma BCAAs and the development of future diabetes.[25] Moreover, studies show elevated levels of BCAAs in obese vs lean humans, and this metabolic signature was found to have a significant linear relationship with insulin sensitivity, shown by BCAA-related principal component analysis (PCA) factor score and HOMA (Homeostatic Model

Assessment of Insulin Sensitivity, or resistance).[26,27] Another study showed elevated levels of BCAAs in the plasma of *ob/ob* mice, a mouse model of obesity, and a mouse model of Type 2 Diabetes compared to wild-type (WT) mice.[28] Indeed, several studies have shown a relationship between lipids, BCAAs, and insulin resistance.[26] Together, these aforementioned studies in humans and animals show a strong association or causality of BCAAs in heart failure and metabolic disease.

BCAA OXIDATION

Branched-Chain Amino Acids (BCAAs)

Branched-chain amino acids (BCAAs) are three of nine essential amino acids that include leucine (Leu), isoleucine (Ile), and valine (Val). Essential amino acids are obtained from the diet and non-essential amino acids are synthesized in the body. BCAAs are amino acids that have an aliphatic side chain with a branched functional R group and have roles in protein synthesis, nutrient sensing, and cellular signaling. However, the primary focus will be in the oxidation of BCAAs.

BCAAs Oxidation Pathway & Catabolic Enzymes

The first step in the oxidation pathway of BCAAs is the reversible transamination of the BCAA to its respective branched-chain α-ketoacid (BCKA) by the branched-chain amino-transaminase (BCAT), an enzyme found in the cytoplasm (BCAT1) and mitochondria (BCAT2) (scheme 4). BCAT transfers an amine group (NH_3) from the BCAA to α-ketoglutarate (αKG) and converts it to glutamate, where the K_m is 0.1-1.0 mM. This gives rise to α-ketoisocaproate (KIC), α-keto-β-methylvalerate (KMV), and α-ketoisovalerate (KIV) from Leu, Ile, and Val, respectively. The K_m for BCAT having Leu or Ile as substrates is approximately 0.4-0.8 mM and 1.2-2.5 mM for Val. This transamination reaction is primarily regulated by the concentration of enzyme [E] and concentration of substrate [S]. Of note, physiological concentrations of BCAAs are 0.1-0.2 mM.[29]

The second, rate-limiting and irreversible step in the oxidation of BCAAs is the oxidative decarboxylation of the BCKAs by the branched-chain α-ketoacid dehydrogenase (BCKDH) complex, producing their respective R-chain coenzyme A (R-CoA) derivative which includes isovaleryl-CoA (IV-CoA) from KIC, 3-methylbutyryl-CoA (MB-CoA) from KMV, and isobutyryl-CoA (IB-CoA) from KIV. The K_m for the BCKDH and the BCKAs are 15 μM for KIC, 14 μM for KMV, and 28 μM for KIV. The branched-chain acyl-CoAs can competitively inhibit the BCKDH. The acyl-CoAs produced then undergo further oxidation through a series of catabolic steps leading to the production of acetyl-CoA (from Leu and Ile), propionyl-CoA (from Ile), and succinyl-CoA (from Val), where they can then enter the tricarboxylic acid (TCA) cycle (**Scheme 2**).

The BCKDH complex is found in the inner mitochondrial membrane (IMM) and is a member of the 2-oxoacid family, which also include the pyruvate dehydrogenase (PDH) complex and the α-ketoglutarate dehydrogenase (α-KGDH) complex. These family members are composed of an E_1 component (dehydrogenase), E_2 core (dihydrolipoyl transacetylase), and E_3 component (dihydrolipoyl dehydrogenase). First, the E_{1b} component (decarboxylase) of the BCKDH complex catalyzes the thiamin diphosphate (ThDP)-mediated decarboxylation of the BCKA, releasing CO_2. The lipoyl domain in E_2 behaves like a swinging arm to transfer the acyl group from E_1 to CoA in E_2 during reductive acylation, resulting in the branched-chain acyl-CoA.[30]

The E_{2b} dihydolipoyl transacetylase component of the BCKDH with a lipoate prosthetic group is non-covalently bounded to the E_{3b} dihydrolipoyl dehydrogenase, which has a flavin adenine dinucleotide (FAD) as a prosthetic group. The FAD re-oxidizes the reduced form of the dihydrolipoyl residue (dithiol) of E_2, resulting in $FADH_2$ and the oxidized form of the dihydrolipoyl residue (with disulfide bond). $FADH_2$ gets re-oxidized to FAD by donating electrons and a proton to nicotinamide adenine dinucleotide (NAD^+), which is the ultimate electron acceptor, thereby producing NADH. BCKDH, a multienzyme complex composed of these three E_1- E_3 catalytic

components, also utilizes $Ca^{2+,}$ and Mg^{2+} for its activity and catalyzes the overall reductive decarboxylation reaction of BCKAs.

BCAA Regulation

The oxidation of BCAAs is mainly regulated by the reversible phosphorylation and dephosphorylation of the BCKDH. The branched-chain α-ketoacid dehydrogenase kinase (BCKDK) phosphorylates the BCKDH, thereby inactivating it. Dephosphorylation of the BCKDH by the protein phosphatase 2Cm (PP2Cm) leads to its activation.

The BCKDK binds tightly to the BCKDH and phosphorylates Serine (Ser)-292α in the E_{1b} 15 Angstrom long active site channel of the BCKDH. Although it also gets phosphorylated at Ser-302, Ser-292α is the major phosphorylation site on the BCKDH and its phosphorylation is enough to inactive BCKDH.[31] Phosphorylation at Ser-292α results in an order-to-disorder transition of the conserved phosphorylation loop. The disordered conformation of this loop does not allow the E_{1b} to bind the E_{2b} lipoyl-bearing domain of the BCKDH. This results in the inhibition of the E_{1b} -catalyzed reductive acylation reaction of BCKDH and thus inactivating it.[32]

The PP2Cm, also known as the BCKDH phosphatase or PPM1K, is a Mn^{2+}-dependent phosphatase. It regulates the BCKDH by loosely binding to BCKDH and dephosphorylating the Ser-292α in $E_{1\alpha}$ component, thereby activating it. The two coordinated Mn^{2+} metal ions, which are bridged by Asp-127, can neutralize the negative charge of the leaving group in the phosphoryl group at Ser-292α of the BCKDH, and thus inducing dephosphorylation of the BCKDH at this site.[33]

In addition to hormones, exercise, and dietary stimulus having roles in regulating phosphorylation status of the BCKDH, there are other metabolic routes of regulating BCAA oxidation. KIC can inhibit the function of the BCKDK at IC_{50} of 74.9 uM,[32] which allows for the BCKDH to be activated and metabolize BCKAs. On the other hand, the BCKDH can be regulated

through end-product inhibition by branched-chain acyl-CoAs and NADH. More specifically, elevated acyl-CoA/CoA and NADH/NAD^+ ratios decrease oxidation of BCKAs through BCKDH.

BCAA Metabolism in Tissues

The liver has low BCAT concentrations and therefore low BCAA transamination activity. Due to high BCKDH activity however, BCKAs from peripheral tissues can be further oxidized in the liver.

The skeletal muscle is the main contributor to BCAA oxidation (59%) at the whole-body level, followed by brown adipose tissue (19%), liver (8%), and heart (4%), quantified by *in vivo* isotope tracing.[4] It is noteworthy to mention that metabolism of BCAAs can change due alterations in diet, endurance exercise, and hormonal changes.

BCAA Signaling

BCAAs affect mTOR (mammalian target of rapamycin) signaling in cardiac insulin resistance and cardiac hypertrophy. Leucine specifically is an activator of the mTORC1 pathway.[34] This pathway is involved in the regulation of cell growth and proliferation in addition to insulin signaling. Additionally, it has been shown that Valine-derived metabolites such as β-aminoisobutyric acid (BAIBA) & 3-hydroxyisobutyrate (3-HIB) are involved in fatty acid metabolism.[35]

BCAA Dysregulation in Disease

Maple Syrup Urinary Disease (MSUD) is an autosomal recessive disease with an inborn error in the BCKDH that results in low enzymatic activity or low levels of BCKDH leading to low oxidation of BCAAs and BCKAs, which therefore gives rise to concentrations of these metabolites. Clinical presentation of MSUD includes inability to metabolize amino acids, which results in viscous urine with an odor of maple syrup and changes in muscle tone. Symptoms present themselves weeks after birth in the neonate stage.

Abnormal levels of BCAAs can also result from the dysregulation of the BCKDK and the PP2Cm.[34] Overexpression of the BCKDK has been observed in patients with colorectal cancer.[36]

Studies indicate that elevated levels of the BCKDK may lead to the phosphorylation of MEK and therefore overactivation of the MAPK signaling pathway, which is a well-known pathway involved in driving cell growth and proliferation in cancer. It has been shown that single nucleotide polymorphisms (SNPs) in the PP2Cm gene lead to a constitutively active or inactive mutant form of this protein. Additionally, low expression of the PP2Cm protein has been linked to obesity, type-2 diabetes (T2D), cardiovascular diseases (CVDs), and neurological diseases. [25]

High levels of plasma BCAAs have been linked to obesity, diabetes, and cardiovascular diseases. Elevated levels of leucine can overstimulate the mTORC1 pathway by increasing activation of the p70S6 kinase, which phosphorylates the insulin receptor substrate, resulting in inhibition of insulin signaling and therefore insulin resistance results. Additionally, an overactivated mTORC1 pathway can play a role in cell growth and proliferation during pathological cardiac hypertrophy.

EVIDENCE FOR AND AGAINST ENHANCING BCAA OXIDATION IN HEART FAILURE & METABOLIC DISEASE

Adaptive vs. Maladaptive

As mentioned previously, studies have shown that intramyocardial levels of BCKAs were significantly increased in human cardiomyopathy hearts and furthermore, levels of BCAAs were significantly elevated in plasma of individuals with cardiovascular disease. This pattern is also observed in metabolic disease including diabetes and obesity. However, it is unclear to what extend this is causative or associative. If causative, then enhancing BCAA oxidation in HF and metabolic disease would suffice to improve disease. If associative, then enhancing BCAA oxidation would not directly ameliorate heart failure and metabolic disease. Next, I will dive deep into the evidence that is for and against enhancing BCAA oxidation in alleviating HF and metabolic disease. These studies will allow us to better predict whether elevated BCAAs/BCKAs cause HF and metabolic disease.

BT2 (dichloropheno[b]thiophene-2-carboxylic-acid

Researchers asked whether the kinase/phosphatase regulation of BCKDH can be manipulated to adjust BCAA & BCKA levels with a pharmacological agent. Therefore, a pharmacological compound named BT2 (dichlorophenо[b]thiophene-2-carboxylic-acid) with IC_{50}= 3.19 μM was designed as a BCKA analog with the intention to allosterically inhibit the BCKDK and induce BCAA oxidation. Upon binding, BT2 induces a conformational change at the N-terminal domain of the BCKDK, thus triggering the dissociation from the BCKDH. By inhibiting the BCKDK, this would result in promoting BCAA/BCKA oxidation removing the break on the activation of the BCKDH. Therefore, the goal of this pharmacological agent was to decrease phosphorylation of BCKDH by inhibiting BCKDK and thereby activating BCKDH to allow it to catabolize BCKAs to their respective R-CoAs.[37,32]

Pharmacological Evidence

Studies showed BT2 indeed induced BCAA oxidation. Sun *et al*. showed that treating WT mice with BT2 reduced the levels of plasma BCKAs compared to vehicle-treated mice, exhibiting the efficacy of the pharmacological agent BT2.[13] Moreover, echocardiographic results showed BT2 treatment improved heart function post-TAC (trans-aortic constriction) surgery, compared to heart function of mice treated with vehicle and subjected to TAC surgery or sham surgery. More specifically, the rescue in heart function was observed in mice treated with BT2 pre-TAC surgery and post-TAC surgery, as shown by the enhancement of fractional shortening (ΔFS%) and left-ventricular inter-diameter (LVID).[38]

BT2 also improved cardiac function in other mouse models including the LAD (left anterior descending artery) ligation mouse model of MI and the mouse model of cardiac ischemia-reperfusion injury (I/R). In mice treated with BT2 and subjected to LAD ligation to induce MI, the LVEF (left-ventricular ejection fraction), LVEDD (left-ventricular end-diastolic diameter), and LVESD (left-ventricular end-systolic diameter), was significantly improved compared to mice

subjected to LAD ligation alone. Mice fed high levels of BCAAs and treated with BT2 significantly reduced I/R injury compared to mice fed with BCAAs alone.

Treatment with BT2 in the Zucker fatty rats, a murine model of obesity, reduced levels of plasma BCAAs and BCKAs, as expected.[39] Additionally, BT2 improved metabolic function by reducing glycemia and insulin levels over time. Moreover, these results were concomitant with decreased hepatic triglyceride levels in Zucker fatty rats treated with BT2, suggesting an increase in fatty acid oxidation or decrease in *de novo* lipogenesis. The authors of this study reasoned that BT2 was having off-target effects and that these effects were due to BCKDK and PP2Cm potentially targeting other enzymes in addition to the BCKDH. White *et al*. found that this kinase/phosphatase pair also modulates the ATP-citrate lyase (ACL), an enzyme involved in *de novo* lipogenesis (DNL). They concluded that this was the reason why BT2 treatment led to a decrease in fatty acids in the liver of Zucker fatty rats.

Finally, a recent study by Flach *et al.* showed the role of BT2 in mouse models of NAFLD (non-alcoholic liver disease) and diet-induced obesity. BT2 treatment in a mouse model of NAFLD indeed reduced levels of BCKAs in the heart and muscle. Results also showed BT2 improved insulin sensitivity, as shown by improved glucose infusion rate (GIR) and clamped GIR data.[40] Moreover, BCKDK KD in the liver of diet-induced obese mice does not protect from metabolic disease even though BCAA and BCKA levels were reduced.

Genetic Evidence

A study showed that mice with the PP2Cm KO exhibited elevated levels of BCKAs in the heart vs heart of WT mice.[37] In addition, subjecting PP2Cm KO mice to TAC surgery worsened heart function compared to WT mice subjected to TAC surgery. These studies suggested elevated levels of BCKAs, due to inactivation of the BCAA catabolic pathway, exacerbated heart function in the TAC mouse model of HF. In addition, tissue-specific overexpression of PP2Cm led to the reduction in BCAA and BCKA levels, which resulted in protection from ischemia reperfusion injury, improved hepatic glucose tolerance, and a decrease in triglyceride accumulation in the liver.

Although these studies suggest a causative role of BCAA catabolism in heart failure, more recent evidence based on BCKDK KO and KD indicate an association.

Another research group reasoned that if pharmacologically inhibiting the BCKDK led to the rescuing of heart function in various models of heart failure (TAC surgery, LAD ligation, and cardiac I/R injury), then it would be expected that by knocking out the BCKDK one would observe results mirroring BT2 treatment in the rescue of heart function in the failing heart. Murashige *et al*. specifically knocked-out the BCKDK in the mouse heart (BCKDK cKO) and subjected control mice and BCKDK cKO mice to LAD ligation to induced MI.[41] Results showed no changes and therefore no improvement in systolic function and ventricular dilation in BCKDK cKO mice vs control mice. These results indicate that BT2 is cardioprotective independent of BCAA oxidation in the heart. This data was accompanied by a significant increase in the enrichment of TCA cycle intermediates in BCKDK cKO mice vs control mice, indicating successful activation of BCAA catabolism. However, no changes in relative abundances of BCAAs and BCKAs were observed in the heart of BCKDK cKO mice.

Moreover, an inducible skeletal muscle BCKDK KO mouse model (iSkM-BCKDK-KO) was created and subjected to LAD ligation showed no improvement in heart function 2-4 weeks post-MI, as observed by no changes in LVEF. Furthermore, no cardioprotection was observed despite observing an increased in BCAA oxidation, as quantified by a reduction in cardiac BCAAs, decrease in BCAA and BCKA abundances in the quadriceps and plasma, including an increase in ^{13}C enrichment of TCA cycle intermediates of skeletal-muscle specific BCKDK KO mice.[41] Therefore, iSkM-BCKDK-KO mice showed changes in whole-body systemic BCAA levels but no cardioprotection was observed. This data on cardiac and skeletal muscle specific BCKDK KO point to another mechanism by which BT2 is conferring cardioprotection.

Finally, the previous evidence showing the contribution of the heart to whole-body BCAA oxidation is only about 4%, according to Neinast *et al,* also supports the unlikelihood of BT2 being cardioprotective through the BCAA catabolic pathway.[24] *In vivo* isotope tracing also showed

skeletal muscle to have the highest rates of BCAA oxidation, approximately 59%. Therefore, enhancing BCAA oxidation in a tissue with a small percentage of BCAA oxidation (heart) and a tissue with high rates of BCAA oxidation (skeletal muscle) did not suffice to rescue the failing heart.

The pharmacological and genetic evidence raises several questions. Why does PP2Cm KO show elevated levels of BCAAs does cause heart failure? In other words, why does this data show that disruption of BCAA oxidation does indeed cause HF? However, BCKDK KO does not rescue HF and does not reproduce the effects of BT2, thus raising the question as to whether the mechanism of action of BT2 is indeed through targeting the BCKDK.

Hypothesis

Thus far, I have delineated the existing evidence supporting a role of impaired BCAA catabolism in heart failure and metabolic disease and rescuing by the pharmacological agent BT2. Most importantly, the tissue specific BCKDK KO and KD experiments unmasked the likelihood of an alternative mechanism of BT2 protecting from heart failure and metabolic disease independently of inducing BCAA oxidation. Consequently, we asked whether BT2 confers cardioprotection and protects from metabolic disease by a mechanism independent of enhanced BCAA oxidation? We therefore hypothesized based on its chemical structure as a lipophilic weak acid, ***BT2 is a mitochondrial uncoupler that decreases ROS production and increases energy expenditure and thus protect from cardiovascular and metabolic disease.***

Indeed, BT2's chemical structure suggests its potential capability to lose and gain a proton (**Scheme 5**). BT2 can therefore have a similar mechanism as the other common mitochondrial uncouplers (also known as protonophores) which include DNP, FCCP, and Bam15. Of note, a mitochondrial uncoupler can be protonated and deprotonated while it transports or shuttles protons across the mitochondrial inner membrane and depolarizes the mitochondrial membrane potential. This leads to uncoupling ATP synthesis from the electron transport chain.

Measurements of respiration, mitochondrial membrane potential, and mitochondrial inner membrane electrophysiology all characterize BT2 as a chemical uncoupler (**Scheme 5**). Furthermore, the evidence provided here elucidate BT2 lowers mitochondrial H_2O_2 efflux and reduced *de novo* lipogenesis via mitochondrial uncoupling, similarly to 2,4-dinitrophenol (DNP). After diving deep into the evidence, we will discuss how mitochondrial uncoupling by BT2 can explain its therapeutic effects against heart failure and cardiometabolic disease, independently of its effects on BCAA catabolism. Therefore, we began unraveling the alternative mechanism of BT2 with the following experiments.

CHAPTER 2

BT2 UNCOUPLES MITOCHONDRIA IN INTACT CELLS

BT2 Uncouples Mitochondria in NRVMs and iCell Cardiomyocytes

Considering that BT2 confers cardioprotection and protects from metabolic disease and furthermore, the evidence pointing to a distinct, uncharacterized mechanism, we decided to identify uncharacterized metabolic targets or mechanisms of BT2 independent of its inhibition on the BCKDK. We accordingly took the initial steps to study BT2's potential effects as a chemical uncoupler in intact cells.

To achieve this, we used a common method to study changes in mitochondrial metabolism and bioenergetics in response to pharmacological agents (or genetic interventions), which is to measure oxygen consumption rates (OCR, pmol O_2/min/μg mito. protein or cells) using the seahorse assay (Seahorse XF Analyzer). This assay allows for measurements of energy metabolism in intact cells, permeabilized cells, and isolated mitochondria by the addition of drugs including oligomycin, FCCP (carbonyl cyanide 4-(trifluoromethoxy)phenylhydrazone), Rotenone, and Antimycin A. Oligomycin is an inhibitor of the ATP synthase, FCCP is a protonophore which shuttles protons back into the mitochondrial matrix, Rotenone is a complex I inhibitor, and Antimycin A is complex III inhibitor. In intact cells, the addition of FCCP would allow us to measure the maximal-respiratory capacity of a cell. Addition of Rotenone and Antimycin A allows for the measurement of non-mitochondrial respiration. Using these drugs, one can obtain respiratory measurements from intact cells including basal respiration (endogenous OCR), ATP-linked respiration, proton-leak linked respiration, and maximal respiration. Additionally, the reserve/spare respiratory capacity and non-mitochondrial respiration can be determined. For more details regarding this method, refer to the following publications that explain the seahorse assay in depth using the Seahorse Extracellular Flux (XF) Analyzer.[42,43]

We therefore sought to determine the uncharacterized mechanism of BT2 by measuring respiration in intact neonatal rat ventricular myocytes (NRVMs) and iCell human iPSC-derived cardiomyocytes. NRVMs were offered glucose, pyruvate, and glutamine and iCell cardiomyocytes were offered galactose, pyruvate, and glutamine (**Figure 1A, B**). These intact human and rodent cardiomyocytes were then acutely treated with 40μM BT2, 80μM BT2, or vehicle, 5 minutes prior to initial measurements. Oxygen consumption rates revealed BT2 increased basal respiration BT2 indeed induces a significant increase and furthermore an increase in proton-leak linked respiration in NRVMs and iCell cardiomyocytes, as expected of a mitochondrial uncoupler (**Figure 1B, C**). These results were concomitant with no changes in maximal respiratory capacity. Moreover, we identify the effects of BT2 in a more physiologically relevant system by physiologically challenging NRVMs and iCell cardiomyocytes through adrenergic stimulation with norepinephrine (+NE). Similarly, an elevation in proton-leak linked respiration and basal respiration was observed in NE-activated NRVMs and NE-activated iCell cardiomyocytes upon 40 and 80 μM BT2 treatment (**Figure 1B, C**). No changes in maximal reparatory capacity rates were observed. These results confirm that BT2 can indeed induce an increase in uncoupled respiration in intact cells and therefore act as a chemical uncoupler.

Classical chemical uncouplers like DNP and FCCP induce the consumption of the mitochondrial membrane potential (MMP) independently of ATP synthesis and therefore increase the oxygen consumption rate in order to maintain the MMP. Accordingly, alongside the effects of BT2 on respiration, the MMP ($\Delta \boldsymbol{\psi}$) of NRVMs and iCell cardiomyocytes treated with BT2 was measured and compared with the chemical uncouplers DNP and FCCP (**Figure 1D, E**). MMP was measured using TMRE and mitochondrial content was measured using MitoTracker Green for imaging. Average TMRE intensity measurements showed acute, 30-45 min. treatment with 80 μM BT2 caused and an approximately 10% significant reduction in $\Delta\boldsymbol{\psi}$ vs control in both NRVMs and iCell cardiomyocytes, similarly to 10 μM DNP. Furthermore, 1 μM FCCP significantly

decreased $\Delta\psi$ at a much larger degree than both BT2 and DNP, as expected of a very highly potent chemical uncoupler. Mitochondrial morphology was not affected much by BT2 and DNP treatment in these cells.

Furthermore, we sought to determine if our *in vitro* models using neonatal rat ventricular myocytes (NRVMs) and iCell human iPSC-derived cardiomyocytes show low rates of BCAA oxidation (compared to other substrates) similarly to recent *in vivo* human and rodent studies.[41,44] To do so, we used stable isotope tracing and offered NRVMs either $^{13}C_6$-Leucine or $^{13}C_6$ glucose. As reviewed in the introduction, complete oxidation of leucine leads to its final product of acetyl-CoA in the BCAA catabolic pathway. Leucine-derived carbons into acetyl-CoA can then enter the TCA cycle and labeled ^{13}C intermediary metabolites can then be measured by calculating the mole percent enrichment (MPE) from the $^{13}C_6$-Leucine. Results demonstrated that NRVMs had very little oxidation rates of leucine (BCAA), as shown by low MPE in citrate and malate from $^{13}C_6$-Leucine (**Figure 1F**). For comparison, tracing NRVMs with $^{13}C_6$ glucose showed higher glucose oxidation, as illustrated by 10-fold higher incorporation of glucose-derived carbons into citrate and malate from $^{13}C_6$ glucose. Overall, these results demonstrated that in these cardiomyocytes with low rates of BCAA oxidation, BT2 increases proton-leak linked respiration independently of its effects on BCAA oxidation.

BT2 increases proton leak-linked respiration in intact HepG2 hepatocytes and C2C12 myoblasts

Furthermore, BT2 also significantly increased proton leak-linked respiration in intact HepG2 hepatocytes and intact C2C12 myoblasts oxidizing glucose, pyruvate, and glutamine (**Figure 2**). BT2's mitochondrial uncoupling effects in intact cells are observed with no significant changes in basal respiratory rates. These results in intact HepG2 hepatocytes and C2C12 myocytes with BT2 treatment mirror the above results observed in rat and human cardiomyocytes. Next, we sought to verify these results using reductionist systems where specific metabolic pathways could be isolated.

CHAPTER 3

BT2 UNCOUPLES IN ISOLATED MITOCHONDRIA AND PERMEABILIZED CELLS

BT2 increases State 4_o respiration in isolated mitochondria

Since mitochondrial uncoupling was observed in intact cells treated with BT2, we next wanted to determine if mitochondrial uncoupling was also observed in isolated mitochondria, independent of BCKDK. Isolated mitochondria are a reductionist system that allows for specific metabolic pathways and reactions to be isolated. In brief, analogous to intact cells, respiratory measurements in isolated mitochondria (and permeabilized cells) include State 3 (ADP-stimulated respiration), State 4_o, and state 3_u (protonophore-stimulated respiration). In isolated mitochondria and permeabilized cells, State 3 OCR is measured by the addition of ADP (adenosine diphosphate) and oxidizable substrates. State 4_o OCR is measured by adding the drug Oligomycin, which is an inhibitor of the ATP synthase. In this manner, one can calculate the proportion of OCR originating from the synthesis of ATP and the OCR deriving from proton leak pathways. State 4_o or proton leak-linked respiration is specifically respiration that results from protons leaking back into the mitochondrial matrix, thus uncoupling ATP synthesis from the electron transport chain, and thereby consuming the mitochondrial membrane potential (MMP, $\Delta\boldsymbol{\psi}$). Finally, state 3_u (or protonophore-stimulated respiration) is the respiration upon addition of the protonophore FCCP, which allows us to determine any potential changes in fuel supply and oxidation.

Now that we briefly reviewed measurements of oxygen consumption rates in isolated mitochondria and permeabilized cells, we can now determine the effects of BT2 on targeted metabolic pathways independent of BCKDK in isolated mitochondria. Mitochondria was isolated from rat liver and heart or mouse liver and heart following the protocol outline in the Materials and Methods section. In **Figure 3**, isolated rat liver mitochondria were offered pyruvate/malate and ADP in all the control and experimental groups. State 3 (ADP-stimulated) and State 3_u (FCCP-stimulated) respiration (pmol O_2/min/μg mito. protein) in isolated mitochondria were unchanged

upon acute treatment with 20μM and 40μM BT2 compared to vehicle-treated mitochondria, as shown (**Figure 3A, B**). However, State 4_o (+Oligomycin) OCRs significantly increase with 20μM and 40μM BT2 treatment in isolated mitochondria. These results indicate that BT2 induces State 4_o respiration (proton-leak) in isolated mitochondria similarly to intact cells (**Figures 1 and 2**).

Moreover, in liver mitochondria isolated from rat and mouse, BT2 caused a significant increase in State 4_o respiration in a dose-dependent manner, regardless of whether the substrates offered were pyruvate/malate (Pyr/Mal), glutamate/malate (Glu/Mal), or succinate/rotenone (Succ/Rot) (**Figure 3C**). Depending on the substrate offered and species, BT2 increased proton-leak linked respiration as little as 2.5μM. In heart mitochondria isolated from rat and mouse, BT2 also induced an increased in State 4_o respiration irrespective of substrate offered (pyruvate or succinate) to the heart mitochondria (**Figure 3D**)**.** Recall that BT2 is a weak inhibitor of the BCKDK with half maximal effect at nearly 4μM. Here, BT2 starts to uncouple mitochondria at about 2μM-5μM, corresponding to a concentration below or nearly identical to the half maximal effect concentration. In total, this data suggest that it is highly probable that BT2 uncouples mitochondria *in vivo*. These results indicate BT2 can uncouple isolated mitochondria at single digit micromolar concentrations, where its chemical uncoupling effects manifest regardless of substrate (pyruvate, glutamate, succinate), tissue (heart or liver) and species (rat or mouse). Thus, BT2 is uncoupling isolated mitochondria, an effect that is independent of inhibiting the BCKDK.

BT2 increases State 4_o respiration in permeabilized HepG2 hepatocytes and permeabilized C2C12 myoblasts

To confirm BT2's mitochondrial uncoupling effects are biologically more relevant and eliminate any possible effects during mitochondrial isolation, permeabilized cells were used to measure oxygen consumption rates upon treatment with BT2 (**Figure 4**). Permeabilized cells were offered different substrates and treated with various concentrations of BT2. Permeabilized HepG2 hepatocytes were treated acutely with vehicle, 20, 40, or 80μM BT2 and fed pyruvate/malate, succinate/rotenone, or glutamate/malate (**Figure 4A**). Results show BT2

elevates State 4_o respiration at 40 and 80μM BT2, regardless of substrate given. Furthermore, State 4_o respiration increases at a concentration of BT2 as low as 20μM BT2 when cells are fed pyruvate or succinate. Similarly, increasing State 4_o respiration is observed 20, 40, or 80μM BT2 of BT2 in permeabilized C2C12 myoblasts (**Figure 4B**).

In addition to BT2 uncoupling mitochondria in permeabilized cells, it should be noted that permeabilized cells offered pyruvate and malate and treated with a high concentration of BT2 at 80μM showed to have off-target effects on mitochondrial metabolism. This is shown by the significant decrease in State 3 respiration rates in permeabilized HepG2 hepatocytes and permeabilized C2C12 myoblasts oxidizing pyruvate and malate. It is possible that an off-target effect could be inhibition on pyruvate dehydrogenase activity or inhibition on the mitochondrial pyruvate carrier**.** State 3 respiration rates decreased in permeabilized C2C12 myoblasts offered glutamate as an oxidizing substrate, which further illustrates the possibility that BT2 is targeting other dehydrogenases.

However, 80μM is at supraphysiological concentration of BT2 and therefore its cardioprotective effects are highly likely originating primarily from uncoupling mitochondria since these uncoupling effects of BT2 appear at a concentration as low as 20μM in permeabilized cells. Furthermore, BT2 starts to uncouple at approximately 2-5μM in isolated mitochondria (**Figure 3**), which line up with BT2's half maximal effect as an inhibitor of the BCKDK (at approximately 4μM), as mentioned above.

BT2 decreases mitochondrial membrane potential and increases membrane proton conductance

It is well-known that proton-leak is dependent on mitochondrial membrane potential, as described in Figure 1. Next, we sought to validate the above results by determining mitochondrial membrane potential (MMP, $\Delta\psi$) in isolated mitochondria to characterize BT2 as a mitochondrial uncoupler. We used the cationic, red-orange dye TMRE (tetramethylrhodamine, ethyl ester), to measure fluorescence in quench mode to measure the MMP.[45] In this assay, TMRE is used at a

relatively high concentration and thus self-aggregates in the alkaline mitochondrial matrix, thereby diminishing and quenching the red-orange fluorescence (self-quench). During mitochondrial hyperpolarization with Oligomycin addition (ATP synthase inhibition), TMRE enters the even more alkaline mitochondria leading to further quenching of TMRE and thus decreasing the fluorescent signal. Finally, during mitochondrial depolarization with FCCP, TMRE unquenches and thus exits the mitochondrial, leading to an increase in fluorescent signal. In **Figure 5A**, the quenched fluorescence in isolated mitochondria is measured and compared to vehicle. As expected, the quenched fluorescence in Oligomycin-treated isolated mitochondria is significantly increased compared to vehicle-treated mitochondria. Quenched-fluorescence in FCCP-treated mitochondria is significantly decreased as predicted, hence the increase in fluorescence upon mitochondrial depolarization. These results validate our assay measuring MMP with TMRE in quench mode.

We then sought to determine whether BT2 potentially affects the MMP in isolated mitochondria using TMRE in quench mode. In line with our hypothesis, we expected BT2 to decrease MMP. Indeed, **Figure 5B** shows that BT2 significantly depolarizes the mitochondrial $\Delta\boldsymbol{\psi}$ at both 40μM and 80μM in mitochondria isolated from rat heart and liver, as shown by the large decrease in measured quenched fluorescence compared to vehicle-control. However, for comparison the effects of BT2 on mitochondrial depolarization are lesser than the FCCP-induced depolarization observed in **Figure 5A.** Insofar as the results show, BT2 seems to be a mild uncoupler in comparison to the highly potent, well-known uncoupler FCCP.

The hitherto evidence on increased State 4o respiration and decreased MMP provides a rationale for determining the direct effects of BT2 on proton current (I_H) amplitude (H^+ current amplitude, pA/pF) across the mitochondrial inner membrane. In brief review, recall that the MMP ($\Delta\boldsymbol{\psi}$) consists of the difference in electrical potential across the mitochondrial inner membrane. In addition, the concentration difference of protons across the mitochondria inner membrane is

the ΔpH. Therefore, the proton motive force (pmf, Δp in Volts) is equal to ΔpH + Δ $\boldsymbol{\psi}$. The Δp + H^+ current (Amps) can then be used to derive proton conductance across the MIM by applying Ohm's law.[46] To measure proton current, which gives us more information on proton leak, patch-clamp electrophysiological technique was therefore implemented in these next studies. This technique uses mitoplasts that are derived from heart mitochondria isolated from mice and stripped of the outer membrane and are used as a model to measure ion conductance by patch-clamp.[47,48] Isolated mitoplasts treated with 100μM BT2 led to an increase in H^+ current amplitude (pA/pF) across the mitochondrial inner membrane compared to vehicle-control (**Figure 5C, D**). This concentration was chosen based on presumption that BT2 is a mild uncoupler and therefore in alignment with the published literature on I_H in mitoplasts treated with the well-known mitochondrial uncouplers DNP, FCCP, and Bam15.[49] BT2 was calculated to require a much higher concentration to be able observe a signal in proton current. Once again, these results support the observation that BT2 is indeed a chemical uncoupler independent of its inhibitory effects on the BCKDK.

BT2 is a mild mitochondrial uncoupler that is less potent than DNP, Bam15, and FCCP

Next, we pursued our hypothesis that BT2 is a mitochondrial uncoupler and proceeded to confirm this by comparing its chemical uncoupling effects to the well-characterized mitochondrial uncouplers FCCP, Bam15, and DNP (**Figure 6A**). As shown, BT2 is lipophilic and has a functional group capable of reversibly dissociating a proton, similarly the well-known chemical uncouplers FCCP, Bam15, and DNP. **Figure 6B** shows the OCRs from isolated liver mitochondria given succinate and rotenone and ADP and treated with either 40μM BT2, 10μM DNP, or 50nM Bam15 compared to vehicle-control. As shown in these seahorse assay traces and the concentration response curves for State 4_o respiration (**Figure 6C**) and the potency of BT2 versus these well-known uncouplers based on the State 4_o respiration depicts BT2 indeed acting as a mitochondrial uncoupler slightly milder than DNP, and much less potent than FCCP and Bam15. Here we show

approximately 10^3-fold more BT2 is required to reach a similar level of proton leak-linked respiration as both FCCP or Bam15 (**Figure 6D**). These results illustrate that BT2 is about 4000 times weaker than FCCP, meaning that for every one unit of FCCP to uncouple, you need 4000 times more BT2 to give a similar result. Furthermore, Bam15 is approximately 1500 times more potent than BT2. Whereas BT2 is about five times weaker than DNP in comparison. Approximately five times the concentration of BT2 is needed to attain nearly the same level of increased State 4_o respiration as DNP in mitochondria isolated from both rat liver (**Figure 6D**) and heart (**Figure 6E**), hence BT2's mild uncoupling effect in isolated mitochondria.

Finally, we asked at which concentrations do we start to see the same uncoupling effects reflected on the changes in MMP in the other mitochondrial uncouplers as in BT2. Here, we once again used TMRE fluorescence in quench mode to measure MMP, an assay validated in **Figure 5**. **Figure 6F** shows the concentration of chemical uncouplers required to give roughly the same MMP as 80μM BT2, measured by quenched fluorescence compared to vehicle. The concentrations of each chemical uncoupler that results in a relatively equivalent $\Delta\psi$ as 80μM BT2 is 25 nM for FCCP, 50 nM for Bam15, and 20μM for DNP. Moreover, measuring the H^+ current amplitude (pA/pF) in isolated heart mitoplasts treated with 100μM BT2 cause a H^+ current that is 6-fold lower (2.52, n=5) than in mitoplasts treated with 100μM DNP (15.82, n=9).[49] These results confirm that BT2 undeniably uncouples 6 times milder than DNP, supporting the results in **Figure 5C and D**. Overall, these respiration and membrane potential measurements in isolated liver mitochondria characterize BT2 as a mild chemical uncoupler that 5-fold less potent than DNP and three orders of magnitude less potent than Bam15 and FCCP.

BT2 uncouples via AAC-dependent and AAC-independent mechanisms

In light of BT2's novel role as a mild mitochondrial uncoupler, we sought to determine whether BT2 uncouples via AAC-dependent and AAC-independent mechanisms. Given that chemical uncouplers induce proton conductance via the ADP/ATP Carrier (AAC) by binding to its

nucleotide translocation site, in addition to dissipating the proton gradient across the mitochondrial inner membrane via weak acid/anion cycling.[49] AAC is part of the solute carrier 25 (SLC25) family of mitochondrial anion carriers, a family which consists of approximately 50 members which include the mitochondrial uncoupling proteins (UCPs), the dicarboxylate carrier, the phosphate carrier, and the aspartate-glutamate carrier. AAC is one of the most abundant proteins in the IMM and there are four isoforms in humans, including *AAC1*, *AAC2*, *AAC3*, and *AAC4*. AAC is a mitochondrial carrier with two modes of transport. One mode consists of binding Mg^{2+} free ADP^{3-} at its single substate binding site (SBS) from the cytosolic side (c-state) and imports it into the matrix side (m-state) for the exchange of exporting ATP^{4-} from the mitochondrial matrix out into the cytosol. Additionally, this carrier protein uncouples mitochondria by increasing fatty acid (FA)-induced H^+ leak in a similar manner as the uncoupling protein 1 (UCP1).[50]

Previous studies have shown that this FA-induced uncoupled respiration can be diminished by the drug carboxyatractyloside (CATR).[51] Furthermore, mitochondrial uncouplers induce proton leak (I_H) through AAC dependent and independent mechanisms. The well characterized mitochondrial uncouplers bind at the translocation site and induce the binding and translocation (shuttling) of protons in a similar manner as FA-induced uncoupling.[49] This mitochondrial uncoupler-induced I_H can also be inhibited by CATR.

CATR, an exceedingly specific inhibitor of AAC, was therefore used in these studies to delineate BT2's mitochondrial uncoupling mechanism. We then sought to measure via a pharmacological strategy whether BT2 shuttles protons across the inner membrane and/or through AAC and thus decreasing mitochondrial membrane potential. Therefore, we asked how much of BT2's mitochondrial uncoupling effect on the respiration rates is CATR sensitive and how much is not. **Figure 7A-C** shows the OCRs of isolated liver mitochondria in the presence of Pyr/Mal or Succ/Rot. Isolated liver mitochondria were acutely treated with vehicle, 80μM BT2, 80μM BT2 with the addition of 5μM CATR (BT2+CATR), or 5μM CATR alone. The difference

between control BT2 and CATR + BT2 is reflective of the proportion of BT2 that is dependent on AAC, as CATR treatment results in BT2 partially uncoupling through AAC, shown by the decrease in State 4_o respiration rate in isolated mitochondria treated with 80μM BT2 and 5μM CATR compared to isolated mitochondria treated with 80μM BT2 alone (control BT2). These results are observed similarly with isolated liver mitochondria either in the presence of the substrate pyruvate/malate or succinate/rotenone (**Figure 7B**). However, Succ/Rot gives higher OCRs because it bypasses complex I and so there are two proton pumps working instead of three, therefore complex III works harder to maintain the MMP & thus results in higher respiratory rates. This phenomenon therefore shows that presence of Succ/Rot increases MMP, which leads to higher proton leak as expected, than in the presence of Pyr/Mal shown by the BT2-stimulated State 4_o respiration rates between the Succ/Rot and Pyr/Mal groups. BT2-stimulated State 4_o respiration rates are therefore both CATR-dependent and CAT-R independent (**Figure 7C**).

Moreover, because previous studies have demonstrated chemical uncouplers induce mitochondrial uncoupling via AAC by binding to the nucleotide translocation site, we therefore sought to determine via a genetic strategy whether BT2 is uncoupling mitochondria in C2C12 myoblasts with both *Slc25a4* (encoding AAC1) and *Slc25a5* (encoding AAC2) genetically deleted ('double-knockout' DKO)**.** In both intact C2C12 myoblasts (**Figure 7D-F**) and permeabilized C2C12 myoblasts (**Figure 7F**), mitochondrial uncoupling by BT2 was partially loss by knocking out AAC1 and AAC2, again showing that BT2 indeed uncouples mitochondria via AAC-dependent and AAC-independent mechanisms, similarly to other well-characterized chemical uncouplers.

The results obtained from both pharmacologic loss of AAC with CATR inhibition and genetic loss of AAC with the AAC DKO intact and permeabilize cells show that BT2 partially uncouples through AAC, which is consistent with the observation in previous studies showing well-characterized mitochondrial uncouplers working via the AAC. Bertholet *et al*. previously published that the mitochondrial uncouplers FCCP, Bam15, and DNP shuttle protons through

both weak acid/anion cycling and the AAC across the inner mitochondrial membrane.[49] Therefore, our results are consistent with these previous studies on well-characterized mitochondrial uncouplers and support our data illustrating that BT2 is indeed uncoupling via proton shuttling through the IMM and through AAC-dependent (or CAT-dependent) mechanisms, further confirming BT2 is a chemical uncoupler.

CHAPTER 4

PHYSIOLOGICAL ENDPOINTS IN CELLS ALTERED BY BT2 CAN BE EXPLAINED BY UNCOUPLING AND MIRRORED WITH DNP, BAM15, AND FCCP

Uncoupling with BT2 can reproduce hallmarks of BT2 associated with cardioprotection

Thus far, we have demonstrated evidence supporting BT2's mitochondrial uncoupling effects by observing and induction in H^+ current and an elevation in State 4_o respiration and proton leak-linked respiration in isolated mitochondria and intact cells, respectively. We now asked why would a mitochondrial uncoupler confer cardioprotection? A previous study by Minners *et al*. demonstrated that DNP pretreatment of an *ex vivo* model of heart failure protected the heart from ischemia/reperfusion injury. Indeed, the isolated rat heart was mounted on a Langendorff apparatus, pretreated with DNP for 5 minutes, a 35-minute ischemia was induced, and reperfusion was allowed for 120 minutes. Infarct size was significantly reduced in the DNP-treated isolated rat heart vs control. This study therefore shows that mitochondrial uncouplers can indeed confer cardioprotection. Furthermore, it has been well-documented the involvement of ROS production during ischemia/reperfusion injury. Korshunov *et al.* clearly demonstrated an attenuation in ROS production with treatment of a chemical uncoupler in isolated heart mitochondria offered succinate as a substrate. This study concluded that titration of a chemical uncoupler in mitochondria producing ROS through reverse-electron transport (RET) chain activity led to a decrease in MMP and thus with a concomitant decrease in H_2O_2 production, as expected.

Moreover, previous studies have shown that BT2 diminishes oxidative stress in cells. Additionally, studies with BT2 administration in *in vivo* preclinical models of heart failure show BT2 rescues cardiac function associated with oxidative stress and protects from ROS-associated I/R and M/I injury. However, these studies did not resolve whether the protective effects of BT2 emanate from BCKDK inhibition or other uncharacterized mechanisms.

Therefore, we sought to determine whether BT2's uncoupling effects directly lower rates of superoxide production. Furthermore, we asked whether BT2 replicates the effects chemical

uncouplers have on ROS production rates. Here, we used isolated heart mitochondria and first made a standard curve to detect known amount (pmol) of H_2O_2 efflux with Amplex Red by fluorescence. H_2O_2 efflux detection was measured to determine production of superoxide, since superoxide gets converted to H_2O_2 (**Figures 8A**). In parallel, isolated rat heart mitochondria were offered succinate to induce reverse-electron-transport (RET)-driven ROS production as a result of a high proton motive force and a highly reduced CoQ pool. Isolated heart mitochondria were then treated with either 80μM BT2, 20μM DNP, or 100nM FCCP and 1μM Antimycin A treatment was used as a control. BT2 was undoubtedly able to significantly reduce ROS production rates vs vehicle treated mitochondria (**Figure 8B**). Likewise, DNP and FCCP significantly decreased H_2O_2 efflux in isolated heart mitochondria, as expected of a chemical uncoupler, vs treatment with Antimycin A, which caused a significant increase in H_2O_2 efflux as expected (**Figure 8B**). These results therefore show that BT2 can attenuate ROS production via mitochondria uncoupling, indeed replicating the observed effects of mitochondrial chemical uncouplers have on rates of ROS production. This highly suggests that BT2 is likely conferring cardioprotection by reducing ROS production via mitochondrial uncoupling, independently of BCAA and BCKA metabolism.

Uncoupling mitochondria with BT2 can reproduce hallmarks of BT2 associated with protection from metabolic disease

We next sought to investigate why mitochondrial uncoupling with BT2 improve metabolic function. A study conducted by Shulman *et al*. showed that treating diabetic rats with the chemical uncoupler CRMP, a derivative of DNP, led to a reduction in the glucose tolerance test vs vehicle-treated diabetic rats. Furthermore, CRMP treatment caused a decrease of plasma triglycerides in diabetic rats vs vehicle treated diabetic rats, therefore demonstrating that a chemical uncoupler can indeed improve metabolic function *in vivo*. Moreover, a recent study by Flach *et al*. provided evidence demonstrating that treatment of diet-induced obese mice with BT2 caused a reduction in liver triglycerides and improvement in the oral glucose tolerance test (oGTT). These results

confirmed that indeed, BT2 improves metabolic function *in vivo*, mirroring the results found in treatment of CRMP in diabetic rats.

Furthermore, it is well established that chemical uncouplers increase energy expenditure by dissipating the mitochondrial membrane potential, thereby stimulating electron transport chain activity. This causes a shift in the energy balance toward nutrient oxidation and away from lipid synthesis and storage.[52,53] Chemical uncoupling by BT2 can therefore likely explain the quick effects of BT2 in various models of metabolic disease.

We therefore sought to determine whether BT2 can improve metabolic function via increasing energy expenditure and decreasing *de novo* lipogenesis (DNL) similarly to the chemical uncoupler DNP (**Figures 9**). Differentiated 3T3-L1 adipocytes were treated with 40μM BT2, 10μM DNP, or vehicle, 10 minutes prior to measurements. BT2 treatment induced an increase in basal and proton leak-linked respiration vs vehicle treatment (**Figures 9A, B**). Furthermore, these results phenocopied the results observed in DNP-treated differentiated 3T3-L1 adipocytes, where basal oxygen consumption rate was increased due to increased proton leak-linked respiration. Next, we further characterized BT2 as a chemical uncoupler by conducting stable isotope tracing with uniformly labeled $^{13}C_6$-glucose and GC/MS analysis in differentiated 3T3-L1 adipocytes and determined whether BT2 shared effects with DNP. Differentiated 3T3-L1 adipocytes were treated with 120μM BT2 or 40μM DNP for 72 hours in medium with very low serum. Results demonstrated BT2 significantly increased glucose-derived carbons into citrate and malate, mirroring the results observed with DNP treatment (**Figures 9C**). Additionally, the relative steady-state abundances of the TCA cycle metabolites citrate, α-ketoglutarate, succinate, fumarate, and malate were reduced with BT2 and DNP treatment, further illustrating the increase in metabolic rate and therefore energy expenditure via mitochondrial uncoupling (**Figures 9D**).

We then investigated the effects of BT2 on *de novo* lipogenesis (DNL) in differentiated 3T3-L1 adipocytes vs the chemical uncoupling effects of DNP on DNL. We reasoned that

increased chemical uncoupling would decrease lipid synthesis. Differentiated 3T3-L1 adipocytes were treated with 120μM BT2, 40μM DNP, or vehicle for 72 hours. Expression of several genes involved in DNL and fatty acid oxidation were then measured (**Figures 9E**). Results demonstrated both BT2 and DNP caused a significant reduction in the mRNA levels of expression of enzymes involved in DNL *Acly*, *Acaca,* and *Fasn*. In addition, gene expression of the transcriptional regulators of lipid synthesis *Srebpf1* and *Ppargc1a* were significantly reduced. Lastly, BT2 increased expression of the fatty acid oxidation gene *Cpt1a*, the gene that encodes for carnitine palmitoyltransferase-1a, which is rate-controlling for long-chain fatty acid oxidation. However, DNP treatment did not change gene expression levels of *Cpt1a*. Altogether, these results showed chemical uncoupling by BT2 reduces lipid synthesis.

To confirm the above results on BT2's effects on DNL, abundances of fatty acids were measured by GC/MS. Results showed that treatment with either 120μM BT2 or 40μM DNP for 72 hours in differentiated 3T2-L1 adipocytes led to the reduction in steady state abundance levels of myristate (14:0), palmitate (16:0), and stearate (18:0) (**Fig. 9F**). However, reduction in fatty acid abundance does not indicate whether there is less lipid synthesis or there is a reduction in fatty-acid oxidation. We therefore measured *de novo* lipogenesis by tracing differentiated 3T3-L1 adipocytes with $^{13}C_{6}$-glucose and quantifying the MPE of palmitate from $^{13}C_{6}$-glucose-derived carbons (**Fig. 9G**)**.** Results showed that BT2 reduced incorporation of $^{13}C_{6}$-glucose-derived carbons into newly synthesized palmitate, as shown by the reduction in MPE of palmitate from $^{13}C_{6}$-glucose. These results suggest that BT2 indeed decreases lipid synthesis. Similarly, DNP treatment led to a reduction in incorporation of $^{13}C_{6}$-glucose into palmitate (**Fig. 9G**)**.** Unfortunately, measuring FA oxidation with ^{13}C-palmitate was not amenable because, given that albumin binds fatty acids and would have therefore interfered with such assay. Finally, the approximate quantitative rate of *de novo* palmitate synthesis was measured by applying the isotopomer spectral analysis (ISA) to model the rate of *de novo* palmitate synthesis [g(t)

parameter] (**Fig. 9H**) and contribution of glucose-derived carbons to the lipogenic acetyl CoA pool ('D' parameter) (**Fig. 9I**). Results demonstrated that both BT2 and DNP caused a decrease in the estimated rate of DNL (**Fig. 9H**). However, no changes were observed in the 'D' parameter (**Fig. 9I and Table 1**). Overall, respiratory rate, gene expression, and mass spectrometry data demonstrate that BT2 indeed induces energy expenditure and reduces *de novo* lipogenesis via mitochondrial uncoupling similarly to DNP, providing support for the observed improved metabolic function in *in vivo* models of metabolic disease.

Using stable isotope tracing to confirm BT2s effects on BCAA oxidation & glucose oxidation in C2C12 myoblasts, HepG2 hepatocytes, and differentiated 3T3-L1 adipocytes

Finally, we sought to confirm the increase in glucose-derived carbons into TCA cycle metabolites with BT2 treatment in C2C12 myoblasts and HepG2 hepatocytes, in addition to differentiated 3T3-L1 adipocytes, in addition to BCAA oxidation using ^{13}C-leucine**. Figure 10** shows that there is a small percentage of BCAA oxidation in C2C12 myoblasts and HepG2 hepatocytes as shown by the mole percent enrichment (MPE) from ^{13}C-leucine in citrate and succinate (**Fig. 10A**), compared to BCAA oxidation in differentiated 3T3-L1 adipocytes where these cells had higher rates of leucine oxidation. C2C12 myoblasts are already known to oxidize very little BCAAs. Furthermore, C2C12 myoblasts and HepG2 hepatocytes show higher rates of glucose oxidation, as demonstrated by larger MPEs from $^{13}C_6$-glucose (**Fig. 10B**). Upon treatment with 80μM BT2, an increase in leucine-derived carbons into citrate and succinate in differentiated 3T3-L1 adipocytes was observed (**Figure 10A**). Furthermore, BT2 increases glucose-derived carbon incorporation into citrate and succinate in differentiated 3T3-L1 adipocytes and C2C12 cells treated with 80μM BT2, further demonstrating that BT2 is increasing energy expenditure via mitochondrial uncoupling.

The evidence elucidated in these studies reveal the proposed mechanism in **Figure 11** by which BT2 is likely conferring protection from cardiovascular and metabolic disease via mitochondrial uncoupling.

CHAPTER 5

CONCLUSIONS AND DISCUSSION

In these studies, we provide evidence on a novel mechanism by which the BCKDK inhibitor BT2 is likely conferring protection from cardiometabolic disease via mitochondrial uncoupling. The data on respiration, mitochondrial membrane potential, and proton conductance illustrate BT2 uncouples mitochondria and therefore elucidate BT2 is also a chemical uncoupler, independent of its inhibitory effects on the BCKDK. Moreover, we demonstrate that chemical uncoupling by BT2 reduces ROS production and decreases *de novo* lipogenesis, likely explaining its role in cardioprotection and alleviating metabolic disease independently of BCAA metabolism.

Mitochondrial uncouplers reduce ROS production by lowering membrane potential

Mechanistically, it has been well documented that mitochondrial uncoupling leads to reduced mitochondrial membrane potential (MMP). Moreover, reduced MMP results in a decrease in reactive oxygen species (ROS) production. Increase of ROS production occurs when there is elevated mitochondrial membrane potential and induction of reverse-electron-transport (RET) chain activity. RET activity occurs when the proton motive force (pmf) is at its maximum, there is little to no ATP synthesis, and reduced CoQ levels are high. A significantly high pmf thermodynamically pushes elevated levels electrons to reduce ubiquinone (Q) to ubiquinol (QH_2) into complex I (CI), thereby reducing NAD^+ to NADH at the FMN site. Elevated NADH/NAD^+ ratio and highly reduced FMN causes the production of superoxide. This can occur in the case where there are high levels of succinate and therefore succinate becomes the source of electrons used to drive CI in reverse and produce ROS species.[54]

As mentioned above, earlier studies by Korshunov *et al*. showed H_2O_2 (produced from superoxide) production as a function of MMP, where H_2O_2 generation was increased with increasing mitochondrial membrane potential. And furthermore, titration of the uncoupler SF6847 in isolated heart mitochondria offered succinate indeed decreased MMP that resulted in lowering ROS production.[55] More specifically, lowering the mitochondrial MMP by chemical uncouplers

leads to the oxidation of the $NADH/NAD^+$ and QH_2/Q pools and thus limits and lowers the production of superoxide.[55,54] It is well-known that there is an increase in ROS production during myocardial oxidative stress. Chouchani *et al*. showed succinate-induced ROS production increased during 15-minute reperfusion, after a 30 minute ischemia, in an I/R mouse model of HF, as shown by an increase in MitoP to MitoB ratio in heart tissue at risk.[56] Indeed, Nickel *et al*. showed elevation of 8-OHdG staining in left ventricular myocardium of C57BL/6N mice subjected to TAC surgery, another mouse model of HF, indicating intracellular ROS formation.[57] Altogether, these studies illustrate that mild uncoupling of mitochondria can therefore help reduce ROS production during oxidative stress in ischemia/reperfusion injury and protect the heart from disease.

Mitochondrial Uncouplers Can Be Cardioprotective (Heart Failure)

It is well-known that mitochondrial ROS production plays a crucial role in the pathogenesis of cardiovascular disease.[58,59] Therefore, at the physiological level, decreased ROS production by mitochondrial uncouplers can explain cardioprotection. Former studies have alluded to chemical uncouplers decreasing ROS production and have shown that attenuation of ROS is cardioprotective. Brennan *et al*. pretreated Langendorff-perfused rat hearts, an *ex-vivo* model of HF, with 100nM FCCP and induced a 25minute-global zero-flow ischemia and 40 minutes of reperfusion.[60] Their results showed FCCP-treated hearts had a significant improvement in left ventricular developed pressure (LVDP) recovery vs control hearts. In addition, treatment with 300 nM FCCP caused mitochondrial depolarization in myocytes, as shown by a reduction in TMRM fluorescence vs baseline. Moreover, a decrease in NADH fluorescence in myocytes treated with 300nM FCCP or 100nM FCCP was observed, as expected of a mitochondrial uncoupler.[61]

Furthermore, Minners *et al*. pretreated Langendorff-perfused rat hearts with DNP and subjected the isolated mounted heart to an ischemia by occlusion for 25 minutes and reperfusion for 120 minutes.[62] Their data exhibited a significant decrease in infarct size in the DNP pretreated isolated rat hearts vs control isolated rat hearts. These studies in an *ex-vivo* model of HF and

treatment with the mitochondrial uncouplers FCCP or DNP further support our evidence that mitochondrial uncouplers can indeed be cardioprotective. It is noteworthy to mention that heterologous expression of UCP1 in the mouse heart protects from ischemic injury and attenuates markers of oxidative stress.[63] Therefore, all these studies illustrate how mitochondrial uncouplers can protect from ischemia damage in the failing heart by reducing production of ROS.

Lastly, regarding ROS production, chemical uncouplers can indirectly reduce ROS production by blocking the opening of the permeability transition pore (PTP) via lowering of the mitochondrial membrane potential. The mitochondrial membrane potential gives rise to the driving force that is used for calcium uptake. During pathological Ca^{2+} overload in the mitochondrial matrix, swelling of the mitochondria results thereby inducing opening of the PTP. Therefore, uncoupling mitochondria can prevent opening of PTP and diminish ischemic injury.[64,65,66]

Mitochondrial Uncouplers Can Protect from Metabolic Disease (Diabetes and Obesity)

There are more recent studies illustrating that mitochondrial uncouplers can protect from metabolic disease. Shulman *et al*. designed a derivative of DNP named CRMP (controlled-release mitochondrial protonophore) and treated diabetic rats with this chemical uncoupler or with vehicle-control.[67] Results in CRMP-treated diabetic rats subjected to intraperitoneal glucose tolerance test showed improved fasting plasma glucose and insulin concentrations with CRMP treatment, indicating improved glucose tolerance, vs the vehicle-treated diabetic rats. Another study showing that mitochondrial uncouplers can protect from metabolic disease comes from Alexopoulos *et al*. where mice fed a Western Diet (WD) were treated with the chemical uncoupler Bam15 for eight days.[68] The intraperitoneal glucose tolerance test showed Bam15 prevented glucose intolerance in mice fed a WD vs control mice. In addition to improved glucose intolerance, Bam15 was able to reduce accumulation of triglycerides in the liver of mice fed a WD vs mice fed a WD alone, and these triglyceride levels were close to hepatic TG levels in mice fed a chow diet. This data suggested that Bam15 increased hepatic lipid oxidation. These encompassing studies illustrate

that increased in energy expenditure via chemical uncoupling can explain the protective effects in preclinical animal models of metabolic disease.

There are several reports demonstrating that BT2 is protective from glucose tolerance, insulin insensitivity, elevated triglycerides, and hepatic inflammation, reflecting what was observed with the chemical uncouplers DNP, CRMP, and Bam15.[39,69,40,67,68]. Although a study showed BT2 does not change body weight of animals, however, BT2 did lightly reduced the respiratory exchange ratio in Zucker fatty rats, further confirming the mild uncoupling properties of BT2 that we observed in our studies.[39] Furthermore, our findings that BT2 altered expression of genes related to lipid metabolism similarly to DNP suggests chemical uncoupling could explain why BT2 treatment in Zucker fatty rats blocked phosphorylation of acetyl CoA carboxylase.[39] These observations were not present when PP2Cm was overexpressed in previous studies. Moreover, studies showing BT2 elicits a rapid euglycemic effect in glucose clamp studies less than an hour after administration are more consistent with the acute effects of DNP on energy expenditure and not with modulation of BCAA metabolism.[40],[67] Collectively, these studies substantiate our findings that mitochondrial uncoupling likely explains the protective effects of BT2 in preclinical models of cardiovascular and metabolic disease.

Chemical Uncoupling is likely an *in vivo* mechanism of BT2

A final aspect that we considered was whether the characterization of BT2 as a chemical uncoupler *in vitro* would explain its *in vivo* mechanism in alleviated cardiometabolic disease. Our data demonstrates that BT2 uncouples mitochondria at concentrations as low as 2.5μM reach the concentrations used *in vivo*, which are at least at the half-maximal inhibitory concentration for BCKDK (IC_{50}=3-4μM) or higher.[37] The peak circulating concentrations of BT2 in the plasma are approximately 1.0μM for 40 mg/kg and 1.8 mM for 120mg/kg.[70] Plasma protein binding measurements show BT2 is 99.3% bound, which indicates that maximal, free BT2 concentrations are at single digit micromolar concentrations or higher.[37] Additionally, pharmacokinetic (PK) data

suggests that BT2 has a longer half-life in plasma vs DNP, where its clearance profile is like CRMP.[67,70] The PK data supports that mitochondrial uncoupling can indeed be an *in vivo* mechanism by which BT2 is conferring protection from cardiometabolic disease.

A recent report conducted structure activity relationship studies on BT2 and derivatives of BT2.[71] In this study, three small-molecule BCKDK inhibitors were found to have higher potency in inhibiting the BCKDK than BT2. One of them, PF-07208254, strongly resembled BT2 in improving heart function and metabolic function in pre-clinical animal models. The efficacy of this new compound was associated with reduced levels of BCAAs and BCKAs, where smaller concentrations of it were used to reach therapeutic efficacy. However, the other two compounds, PF-07238025 PF-07247685, did not improve metabolism and were not protective like BT2 and PF-07208254, even though these two small molecules were much more potent at inhibiting the BCKDK than BT2 and PF-07208254. These observations from this study may indeed substantiate our hypothesis that the therapeutic effects of BT2 are not from BCKDK inhibition but rather via an alternative mechanism. Moreover, the PF-07208254 was more structurally similar to BT2 and retained its lipophilic weak acid properties as BT2, indicating that the protective effect are likely due to mitochondrial uncoupling.

Lastly, it is possible that BT2 may have other off-target effects contributing to its effects observed both *in vivo and in vitro*. A recent study showed structural resemblance in angiotensin ll type 1 receptor blockers (ARBs) and BT2, which may explain BT2's effects on blood pressure upon *Bckdk* deletion.[72,41] Another possible off-target may be inhibition on the mitochondrial pyruvate carrier (MPC), other dehydrogenases and transporters. BT2 was designed as a branched-chain 2 oxoacid analog and previous studies show that BCKAs can inhibit the MPC. Inhibition of pyruvate oxidation may explain why in our studies BT2 induces expression of *Cpt1* in differentiated 3T3-L1 adipocytes, whereas DNP did not.[73] Moreover, it can explain our data showing that acute treatment at high concentrations of BT2, permeabilized HepG2 hepatocytes and C2C12 myoblasts show a significant reduction in State 3 respiratory rates. However, our

stable isotope data showed increased relative incorporation of glucose into TCA cycle metabolites and steady state abundances were decreased, consistent with an increased metabolic rate when cells were offered labeled glucose.

The BCKDK inhibitor BT2 is a mitochondrial uncoupler, likely explaining its protective effects in cardiovascular and metabolic disease

In summary, recent studies show that knocking-out the BCKDK specifically in the heart or skeletal muscle and knocking-down the BCKDK in the liver do not protect from heart failure and metabolic disease, respectively. These studies strongly indicate that BT2 is indeed protecting from cardiovascular and metabolic disease via an alternative mechanism. The evidence provided in this study prove that the BCKDK inhibitor BT2 is a mitochondrial uncoupler, independent of its inhibitor effects on the BCKDK. We demonstrated in a reductionist system that BT2 induces a proton-leak, depolarizes mitochondria, and increases proton conductance in isolated mitochondria and mitochondrial mitoplasts, respectively. BT2 exhibited mild mitochondrial uncoupling compared to the chemical uncouplers DNP, Bam15, and FCCP. Furthermore, induced proton-leak and mitochondrial depolarization with BT2 was replicated in intact NRVMs and iCell adult cardiomyocytes. Functional assays show that BT2's uncoupling effects reduces mitochondrial ROS production in isolated rat heart mitochondria similarly to the well-established chemical uncouplers DNP and FCCP. Moreover, BT2 enhances d*e novo lipogenesis* and likely diminishes fatty acid oxidation. The evidence presented here therefore reveal the mechanism by which BT2 is conferring protection in preclinical models of heart failure and metabolic disease is likely via mitochondrial uncoupling.

SCHEMES

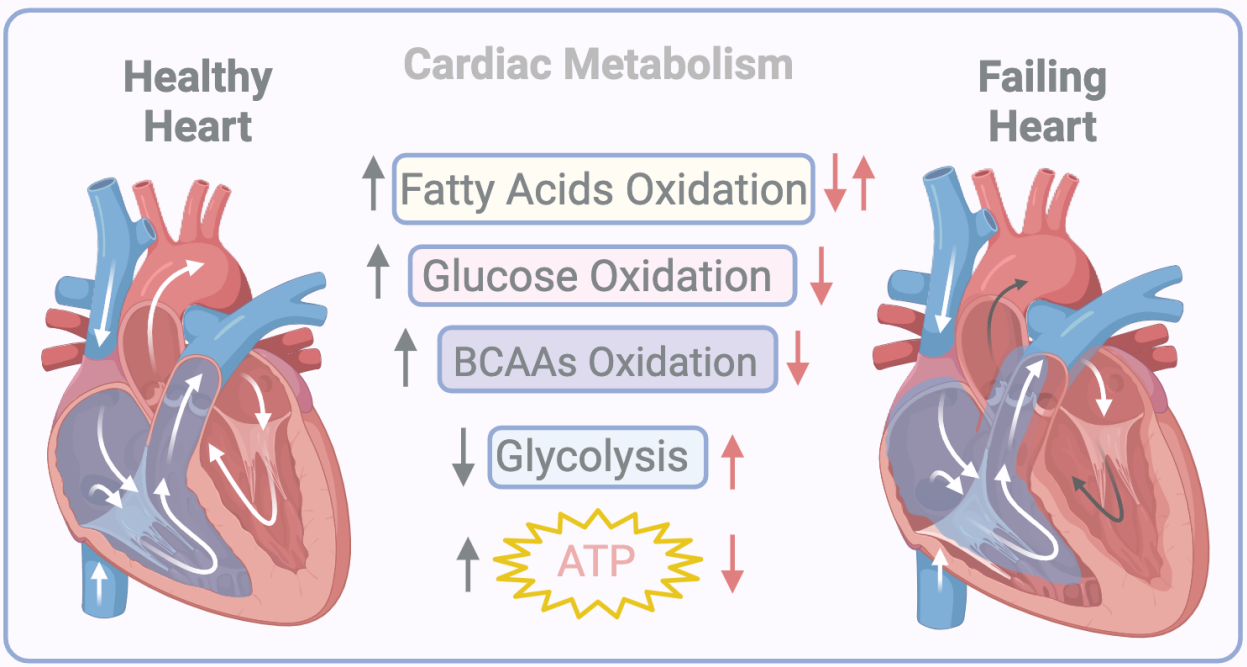

Scheme 1: Healthy Heart vs. Failing Heart

Physiology of the healthy heart vs. the failing heart where there is a decrease in cardiac output in heart failure, as indicated inside the failing heart by the black arrows vs. the white arrows in the healthy heart. Changes in cardiac metabolism in the failing heart vs the healthy heart is indicated by the red arrows vs the grey arrows. Fatty acid oxidation (FAO) can be decreased or increased; however, it is more commonly decreased in the failing heart. Mitochondrial glucose oxidation is decreased in the failing heart, while glycolysis is elevated. BCAA oxidation is reduced in heart failure.

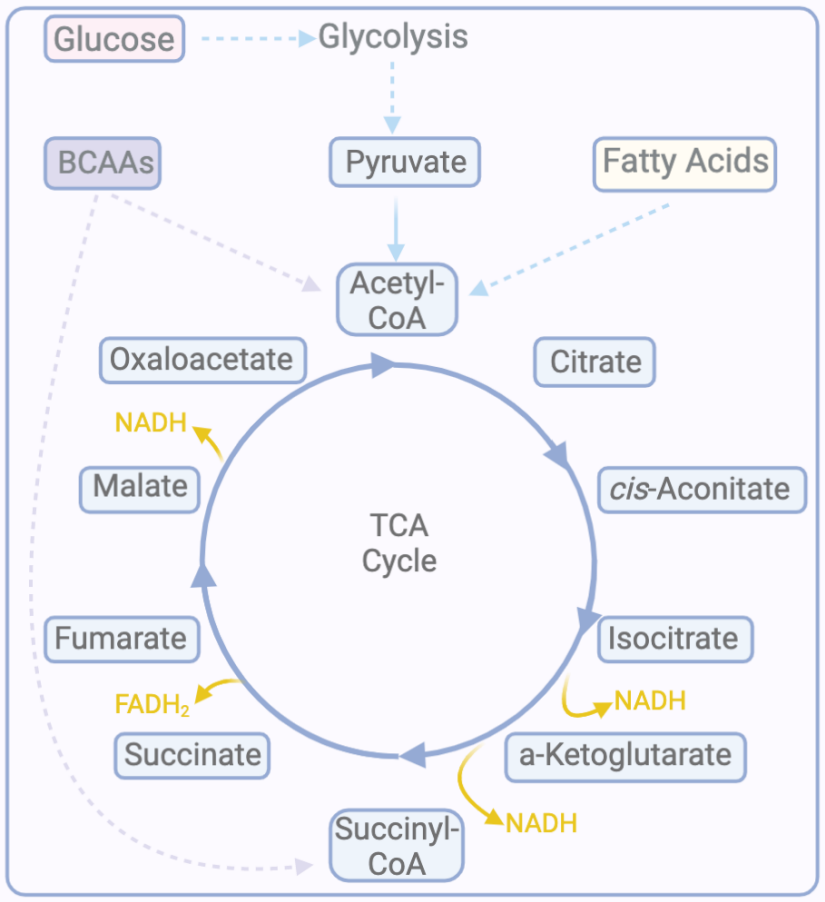

Scheme 2: The Tricarboxylic Acid Cycle

Glucose, fatty acid (FA), and branched-chain amino acid (BCAA) oxidation all converge at acetyl-CoA. Acetyl-CoA is taken through the tricarboxylic acid cycle (TCA), while making various intermediary metabolites. NADH and $FADH_2$ are produced, where they are then fed into the electron-transport-chain (ETC) for further harvesting of electrons.

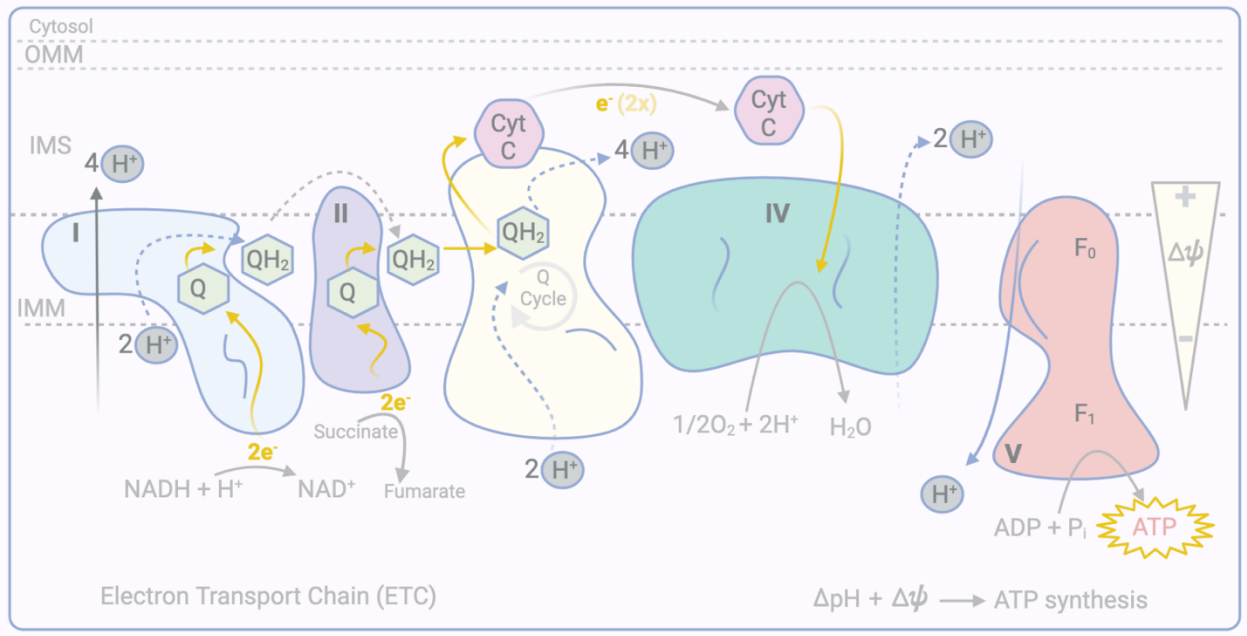

Scheme 3: The Electron-Transport-Chain (ETC)

The electron-transport-chain begins at complex I where it harvests electrons from NADH produce after fuel breakdown in the TCA cycle. Electrons are passed to the FMN site and through the 7 Fe-S centers to Q, thus making QH_2. Harvesting of electrons and H^+ pumping to the IMS creates a proton motive force (pmf) that is used to drive the synthesis of ATP. Cytochrome C donates electrons to the ultimate electron acceptor, O_2. ETC, electron-transport-chain; I-IV, V, ATP synthase, electron-transport-chain complexes; e^-, electron; OMM, outer-mitochondrial-membrane; IMS, intermembrane space; IMM, inner-mitochondrial-membrane; H^+, protons; Q, ubiquinone; QH_2, ubiquinol; Cyt C, cytochrome C; $\Delta\Psi$, mitochondrial membrane potential; ΔpH, pH; O_2, oxygen.

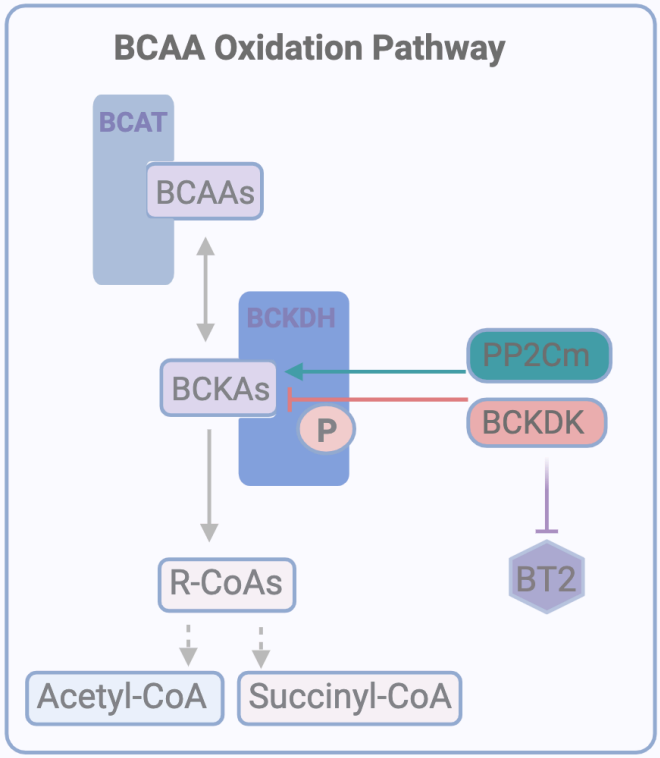

Scheme 4: Branched-chain Amino Acid (BCAA) Oxidation Pathway

Branched-chain amino acids (BCAAs) consist of leucine, isoleucine, and valine, and are first transaminated by the mitochondrial branched-chain amino acid transaminase (BCAT2) into their respective branched-chain α-ketoacids (BCKAs). BCKAs are then decarboxylated by the branched-chain α-ketoacid dehydrogenase (BCKDH), thus producing the respective R-chain CoAs, which are further catabolized by a series of catabolic reactions that eventually leads to the production of acetyl-CoA and succinyl-CoA. The protein phosphatase 2Cm (PP2Cm) activates BCKDH by dephosphorylation and the branched-chain α-ketoacid dehydrogenase kinase (BCKDK) deactivates BCKDH by phosphorylation. BT2 is an allosteric inhibitor of BCKDK.

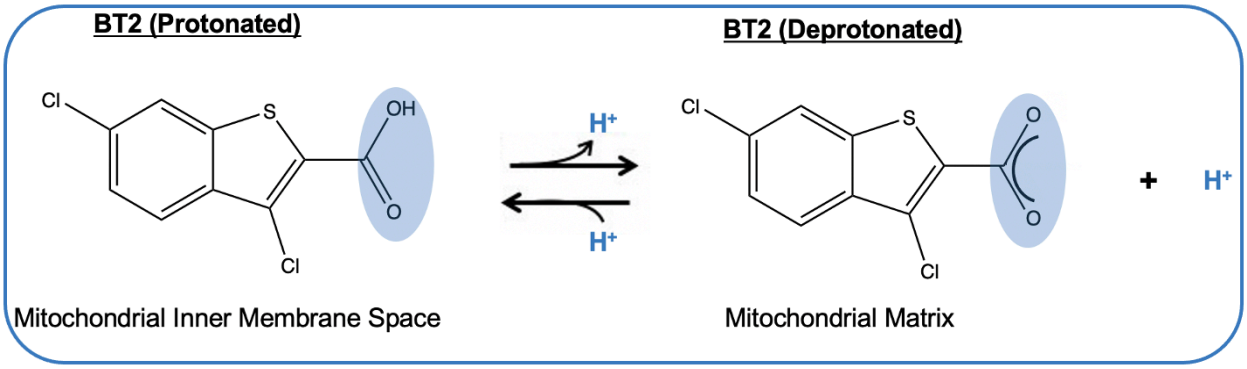

Scheme 5: Hypothesis-The BCKDK inhibitor BT2 is a mitochondrial uncoupler

The BCKDK inhibitor BT2 is a lipophilic weak acid that has a functional group that can reversibly bind a proton. Thus, BT2 can cycle and shuttle protons into the mitochondrial matrix thereby consuming the mitochondrial membrane potential independently of ATP synthesis and uncoupling mitochondria.

FIGURES

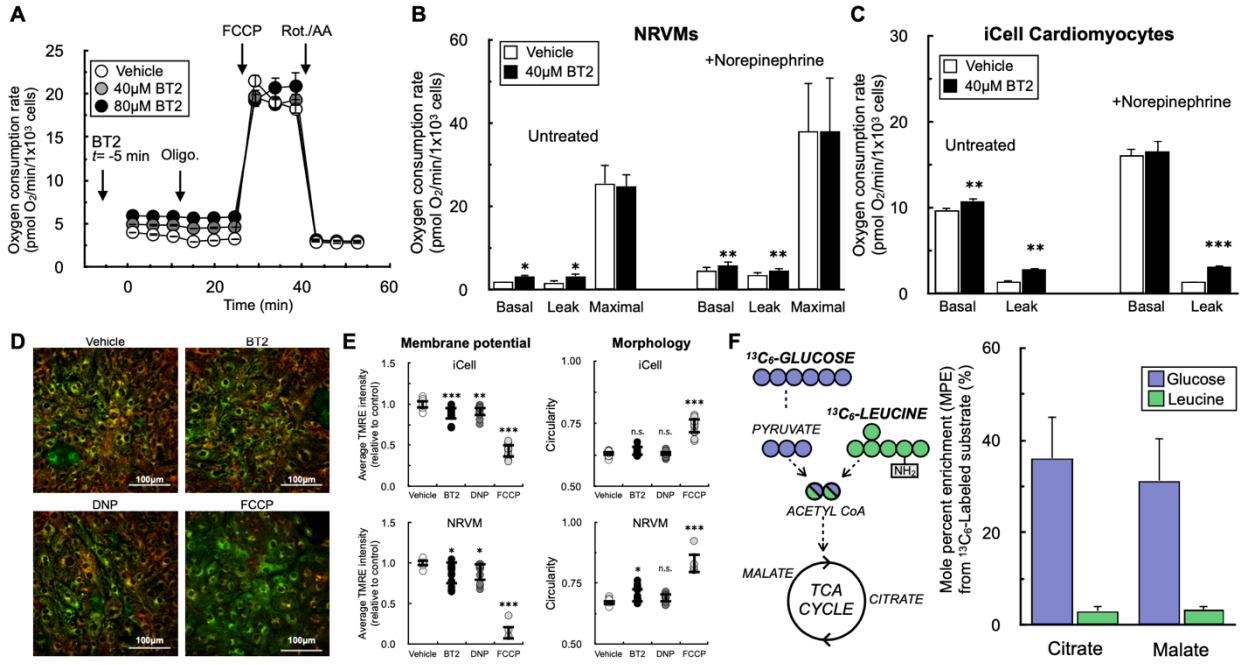

Figure 1: The BCKDK inhibitor BT2 uncouples mitochondria in intact rat and human cardiomyocytes

(A) Representative oxygen consumption rates trace of neonatal rat ventricular myocytes (NRVMs) treated with 40μM BT2, 80μM BT2, or vehicle (DMSO) 5 min prior to conducting measurements. 40μM and 80μM BT2 were chosen as concentrations because they are 10-fold above the EC50 (40μM) or previously used in the literature (80μM) (n=10 technical replicates from a single experiment). (B) Collated oxygen consumption rates of basal, proton-leak linked, and maximal respiration in NRVMs offered 40μM BT2 with or without 1μM norepinephrine. (n=4 biological replicates). (C) Collated oxygen consumption rates of basal, proton-leak linked, and maximal respiration for human iPSC-derived iCell cardiomyocytes treated with 40μM BT2 with or without 1μM norepinephrine as in (B). (n=4 biological replicates). (D) Representative images for iCell cardiomyocytes treated for 30-45 min. with 80μM BT2, 10μM DNP, 1μM FCCP, or vehicle control. (E) (Left) Average TMRE intensity relative to vehicle control for treatments as in (D) with iCell

cardiomyocytes (top) and NRVMs (bottom). (Right) Circularity as a measure of mitochondrial morphology for treatments as in (D) with iCell cardiomyocytes (top) and NRVMs (bottom). (n=7-15 technical replicates collated from n=3 biological replicates for each cell type). (F) (Left) Simplified scheme of uniformly labeled $^{13}C_6$-glucose or $^{13}C_6$-leucine enriching TCA cycle intermediates. (Right) Mole percent enrichment (M.P.E.) of TCA cycle intermediates citrate and malate in NRVMs offered $^{13}C_6$-glucose or $^{13}C_6$-leucine. (n=3 biological replicates). All data are mean ± S.E.M. Statistical analysis was conducted with a pairwise Student's t test [(B) and (C)] or ANOVA followed by Dunnett's post-hoc multiple comparisons tests [(E)] as appropriate. *, $p < 0.05$; **, $p < 0.01$; ***, $p < 0.001$.

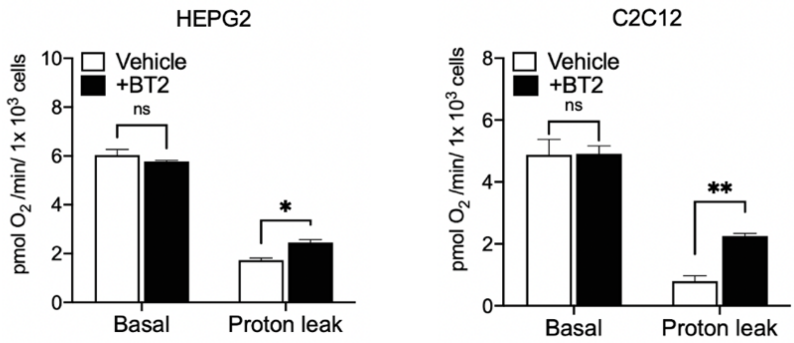

Figure 2: BT2 increases proton leak-linked respiration in mitochondria of intact HepG2 and C2C12 cells.

Oxygen consumption rates of basal respiration and proton leak-linked respiration of intact HepG2 hepatocytes (left, n=4 biological replicates) and intact C2C12 myocytes (right, n=4 biological replicates) offered glucose, pyruvate, and glutamine and treated with vehicle or 80 μM BT2 5 minutes prior to measurements. Each experiment consisted of n=4 or n=5 technical replicates. Statistical analysis was conducted with a pairwise Student's t test or ANOVA followed by Dunnett's post-hoc multiple comparisons tests as appropriate. *, $p < 0.05$; **, $p < 0.01$.

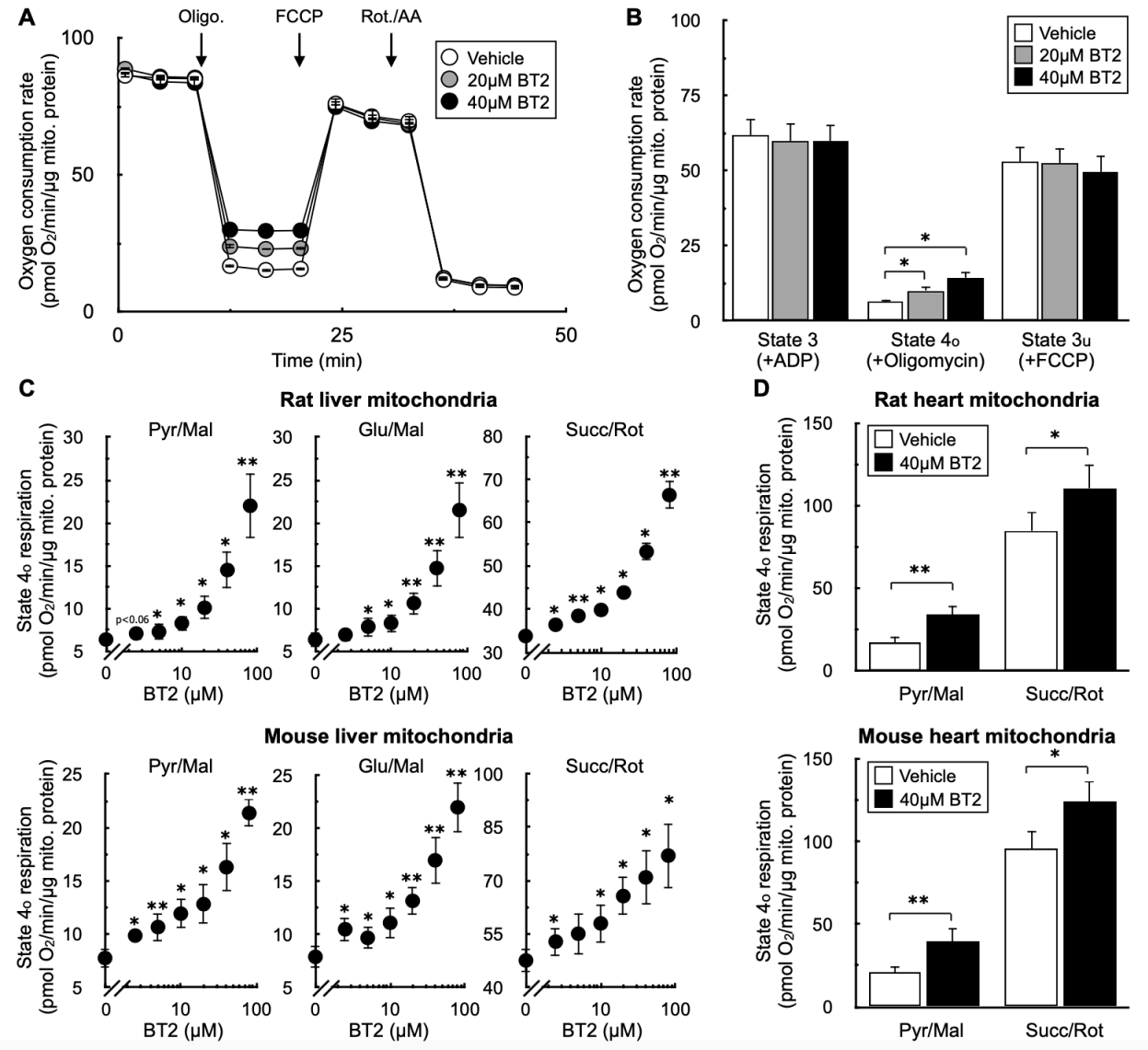

Figure 3: The BCKDK inhibitor BT2 increases State 4$_o$ respiration in isolated mitochondria

(A) Representative oxygen consumption rates (OCR) of isolated rat liver mitochondria offered pyruvate, malate, and ADP and acutely treated with 20 μM BT2, or 40 μM BT2 prior to initial measurements. Respiration was measured in response to sequential injections of oligomycin, FCCP, and rotenone with antimycin A. (n=5 technical replicates from a single experiment. (B) Collated oxygen consumption rate paraments for isolated liver mitochondria as in (A). (n=4 biological replicates). (C) State 4$_o$ respiration in mitochondria isolated from rat liver (top) or mouse liver (bottom). Experiments conducted as in (A) with pyruvate/malate (left), glutamate/malate

(middle), or succinate/rotenone (right) and treated with increasing amounts of BT2, [BT2] = 2.5, 5, 10, 20, 40, and 80μM. (n=4 biological replicates). (D) State 4_o respiration in isolated mitochondria from rat heart (top) or mouse heart (bottom) acutely treated with either vehicle control (DMSO) or 40μM BT2, 5 min prior to initial measurements. Experiments conducted in (A) with either pyruvate/malate (left), or succinate/rotenone (right), offered as respiratory substrates. OCRs were measured with the Agilent XF96 Analyzer. All data are mean ± S.E.M. Statistical analysis was conducted with a pairwise Student's t test [(D)] or ANOVA followed by Dunnett's post-hoc multiple comparisons tests [(B) and (C)] as appropriate. *, $p < 0.05$; **, $p < 0.01$.

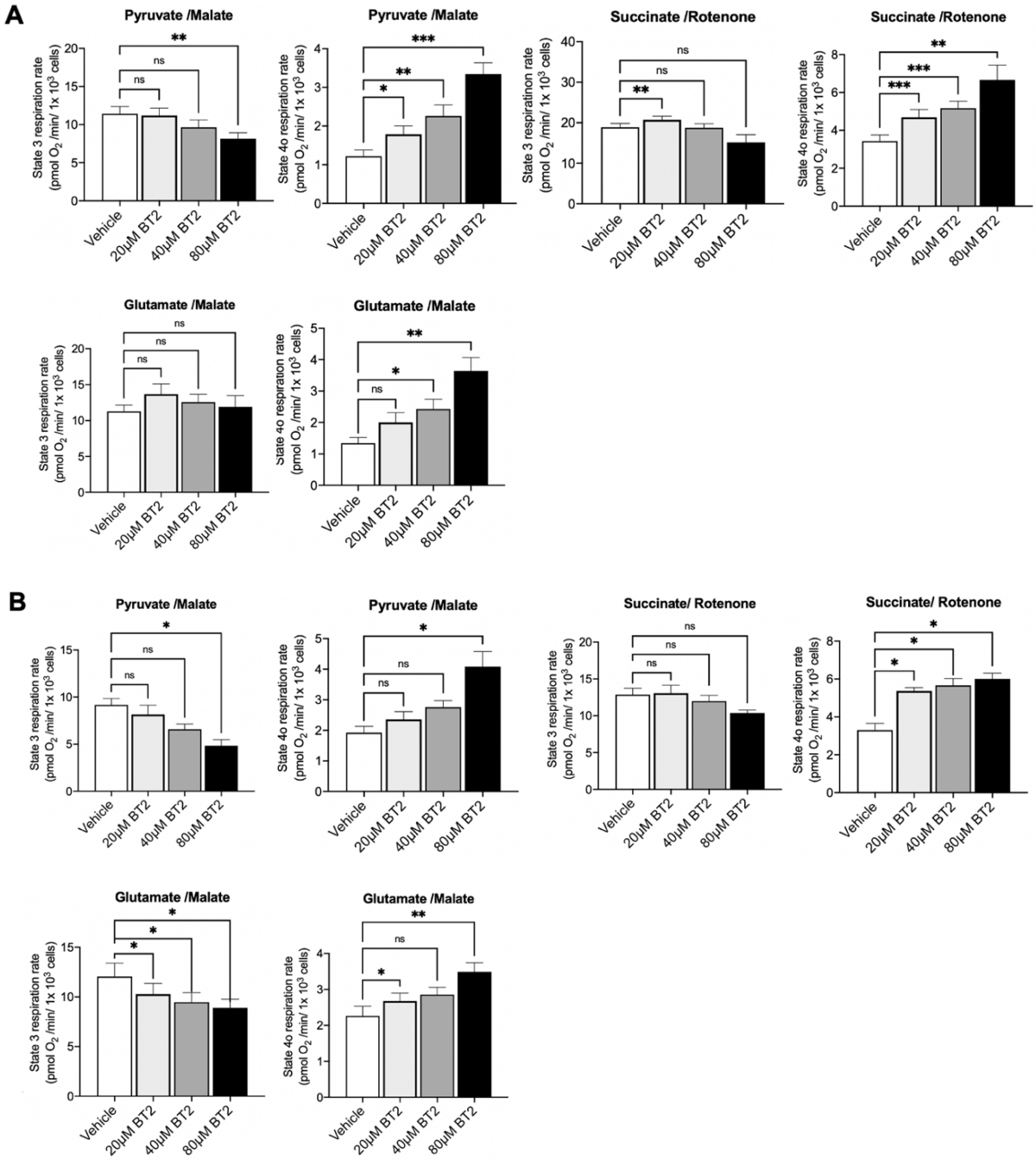

Figure 4: BT2 uncouples in permeabilized HepG2 hepatocytes and permeabilized C2C12 myoblasts

(A) State 3 and State 4_o oxygen consumption rates of permeabilized HepG2 cells treated acutely with vehicle, 20, 40, or 80 μM BT2 5 minutes prior to measurements and offered pyruvate/malate, succinate/rotenone, or glutamate/malate (n=4 biological replicates each). (B) State 3 and State 4_o respiration rates of permeabilized C2C12 myoblasts treated acutely with vehicle, 20, 40, or 80

μM BT2 5 minutes prior to measurements and offered pyruvate/malate (n=5 biological replicates), succinate/rotenone (n=5 biological replicates), or glutamate/malate (n=4 biological replicates). Statistical analysis was conducted with a pairwise Student's t test or ANOVA followed by Dunnett's post-hoc multiple comparisons tests as appropriate. *, $p < 0.05$; **, $p < 0.01$, $p < 0.01$; ***.

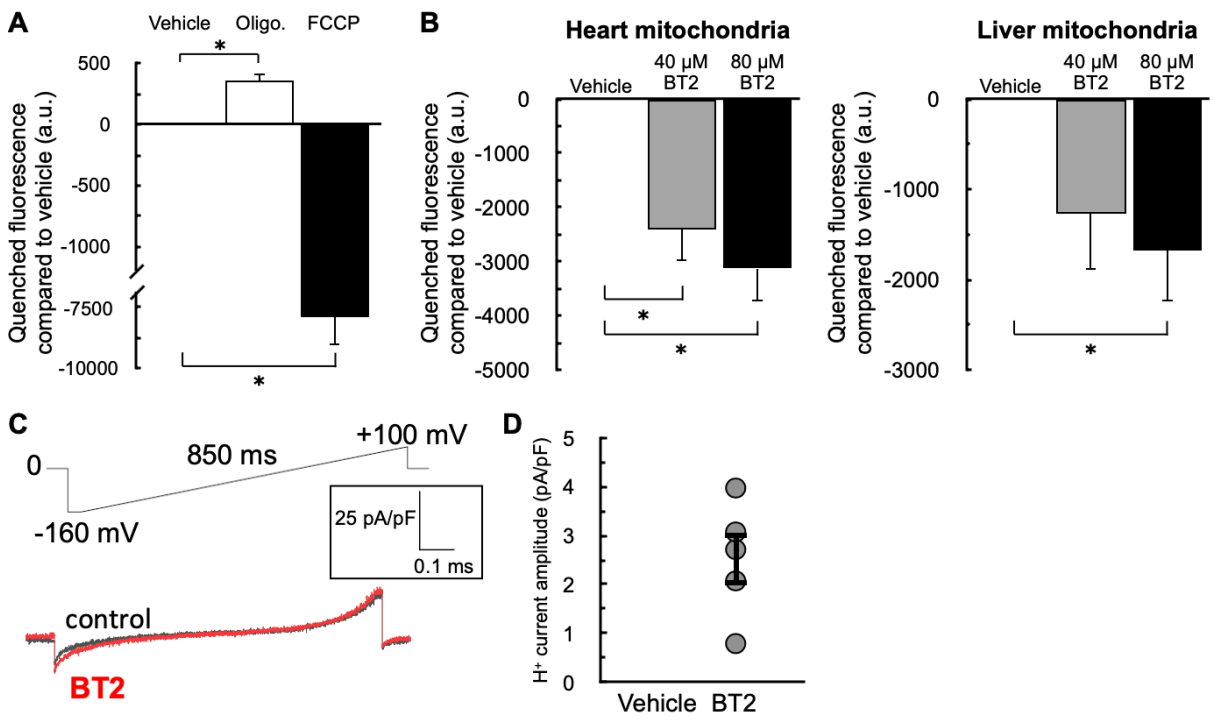

Figure 5: BT2 decreases mitochondrial membrane potential in isolated mitochondria and increases proton conductance across the mitochondrial inner membrane

(A) Quenched fluorescence of TMRE in isolated rat liver mitochondria offered succinate, rotenone, and ADP as described in the Materials and Methods. Mitochondria were offered oligomycin (1μg/mg mitochondrial protein) or FCCP (1μM) 5 min prior to measurements as controls to demonstrate the signal responds appropriately to known effector compounds. (n=3 biological replicates). (B) Quenched TMRE fluorescence as in (A) in response to 40 μM BT2, 80 μM BT2, or vehicle controls in isolated rat heart (left) or rat liver (right) mitochondria. (n=4 biological replicates). (C) Representative current induced by 100 μM BT2 in heart mitoplasts. (D) Current densities at -160 mV from (C). (n=5) All data are mean ± S.E.M. Statistical analysis was conducted with ANOVA followed by Dunnett's post-hoc multiple comparisons tests. *, $p < 0.05$.

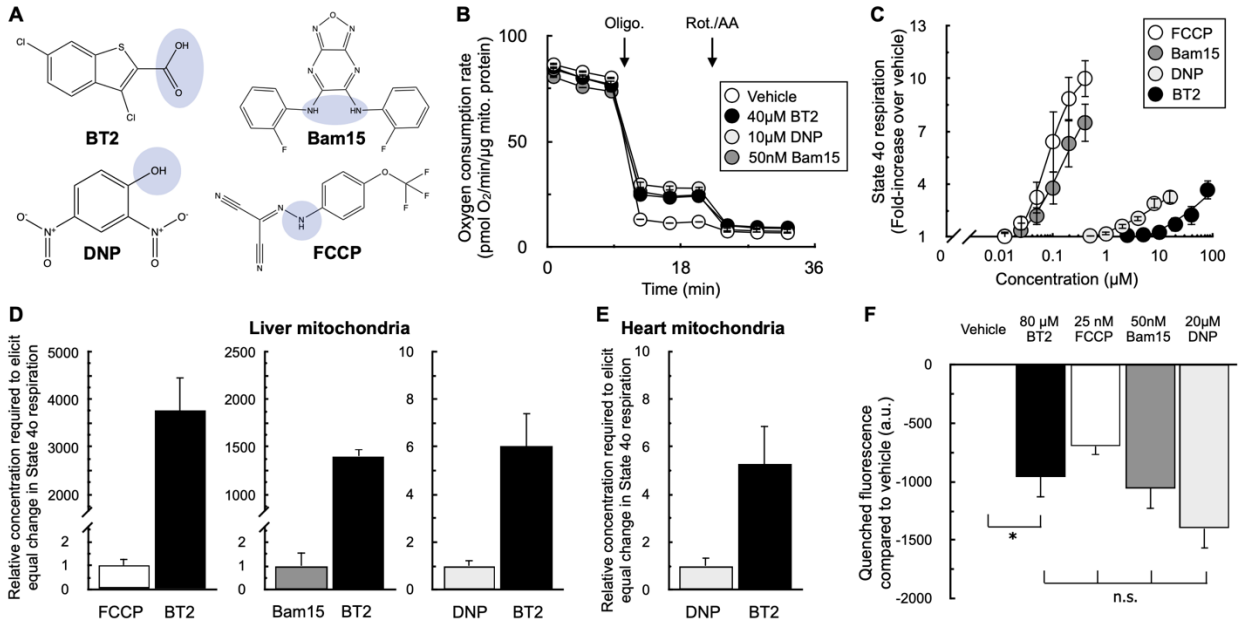

Figure 6: BT2 is a less potent uncoupler than DNP, Bam15, and FCCP.

(A) Chemical structures of BT2, DNP, Bam15, and FCCP with the functional group for protonation and deprotonation for acid/anion cycling highlighted in blue. (B) Representative trace of oxygen consumption rates of isolated rat liver mitochondria offered pyruvate, malate, ADP, and treated with 40 μM BT2, 10 μM DNP, or 50 nM Bam15. (n=4 technical replicates from a single experiment). (C) Aggregate fold-change in State 4_o respiration relative to vehicle controls from experiments conducted as in (B) [FCCP] and [Bam15] = 400 nM, 200 nM, 100 nM, 50 nM; [DNP] = 16 μM, 8 μM, 4 μM, 2 μM, 1 μM, 500 nM; [BT2] = 2.5, 5, 10, 20, 40, and 80 μM. (n=4 biological replicates). (D) Data extrapolated from experiments conducted in (A) and (B) measuring difference in concentration required to elicit a two- and three-fold change in State 4_o respiration relative to vehicle controls. (n= 4 biological replicates). (E) Values calculated as in (A) – (C) except with isolated rat heart mitochondria. (n=4 biological replicates). (F) Measurements of mitochondrial membrane potential using quenched TMRE fluorescence with isolated liver mitochondria as in Figure 3 (A) – (C). (n=4 biological replicates). All data are mean ± S.E.M. Statistical analysis was conducted with ANOVA followed by Dunnett's post-hoc multiple comparisons tests [(F)]. *, $p < 0.05$.

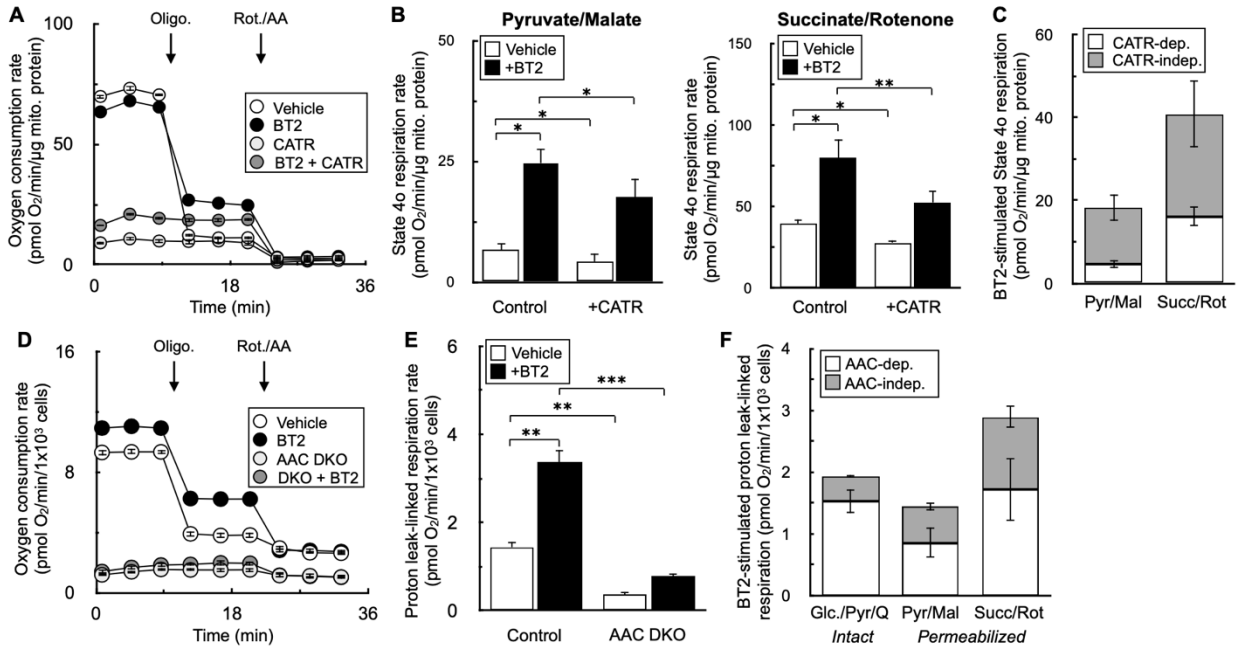

Figure 7: BT2 uncouples via both AAC-dependent and AAC-independent mechanisms

(A) Oxygen consumption rate traces of isolated rat liver mitochondria acutely treated with 80 μM BT2, 5 μM carboxyatractyloside (CATR), both 80 μM BT2 and 5 μM CATR, or vehicle control 5 minutes prior to conducting measurements. Mitochondria were offered pyruvate, malate, and ADP as before. (n=10 technical replicates from a single experiment. (B) Collated State 4_o respiration from isolated rat liver mitochondria in (A) offered either pyruvate/malate (left) or succinate/rotenone (right). (n=4 biological replicates. (C) Collated State 4_o respiration that is CATR-dependent or CATR-independent in isolated rat liver mitochondria offered pyruvate and malate or succinate and rotenone as in (A) and (B). plotted as a stacked bar chart to gauge the proportion of CATR-sensitive (white) and CATR-insensitive (grey) uncoupling. (n=4 biological replicates). (D) Intact C2C12 myoblasts with or without genetic ablation of AAC1 and AAC2 (DKO) assayed in DMEM supplemented with glucose, pyruvate, and glutamine as described in the Materials and Methods. 80μM BT2 was offered acutely 5 min prior to conducting measurements. (n=10 technical replicates from a single experiment). (E) Collated proton leak-linked respiration from experiments using intact C2C12 myoblasts as in (D). (n=5 biological replicates). (F) Collated

proton leak-linked respiration from experiments as in (D) and (E) plotted as a stacked bar chart to gauge the proportion of AAC-dependent (white) and AAC-independent (grey) uncoupling. Conditions are intact cells offered DMEM supplemented as in (A) (left) and permeabilized myoblasts offered either pyruvate/malate (middle) or succinate/rotenone (right). (n=5 biological replicates). All data are mean ± S.E.M. Statistical analysis was conducted with ANOVA followed by Dunnett's post-hoc multiple comparisons tests. *, $p < 0.05$; **, $p < 0.01$; ***, $p < 0.001$.

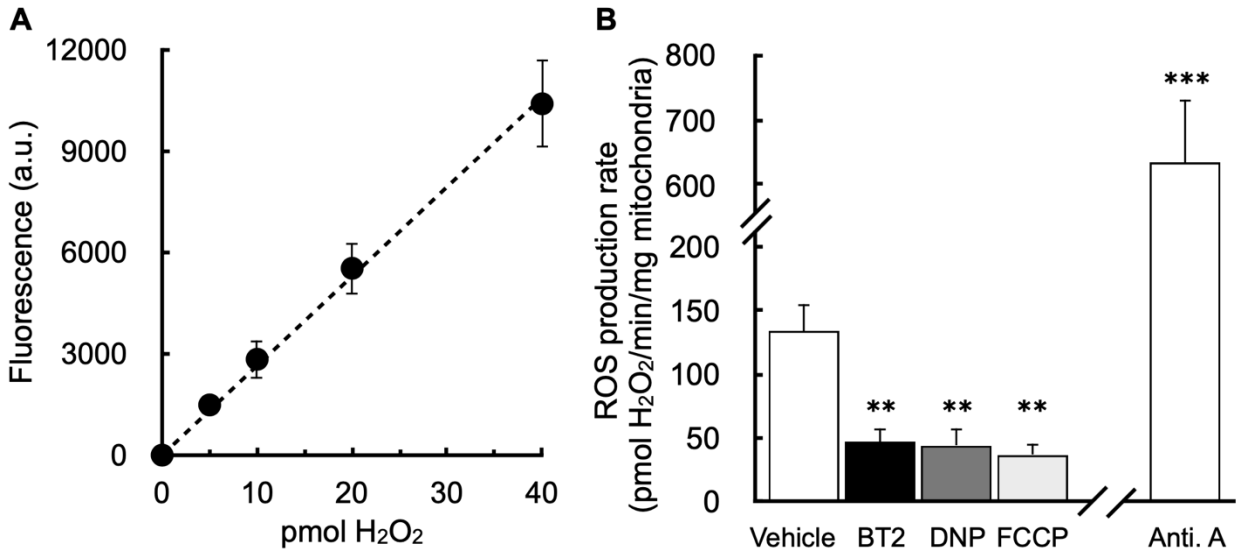

Figure 8: BT2 lowers ROS productions in isolated rat heart mitochondria in parallel with the chemical uncouplers DNP and FCCP.

(A) Representative standard curve of exogenous H_2O_2 added on top of isolated mitochondria and detected with Amplex Red. (n=3 technical replicates from a single experiment) (B) H_2O_2 efflux in isolated mitochondria offered succinate in response to addition of 80μM BT2, 20μM DNP, 100nM FCCP, 1μM antimycin A, or vehicle control. (n=3-4 biological replicates). All data are mean ± S.E.M. Statistical analysis was conducted with ANOVA followed by Dunnett's post-hoc multiple comparisons tests. **, $p < 0.01$; ***, $p < 0.001$.

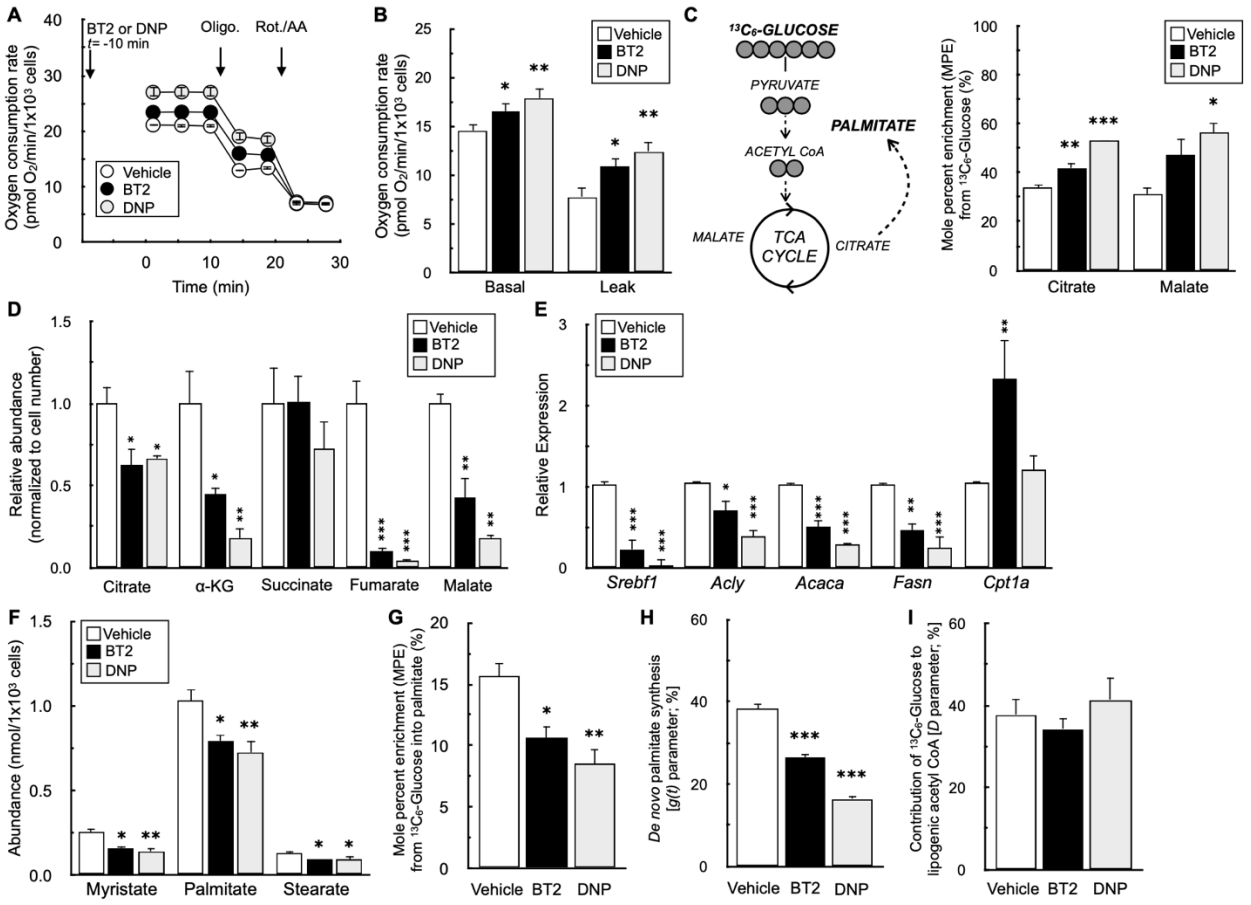

Figure 9: BT2 increases cellular energy expenditure and decreases *de novo* lipogenesis

(A) Representative oxygen consumption trace of differentiated 3T3-L1 adipocytes acutely offered 40μM BT2 or 10μM DNP 10 min. prior to initial measurements in DMEM supplemented with glucose, pyruvate, and glutamine as described in the Materials and Methods. (n=5 technical replicates from a single experiment). (B) Collated oxygen consumption rate parameters for 3T3-L1 cells as in (A). (n=5 biological replicates). (C) (Left) Simplified schematic of uniformly labeled $^{13}C_6$-glucose enriching TCA cycle intermediates and palmitate. (Right) Mole percent enrichment (M.P.E.) from $^{13}C_6$-glucose of TCA cycle intermediates citrate and malate in differentiated 3T3-L1 adipocytes treated for 72 hr. with 120μM BT2 or 40μM DNP in medium containing 2% serum. High concentrations of drug were used to account for drug binding to serum. (n=3 biological replicates). (D) Metabolite abundances of TCA cycle intermediates, adjusted for cell number, for

experiments conducted as in (C). (n=3 biological replicates). (E) qPCR analysis for genes associated with *de novo* lipogenesis as well as *Cpt1a* for cells treated as in (C). (n=5-8 biological replicates). (F) Abundances of fatty acids for experiments conducted as in (C). (n=3-4 biological replicates). (G) M.P.E. from $^{13}C_6$-glucose into palmitate for experiments conducted as in (C). (n=5 biological replicates). (H) Rate of *de novo* lipogenesis [g(t) parameter] calculated by isotopomer spectral analysis (ISA) for experiments conducted as in (C). Averages provided by the model for each biological replicate are presented. Predicted g(t) values and 95% confidence intervals for each technical replicate are provided in Table 1. (n=4 biological replicates). (I) Fractional contribution of glucose to the lipogenic acetyl CoA pool ('D' parameter) calculated by ISA. Averages provided by the model for each biological replicate are presented. Predicted 'D' values and 95% confidence intervals for each technical replicate are provided in Supplementary Table 1. (n=4 biological replicates). All data are mean ± S.E.M. Statistical analysis was conducted with ANOVA followed by Dunnett's post-hoc multiple comparisons tests. *, $p < 0.05$; **, $p < 0.01$; ***, $p < 0.001$.

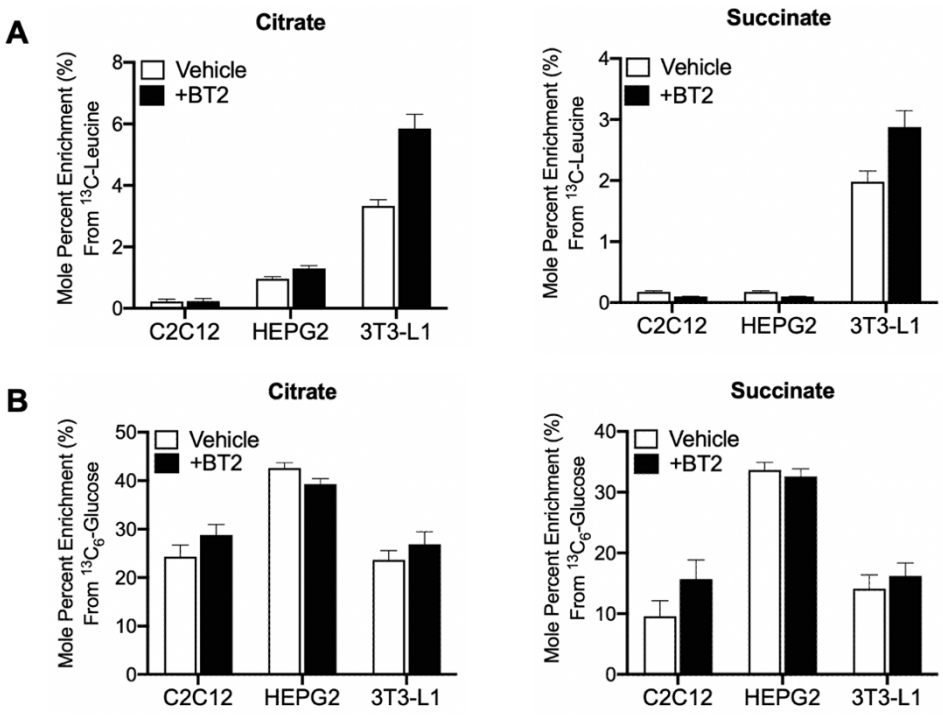

Figure 10: BT2 uncouples in intact cells independently of BCAA oxidation.

(A) Mole percent enrichment (M.P.E.) from ^{13}C-leucine of TCA cycle intermediates citrate and succinate in C212 myoblasts, HepG2 hepatocytes, and differentiated 3T3-L1 adipocytes treated for 24 hours with 80 μM BT2. (B) Mole percent enrichment (M.P.E.) from $^{13}C_6$-glucose of TCA cycle intermediates citrate and succinate in C212 myoblasts, HepG2 hepatocytes, and differentiated 3T3-L1 adipocytes treated for 24 hours with 80 μM BT2. For (A) and (B), C2C12 myoblasts (n=4 biological replicates), HepG2 hepatocytes (n=4 biological replicates), and 3T3-L1 differentiated adipocytes (n=5 biological replicates). All data are mean ± S.E.M.

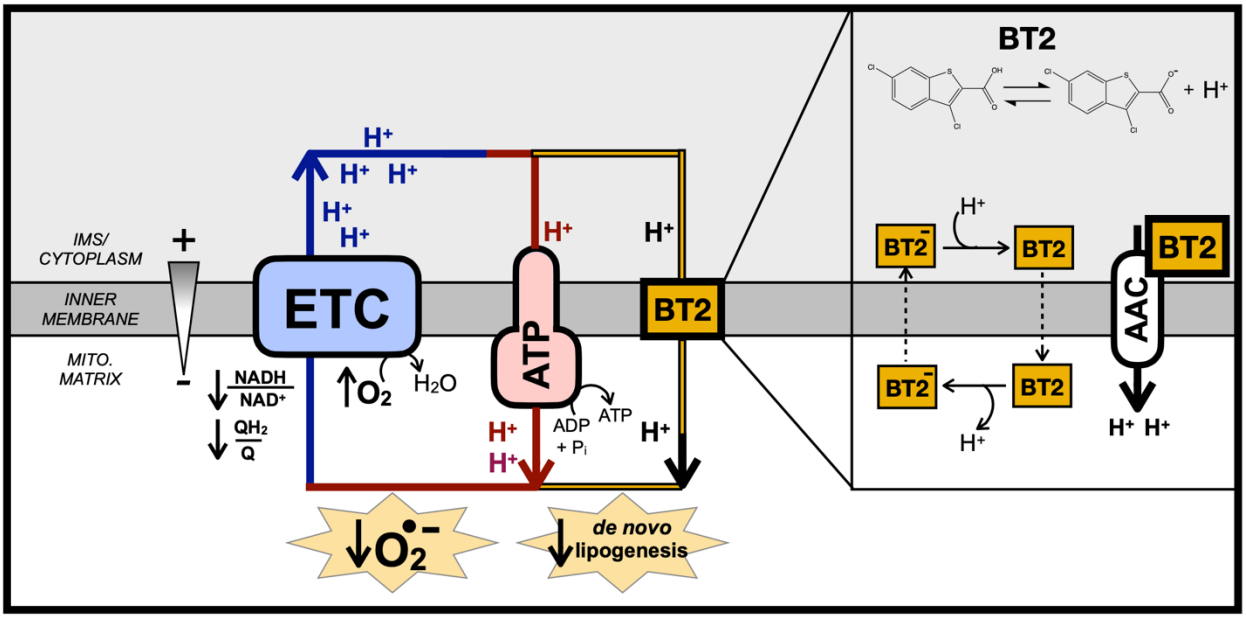

Figure 11: BT2 uncouples mitochondria to increase energy expenditure, lower superoxide production, and reduce *de novo* lipogenesis.

Supplemental Table 1 – ISA modeled values and 95% confidence intervals for individual technical replicates.								
Sample	Measurement	Value	Lower range	Upper range	Sample	Measurement	Value	Lower range	Upper range
N1-NT1	D(M2-AcCoA)	0.309	0.264	0.353	N3-NT1	D(M2-AcCoA)	0.558	0.509	0.605
	D(M1-AcCoA)	0.027	0.006	0.052		D(M1-AcCoA)	0.034	0.010	0.066
	1-D(AcCoA)	0.665	0.621	0.708		1-D(AcCoA)	0.408	0.360	0.457
	g(t) palmitate	0.419	0.375	0.459		g(t) palmitate	0.456	0.408	0.498
	D(TOTAL)	0.335	0.270	0.405		D(TOTAL)	0.592	0.519	0.671
N1-NT2	D(M2-AcCoA)	0.288	0.240	0.335	N3-NT2	D(M2-AcCoA)	0.292	0.236	0.348
	D(M1-AcCoA)	0.027	0.006	0.055		D(M1-AcCoA)	0.030	0.005	0.065
	1-D(AcCoA)	0.685	0.638	0.731		1-D(AcCoA)	0.677	0.624	0.730
	g(t) palmitate	0.394	0.349	0.435		g(t) palmitate	0.354	0.307	0.396
	D(TOTAL)	0.315	0.246	0.390		D(TOTAL)	0.323	0.241	0.412
N1-NT3	D(M2-AcCoA)	0.244	0.194	0.291	N3-NT3	D(M2-AcCoA)	0.326	0.248	0.398
	D(M1-AcCoA)	0.032	0.009	0.064		D(M1-AcCoA)	0.030	0.000	0.078
	1-D(AcCoA)	0.724	0.678	0.769		1-D(AcCoA)	0.644	0.574	0.715
	g(t) palmitate	0.395	0.348	0.437		g(t) palmitate	0.262	0.211	0.306
	D(TOTAL)	0.276	0.204	0.355		D(TOTAL)	0.356	0.248	0.476
N1-BT2-1	D(M2-AcCoA)	0.322	0.255	0.385	N3-BT2-1	D(M2-AcCoA)	0.327	0.282	0.372
	D(M1-AcCoA)	0.029	0.000	0.070		D(M1-AcCoA)	0.023	0.002	0.048
	1-D(AcCoA)	0.650	0.588	0.712		1-D(AcCoA)	0.650	0.605	0.694
	g(t) palmitate	0.285	0.236	0.329		g(t) palmitate	0.366	0.325	0.403
	D(TOTAL)	0.350	0.255	0.455		D(TOTAL)	0.350	0.284	0.420
N1-BT2-2	D(M2-AcCoA)	0.299	0.221	0.370	N3-BT2-2	D(M2-AcCoA)	0.295	0.223	0.362
	D(M1-AcCoA)	0.030	0.000	0.079		D(M1-AcCoA)	0.030	0.000	0.075
	1-D(AcCoA)	0.671	0.603	0.739		1-D(AcCoA)	0.675	0.611	0.739
	g(t) palmitate	0.258	0.209	0.303		g(t) palmitate	0.235	0.191	0.274
	D(TOTAL)	0.329	0.221	0.449		D(TOTAL)	0.325	0.223	0.437
N1-BT2-3	D(M2-AcCoA)	0.231	0.076	0.320	N3-BT2-3	D(M2-AcCoA)	0.316	0.245	0.383
	D(M1-AcCoA)	0.046	0.004	0.169		D(M1-AcCoA)	0.028	0.000	0.072
	1-D(AcCoA)	0.723	0.646	0.826		1-D(AcCoA)	0.655	0.591	0.720
	g(t) palmitate	0.275	0.218	0.325		g(t) palmitate	0.248	0.202	0.289
	D(TOTAL)	0.277	0.079	0.489		D(TOTAL)	0.345	0.245	0.455
N1-DNP-1	D(M2-AcCoA)	0.355	0.236	0.455	N3-DNP-1	D(M2-AcCoA)	0.551	0.483	0.615
	D(M1-AcCoA)	0.024	0.000	0.095		D(M1-AcCoA)	0.023	0.000	0.062
	1-D(AcCoA)	0.621	0.524	0.721		1-D(AcCoA)	0.426	0.360	0.495
	g(t) palmitate	0.197	0.141	0.247		g(t) palmitate	0.111	0.088	0.134
	D(TOTAL)	0.379	0.236	0.550		D(TOTAL)	0.574	0.483	0.677
N1-DNP-2	D(M2-AcCoA)	0.387	0.243	0.505	N3-DNP-2	D(M2-AcCoA)	0.338	0.000	0.483
	D(M1-AcCoA)	0.022	0.000	0.105		D(M1-AcCoA)	0.031	0.000	0.287
	1-D(AcCoA)	0.591	0.476	0.713		1-D(AcCoA)	0.631	0.492	0.993
	g(t) palmitate	0.171	0.114	0.221		g(t) palmitate	0.175	0.110	0.231
	D(TOTAL)	0.409	0.243	0.610		D(TOTAL)	0.369	0.000	0.770
N1-DNP-3	D(M2-AcCoA)	0.346	0.201	0.456	N3-DNP-3	D(M2-AcCoA)	0.295	0.178	0.386
	D(M1-AcCoA)	0.025	0.000	0.109		D(M1-AcCoA)	0.029	0.000	0.100
	1-D(AcCoA)	0.629	0.524	0.743		1-D(AcCoA)	0.677	0.592	0.766
	g(t) palmitate	0.178	0.123	0.228		g(t) palmitate	0.172	0.127	0.212
	D(TOTAL)	0.371	0.201	0.565		D(TOTAL)	0.323	0.178	0.486
N2-NT1	D(M2-AcCoA)	0.224	0.187	0.260	N4-NT1	D(M2-AcCoA)	0.346	0.306	0.386
	D(M1-AcCoA)	0.031	0.012	0.054		D(M1-AcCoA)	0.023	0.004	0.045
	1-D(AcCoA)	0.746	0.711	0.780		1-D(AcCoA)	0.631	0.591	0.672
	g(t) palmitate	0.395	0.358	0.430		g(t) palmitate	0.378	0.340	0.412
	D(TOTAL)	0.254	0.198	0.314		D(TOTAL)	0.369	0.309	0.431
N2-NT2	D(M2-AcCoA)	0.387	0.337	0.436	N4-NT2	D(M2-AcCoA)	0.523	0.475	0.571
	D(M1-AcCoA)	0.024	0.002	0.052		D(M1-AcCoA)	0.029	0.007	0.059
	1-D(AcCoA)	0.589	0.540	0.638		1-D(AcCoA)	0.447	0.399	0.496
	g(t) palmitate	0.420	0.373	0.462		g(t) palmitate	0.429	0.383	0.470
	D(TOTAL)	0.411	0.339	0.488		D(TOTAL)	0.553	0.481	0.630
N2-NT3	D(M2-AcCoA)	0.249	0.203	0.293	N4-NT3	D(M2-AcCoA)	0.435	0.381	0.489
	D(M1-AcCoA)	0.030	0.008	0.059		D(M1-AcCoA)	0.023	0.000	0.052
	1-D(AcCoA)	0.721	0.679	0.763		1-D(AcCoA)	0.541	0.487	0.595
	g(t) palmitate	0.393	0.350	0.432		g(t) palmitate	0.412	0.363	0.455
	D(TOTAL)	0.279	0.212	0.352		D(TOTAL)	0.459	0.381	0.541
N2-BT2-1	D(M2-AcCoA)	0.398	0.295	0.492	N4-BT2-1	D(M2-AcCoA)	0.300	0.246	0.352
	D(M1-AcCoA)	0.029	0.000	0.094		D(M1-AcCoA)	0.026	0.001	0.058
	1-D(AcCoA)	0.573	0.480	0.669		1-D(AcCoA)	0.674	0.624	0.724
	g(t) palmitate	0.231	0.172	0.281		g(t) palmitate	0.266	0.226	0.302
	D(TOTAL)	0.427	0.295	0.586		D(TOTAL)	0.326	0.247	0.411
N2-BT2-2	D(M2-AcCoA)	0.282	0.203	0.354	N4-BT2-2	D(M2-AcCoA)	0.317	0.266	0.367
	D(M1-AcCoA)	0.032	0.000	0.084		D(M1-AcCoA)	0.023	0.000	0.053
	1-D(AcCoA)	0.685	0.619	0.753		1-D(AcCoA)	0.660	0.611	0.709
	g(t) palmitate	0.279	0.227	0.325		g(t) palmitate	0.232	0.198	0.263
	D(TOTAL)	0.315	0.203	0.437		D(TOTAL)	0.340	0.266	0.420

N2-BT2-3	D(M2-AcCoA)	0.369	0.271	0.459	N4-DNP-1	D(M2-AcCoA)	0.365	0.247	0.468
	D(M1-AcCoA)	0.030	0.000	0.091		D(M1-AcCoA)	0.026	0.000	0.093
	1-D(AcCoA)	0.601	0.514	0.690		1-D(AcCoA)	0.609	0.508	0.714
	g(t) palmitate	0.252	0.193	0.303		g(t) palmitate	0.183	0.133	0.229
	D(TOTAL)	0.399	0.271	0.549		D(TOTAL)	0.391	0.247	0.561
N2-DNP-1	D(M2-AcCoA)	0.464	0.319	0.590	N4-DNP-2	D(M2-AcCoA)	0.340	0.271	0.408
	D(M1-AcCoA)	0.021	0.000	0.117		D(M1-AcCoA)	0.019	0.000	0.056
	1-D(AcCoA)	0.515	0.390	0.650		1-D(AcCoA)	0.641	0.576	0.706
	g(t) palmitate	0.150	0.094	0.201		g(t) palmitate	0.163	0.129	0.195
	D(TOTAL)	0.485	0.319	0.707		D(TOTAL)	0.359	0.271	0.464
					N4-DNP-3	D(M2-AcCoA)	0.316	0.239	0.388
						D(M1-AcCoA)	0.021	0.000	0.064
						1-D(AcCoA)	0.663	0.594	0.732
						g(t) palmitate	0.162	0.126	0.194
						D(TOTAL)	0.337	0.239	0.452

Table 1: ISA modeled values and 95% confidence intervals for individual technical replicates

MATERIALS AND METHODS

Animals

All animal protocols and procedures were approved and performed in accordance with the NIH Guide for the Care and Use of Laboratory Animals and the UCLA Animal Research Committee (ARC). C57BL/6J male mice aged 8-12 weeks were purchased from The Jackson Laboratory. Male Sprague Dawley age 7-10 weeks (~200-300 g) were purchased from Envigo.

Chemical Reagents

BT2 (3,6-dichlorobenzo[b]thiophene-2-carboxylic acid) was purchased from MedChemExpress (#HY-114855). BT2 stocks were prepared at 40mM and 400mM in DMSO. All other uncouplers were purchased from Sigma-Alrich. FCCP (Carbonyl cyanide 4-trifluoromethoxyphenylhydrazine) was purchased from Sigma Aldrich (#C2920). FCCP stocks were made at 10 mM in 95% EtOH. Bam15 was purchased from Sigma Aldrich (#SML-1760). Bam15 stocks were made at 40 mM in DMSO. DNP (2,4-dinitrophenol) was purchased from Sigma Aldrich (#42195). DNP stocks were prepared at 20 mM in DMSO. Bam15 was purchased from Sigma Aldrich (#SML-1760) and made at 40mM in DMSO. Al chemical uncoupler stocks were stored at -20°C at the concentrations indicated.

Cell Culture

Neonatal rat ventricular myocytes (NRVMs)

NRVMs were isolated from post-natal P1-P3-day old Sprague Dawley rat pups of mixed sex as previously described.[74,75] Cells were plated onto Agilent Seahorse XF96 cell culture plates or 12-well cell culture dishes coated with 0.1% gelatin (Sigma #G1393) in DMEM/F12 medium (Gibco #11330057) supplemented with 10% (v/v) fetal bovine serum (FBS), 100U/mL penicillin, and 100 μg/mL streptomycin. After 24hr., medium was changed to DMEM/F12 lacking FBS but with antibiotics as before. Cells were grown and maintained in a humidified 5% CO_2 incubator at 37°C.

Human induced pluripotent stem cell (iPSC) cardiomyocytes (iCell cardiomyocytes)

iCell cardiomyocytes were purchased from FUJIFILM Cellular Dynamics, Inc. (#01434) and were grown and maintained according to the protocol guidelines provided by vendor. Cells were grown and maintained in a humidified 5% CO_2 incubator at 37°C.

3T3-L1 adipocytes

3T3-L1 pre-adipocytes were maintained below 70% confluency in DMEM (Gibco #11965) supplemented with 10% (v/v) bovine calf serum (BCS, ATCC 30-2020), 100U/mL penicillin, 100 μg/mL streptomycin, and 1mM pyruvate. Cells were plated onto XF96 cell culture plates or 12-well tissue culture dishes and allowed to grow for 48 hours (plating on Day -2). On Day 0, 3T3-L1 pre-adipocytes were initiated to differentiate into 3T3-L1 adipocytes in maintenance medium that consisted of DMEM supplemented with 10% (v/v) FBS, 1.0 μg/mL insulin (bovine, Sigma #I0515), 0.25 μM dexamethasone (Sigma #D4904), and 0.5 mM methylisobutylxanthine (IBMX, Sigma I5879), and 100 nM rosiglitazone (Sigma #R2408). On Day 2, medium was changed to maintenance medium supplemented only with 1.0 μg/mL insulin, and in Day 4 and 6 medium was replaced to maintenance medium with no further additions. Differentiated 3T3-L1 adipocytes were treated with compound on Day 8 as described in the Materials and Methods. The pre-adipocyte expansion procedure and differentiation procedure were derived from the chemically induced differentiation of ATCC 3T3-L1 protocol guidelines and Green *et al.*[76]

C2C12 myoblasts

C2C12 myoblasts were maintained in high glucose DMEM (Gibco #11965) medium supplemented with 10% (v/v) FBS, 100U/mL penicillin, 100 μg/mL streptomycin, and 1mM sodium pyruvate. C2C123 cells with genetic ablation of *Slc25a4* and *Slc25a5* (encoding AAC1 and AAC2) were generated and described previously.[49]

HepG2 hepatocytes

HepG2 hepatocytes were maintained in MEM (Gibco #11095) medium supplemented with 10% (v/v) FBS, 100U/mL penicillin, 100 μg/mL streptomycin, and 1mM sodium pyruvate.

Mitochondrial Isolation

In brief, rodent heart and liver tissues were isolated and placed in ice-cold PBS buffer immediately after anesthetizing mice with isoflurane and sacrificing. Mitochondria from each tissue were isolated following its own respective protocol. MSHE buffer consisted of 210 mannitol, 70 mM sucrose, 5 mM HEPES, and 1 mM EGTA (Ca^{2+} chelator) was used with or without 0.2% (w/v) fatty acid-free BSA, at pH 7.2 at 4°C. HES buffer consists of sucrose and HEPES. Note, all step in the mitochondrial isolation procedure were conducted on ice or at 4°C and ice water contamination was highly avoided. Mitochondrial protein content was measured by the bicinchoninic acid (BCA) assay.

Heart mitochondria

For isolated heart mitochondria, mouse or rat hearts were removed quickly from euthanized animal while heart was still pumping and had blood immediately drained in saline buffer and then submerged in ice cold relaxing buffer. Hearts were immediately transferred (to avoid ischemic tissue) in HES buffer, minced, and then homogenized in a hand-held tissue disruptor (IKA Ultra-Turrax) in ice-cold MSHE. The heart tissue homogenate was centrifuged at 900*g* for 10 minutes at 4°C. The pellet was discarded, and the supernatant was transferred into a fresh tube and centrifuged at 9,000*g* for 10 minutes at 4°C. Finally, the remaining pellet containing mitochondria was collected and washed with medium lacking BSA and centrifuged at 9,000*g* for 10 minutes at 4°C. The final mitochondrial pellet was resuspended in approximately 20 μL of MSHE lacking BSA and kept at a concentration greater than 25 mg/mL and kept on ice. Mitochondrial protein concentration was determine using bovine serum albumin for a standard curve, the BCA assay, and TECAN plate reader.

Liver mitochondria

A detailed protocol on isolating liver mitochondria can be reviewed elsewhere.[77] Briefly, liver from mouse or rat was immediately emerged and washed in ice-cold PBS buffer after isolation from animal. Liver tissue was minced and transferred into MSHE+ BSA buffer and transferred into a pre-chilled Teflon-on-glass Dounce homogenizer to disrupt and breakdown tissue. Livers were disrupted using 2 strokes of the drill-driven Teflon-on-glass homogenizer with roughly 1 mL of buffer for every 100 mg of tissue. The homogenate was centrifuged at 12,000*g* for 10 minutes at 4°C to remove any contaminating fat. The pellet was resuspended and centrifuged at 800*g* for 5 minutes at 4°C to remove cell debris. The supernatant was filtered through two layers of a buffer-wet cheesecloth and filtered supernatant was centrifuged at 12,000*g* for 10 minutes at 4°C. The light, 'fluffy' layer of the pelleted was removed, and the mitochondrial pellet was resuspended and centrifuged again at 12,000*g* at. For the third and final centrifugation step, the pellet was washed and resuspended in MSHE lacking BSA and kept at a concentration greater than 100 mg/mL (approximately 50-100 μL) and kept on ice. Amount of mitochondrial protein was measured as mentioned above.

Respirometry

All respirometry experiments were conducted using an Agilent Seahorse XF96 Analyzer. Experiments were conducted at 37°C and pH 7.4 for intact cells or 7.2 for isolated mitochondria and permeabilized cells. Oxygen consumption rates (OCRs) were calculated according to the published protocols.[42,43] For experiments with intact or permeabilized cells, only the inner 60 wells were used, and the outer rim was filled with 200 μL of PBS throughout the incubation to minimize variance in temperature and evaporative effects across the plated. All respiratory parameters were corrected for non-mitochondrial respiration and background signal from the instrument with addition of 200 nM rotenone and 1 μL antimycin A and calculated according to well established best practices.[78]

Intact cells

Respiration was measured in NRVMs ($4.0x10^4$ cells/well), iPSC cardiomyocytes ($1.5x10^4$ cells/well), C2C12 myoblasts ($1.5x10^4$ cells/well) and differentiated 3T3-L1-adipocytes ($2.5x10^3$ cells/well) in DMEM assay medium composed of DMEM (Sigma #5030) supplemented with 31.6 mM NaCl, 3mg/L phenol red, 5 mM HEPES, 10 mM glucose, 2 mM glutamine, and 2 mM pyruvate. Where appropriate, cells were offered oligomycin (2 μM) and maximal respiration was estimated with 750 nM FCCP.

Permeabilized cells

Cells were permeabilized with 3 nM recombinant, mutant perfringolysin O (rPFO, Agilent Technologies). Before running the seahorse assay, cells were washed with buffer and then permeabilized cells were assayed as previously described in 1X MAS buffer.[77] 1X MAS buffer was prepared with 220 mM mannitol, 70 mM sucrose, 10 mM KH_2PO_4 5 mM $MgCl_2$, 2 mM HEPES (pH 7.2 at 37°C), and 1 mM EGTA, 0.2% (w/v BSA). This buffer was also supplemented with 3 nM rPFO, 4 mM ADP, AND BSA. Where indicated medium was supplemented with the appropriate respiratory substrates as stated in the figure legends, with either 10 mM pyruvate with 1 mM malate, or 10 mM succinate with 2 μM rotenone. Where indicated, oligomycin was used at 2 μM. Permeabilized cells were given the appropriate mitochondrial uncoupler treatments in the buffer described above.

Isolated mitochondria

Mitochondrial isolation was conducted as described in the Mitochondrial Isolation section above. For respirometry experiments in mitochondria isolated from liver, mitochondria were plated in XF96 plates at 3.0 μg/well. Isolated heart mitochondria were plated in XF96 plates at 1.5 μg/well. Mitochondria were plated in 1X MAS buffer described previously according to well established protocols.[77,79] As indicate in the figure legends, BSA was either omitted from the assay medium or used at 0.001% (w/v) to avoid sequestering lipophilic compounds under investigation. Where indicated, MAS buffer was supplemented with 10 mM pyruvate with 1 mM malate

(Pyr/Mal), 5 mM glutamate with 5 mM malate (Glu/Mal), or 10 mM succinate with 2 μM rotenone (Succ/Rot). Substrates offered are indicated in the figure legends. Mitochondria were offered oligomycin at 2 μM oligomycin and FCCP at 1 μM where indicated, 0.2 μM rotenone with 1 μM antimycin A were added at the end of the assay to subtract OCRs from non-mitochondrial respiration.

Normalization

All intact and permeabilized cell oxygen consumption rates were normalized to cell number. Post-seahorse assay, intact or permeabilized cells were fixed with 2% (v/v) paraformaldehyde in PBS at room temperature and stored at 4°C for up to 14 days. Cell nuclei were stained with 10 ng/mL Hoescht #33342 (ThermoFisher) for 30 minutes or overnight at 4°C. Cells were quantified using the Operetta High Content Imaging System (Perkin Elmer). All oxygen consumption rates in isolated mitochondria were normalized to microgram of total mitochondrial protein in microplate well unless otherwise indicated.

Mitochondrial Membrane Potential

Isolated mitochondria

The MMP of isolated mitochondria was measured using TMRE fluorescence in quench mode on the TECAN plate reader, where high concentration of tetramethylrhodamine, ethyl ester (TMRE) as been previously described.[45] TMRE fluorescence will self-quench upon accumulation in the mitochondrial matrix at high concentrations. As such, lowering the membrane potential will decrease dye uptake and self-quenching, thereby increasing the observed fluorescent signal. Isolated mitochondria from rat liver or heart were plated at 0.6 mg/mL per well in MAS buffer supplemented with 0.001% BSA, 5 μM TMRE, 4 mM ADP, 5 mM succinate, and 2 μM rotenone, with or without treatment of BT2 or chemical uncoupler. The black-walled 96-well plate was then wrapped in foil to shield from light and incubated at 37°C for 10 minutes. After incubation,

fluorescence was measured at 549/575 nm using a Tecan Spark multimode plate reader. Compounds under investigation were added immediately prior to the 10 min. incubation period.

Cardiomyocytes

The mitochondrial membrane potential in cells was measured with TMRE using the Image Xpress Micro Confocal high-content imaging system (Molecular Devices). NRVMs and iPSC-derived iCell cardiomyocytes were plated onto collagen-coated, black-walled PhenoPlates (Perkin-Elmer) at either $6.0x10^4$ (NRVMs) or $1.5x10^4$ (iCell) cells/well and maintained as described earlier in the Materials and Methods. 75 minutes prior to conducting measurements, medium was exchanged for DMEM lacking glucose, phenol red, and sodium bicarbonate (Sigma #5030) supplemented 31.6 mM NaCl, 10 mM glucose, 2 mM glutamine, 2 mM pyruvate, and 5 mM HEPES along with 10 nM TMRE (Invitrogen #T669) and 200 nM MitoTracker Green FM (Catalog # M7514). After allowing the dyes to equilibrate for 1 hr., BT2 (80 μM), DNP (10 μM) and FCCP (1 μM) were added, and measurements of the first microplate well began after 15 minutes. Circularity is defined with “1” being a perfect circle and “0” a straight line.

Patch-clamp recordings

Proton conductance across the mitochondrial inner membrane was conducted on mitoplasts derived from mouse heart mitochondria as previously described.[48,49] Patch-clamp recording was performed from isolated heart mitoplasts of mice. The mitoplasts used for patch-clamp experiments were 3–5 μm in diameter and typically had membrane capacitances of 0.3–1.2 pF. Both the bath and pipette solutions were formulated to record H^+ currents and contained only salts that dissociate into large anions and cations that are normally impermeant through ion channels or transporters. A low pH gradient across the IMM was used (pH 7.5 and 7.0 on the matrix and cytosolic sides, respectively). Pipettes were filled with 130 mM tetramethylammonium hydroxide (TMA), 1 mM EGTA, 2 mM Tris-HCl, and 100 mM HEPES. pH was adjusted to 7.5 with D-gluconic acid, and tonicity was adjusted to ~360 mmol/kg with sucrose. Typically, pipettes had resistances of 25–35 MΩ, and the access resistance was 40–75 MΩ. Whole-mitoplast I_H was

recorded in the bath solution containing 100 mM HEPES and 1 mM EGTA (pH adjusted to 7 with Trizma base, and tonicity adjusted to ~300 mmol/kg with sucrose). All experiments were performed under continuous perfusion of the bath solution. All electrophysiological data presented were acquired at 10 kHz and filtered at 1 kHz. For patch-clamping recordings, refer to the protocols in Bertholet *et al*.[49]

Hydrogen peroxide efflux

H_2O_2 efflux was measured in isolated mitochondria as described previously [39] using a Tecan Spark multimode plate reader and an Amplex Red-based detection system. Mitochondria (2 mg/mL) were incubated in SHE buffer (250 mM sucrose, 10 mM HEPES, 1 mM EGTA, pH 7.2 at 37°C) supplemented with 2.5 μM Amplex Red (ThermoFisher #A12222) and 5 U/mL horseradish peroxidase (ThermoFisher #31491). 10 mM succinate was added to the incubation, and the rate of H_2O_2 was measured over 2-3 minutes. The signal was calibrated to known amounts of H_2O_2 added on top of isolated mitochondria. Compounds under investigation were pre-incubated with mitochondria in the SHE buffer for 2-5 minutes prior to the addition of succinate. Fluorescence was detected using λ_{ex}= 570 nm and λ_{em}= 585 nm.

Stable isotope tracing and *de novo* lipogenesis

Cell culture

3T3-L1 pre-adipocytes were seeded at $2.5x10^4$ cells/well in 12-well dishes and differentiated as described earlier in the Materials and Methods. On Day 8, cells were changed into maintenance medium (made with DMEM A1443001) with the following changes: 2% (v/v) FBS rather than 10% to reduce protein binding of compounds under investigation, and uniformly labeled [$^{13}C_6$]-glucose (Cambridge Isotope Laboratories #CLM-1396) was used instead of ^{12}C unlabeled glucose. BT2 (120 μM) and DNP (40 μM) were added during this step and used at higher concentrations than in other experiments to account for binding to albumin in 2% (v/v) FBS. After 72 hr. cells were extracted for GC/MS analysis as described below. A matched 12-well dish

was used for normalization of metabolite levels to cell number. On the day of the extraction, cells were fixed with 2% (v/v) paraformaldehyde in PBS and stored at 4°C for no less than 7 days. Nuclei were stained with Hoescht (ThermoFisher #33342) overnight at 4°C and quantified using the Operetta High Content Imaging System (Perkin Elmer).

Neonatal rat ventricular myocytes were seeded at $4.0x10^5$ cells/well in 12-well dishes coated with 0.1% (w/v) gelatin in DMEM/F12 medium described earlier. After 24 hr. medium was exchanged into custom DMEM formulated without glucose, glutamine, or leucine (Sciencell Laboratories) and supplemented with 10 mM glucose, 2 mM GlutaMAX, or 0.8 mM leucine, with a uniformly labeled [$^{13}C_6$] label on either glucose or leucine (#CLM-2262). After 24 hr. cells were extracted for GC/MS analysis as described below.

Derivatization and mass spectrometry

Cell preparation and stable isotope tracing measuring incorporation of isotopic labels into polar metabolites and palmitate was conducted as previously described.[80] Metabolite extraction was conducted with a Folch-like extraction with a 5:2:5 ratio of methanol:water:chloroform. 12-well dishes were kept on ice and quickly washed with ice-cold 0.9% (w/v) NaCl. Cells were then scraped in ice-cold methanol and water containing 5 µg/mL norvaline (Sigma #N7502), an internal standard. Chloroform containing 20 µM [U-$^2H_{31}$]-palmitate (Cambridge Isotope Laboratories #DLM-215) as an internal standard was then added to the samples. Samples were then vortexed for 1 min and centrifuged at 10,000*g* for 5 min at 4°C.

The polar fraction (top layer) was removed, and the samples were dried overnight using a refrigerated CentriVap vacuum concentrator (LabConco). Metabolites (50 nmol to 23 pmol) were extracted alongside the cell samples to ensure the signal fell within the linear detection range of the instrument. The dried polar metabolites were reconstituted in 20 µL of 2% (w/v) methoxyamine in pyridine prior to a 45-min incubation at 37°C. Subsequently, 20 µL of MTBSTFA with 1% tert-butyldimethylchlorosilane was added to samples, followed by an additional 45-min incubation at

37°C. Samples were analyzed using Agilent MassHunter software and FluxFix software (http://fluxfix.science) was used to correct for the abundance of natural heavy isotopes against an in-house reference set of unlabeled metabolite standards.[81]

The lower, organic fraction was dried under air and then solubilized in 500 µL of acidified methanol [2% (v/v) H_2SO_4 in methanol] for 2 hr. at 50°C to generate fatty acid methyl esters (FAMEs). After this incubation, 100 µL of saturated NaCl was added, followed by 500 µL of hexane. This mixture was vortexed for 2 min and the upper hexane layer was collected in a new microfuge tube. An additional 500 µL of hexane was added to the original MeOH/NaCl tube and the process repeated to collect any residual FAMEs not obtained by the first addition. The pooled hexane extracts were then dried under airflow and resuspended in 75 µL of hexane. FAMEs were analyzed by GC-MS analysis. *De novo* lipid synthesis was estimated by isotopomer spectral analysis (ISA) and calculated using MATLAB software.[71] Samples were analyzed using a DB-35 column (Agilent Technologies). Information regarding additional technical specifications is available elsewhere.[80]

qPCR

3T3-L1 adipocytes were plated, maintained, and treated with either BT2 or DNP in 12-well dishes identically to those used for GC/MS analysis. Transcript levels were measured using quantitative polymerase chain reaction (qPCR). RNA was extracted using the RNeasy Mini Kit (Qiagen, 74106), and cDNA was generated using the High-Capacity cDNA Reverse Transcription Kit (Applied Biosystems, 4368814). The PowerUp SYBR Green Master Mix kit (Applied Biosystems, A25743) and a QuantStudio 5 (Applied Biosystems) were used for qPCR analysis. Relative gene expression was calculated using the $\Delta\Delta C_t$ method with *36b4* as a reference gene.

Statistical analysis

All statistical parameters, including the number of replicates (n), can be found in the figure legends. Statistical analyses were performed using Graph Pad Prism 5 software. Data are

presented as the mean ± SEM unless otherwise specified. Individual pairwise comparisons were performed using two-tailed Student's t-test. For experiments involving two or more groups, data were analyzed by one-way, repeated measures ANOVA followed by Dunnett's post-hoc multiple comparisons tests against vehicle controls. Data were assumed to follow a normal distribution (no tests were performed). Values denoted as follows were considered significant: *, $p < 0.05$; **, $p < 0.01$; ***, $p < 0.001$.

REFERENCES

(1) Nakamura, M.; Sadoshima, J. Mechanisms of Physiological and Pathological Cardiac Hypertrophy. *Nat. Rev. Cardiol.* **2018**, *15* (7), 387–407. https://doi.org/10.1038/s41569-018-0007-y.

(2) Frey, N.; Olson, E. N. Cardiac Hypertrophy: The Good, the Bad, and the Ugly. *Annu. Rev. Physiol.* **2003**, *65* (1), 45–79. https://doi.org/10.1146/annurev.physiol.65.092101.142243.

(3) Lopaschuk, G. D.; Karwi, Q. G.; Tian, R.; Wende, A. R.; Abel, E. D. Cardiac Energy Metabolism in Heart Failure. *Circ. Res.* **2021**, *128* (10), 1487–1513. https://doi.org/10.1161/CIRCRESAHA.121.318241.

(4) Saddik, M.; Lopaschuk, G. D. Myocardial Triglyceride Turnover and Contribution to Energy Substrate Utilization in Isolated Working Rat Hearts. *J. Biol. Chem.* **1991**, *266* (13), 8162–8170. https://doi.org/10.1016/S0021-9258(18)92956-X.

(5) Wisneski, J. A.; Stanley, W. C.; Neese, R. A.; Gertz, E. W. Effects of Acute Hyperglycemia on Myocardial Glycolytic Activity in Humans. *J. Clin. Invest.* **1990**, *85* (5), 1648–1656. https://doi.org/10.1172/JCI114616.

(6) Murthy, M. S.; Pande, S. V. Malonyl-CoA Binding Site and the Overt Carnitine Palmitoyltransferase Activity Reside on the Opposite Sides of the Outer Mitochondrial Membrane. *Proc. Natl. Acad. Sci.* **1987**, *84* (2), 378–382. https://doi.org/10.1073/pnas.84.2.378.

(7) Paulson, D. J.; Ward, K. M.; Shug, A. L. Malonyl CoA Inhibition of Carnitine Palmityltransferase in Rat Heart Mitochondria. *FEBS Lett.* **1984**, *176* (2), 381–384. https://doi.org/10.1016/0014-5793(84)81201-6.

(8) Ho, K. L.; Karwi, Q. G.; Wagg, C.; Zhang, L.; Vo, K.; Altamimi, T.; Uddin, G. M.; Ussher, J. R.; Lopaschuk, G. D. Ketones Can Become the Major Fuel Source for the Heart but Do Not Increase Cardiac Efficiency. *Cardiovasc. Res.* **2021**, *117* (4), 1178–1187. https://doi.org/10.1093/cvr/cvaa143.

(9) Ponikowski, P.; Voors, A. A.; Anker, S. D.; Bueno, H.; Cleland, J. G. F.; Coats, A. J. S.; Falk, V.; González-Juanatey, J. R.; Harjola, V.-P.; Jankowska, E. A.; Jessup, M.; Linde, C.; Nihoyannopoulos, P.; Parissis, J. T.; Pieske, B.; Riley, J. P.; Rosano, G. M. C.; Ruilope, L. M.; Ruschitzka, F.; Rutten, F. H.; van der Meer, P. 2016 ESC Guidelines for the Diagnosis and Treatment of Acute and Chronic Heart Failure: The Task Force for the Diagnosis and Treatment of Acute and Chronic Heart Failure of the European Society of Cardiology (ESC)Developed with the Special Contribution of the Heart Failure Association (HFA) of the ESC. *Eur. Heart J.* **2016**, *37* (27), 2129–2200. https://doi.org/10.1093/eurheartj/ehw128.

(10) van Bilsen, M.; van Nieuwenhoven, F. A.; van der Vusse, G. J. Metabolic Remodelling of the Failing Heart: Beneficial or Detrimental? *Cardiovasc. Res.* **2008**, *81* (3), 420–428. https://doi.org/10.1093/cvr/cvn282.

(11) Aubert, G.; Martin, O. J.; Horton, J. L.; Lai, L.; Vega, R. B.; Leone, T. C.; Koves, T.; Gardell, S. J.; Krüger, M.; Hoppel, C. L.; Lewandowski, E. D.; Crawford, P. A.; Muoio, D. M.; Kelly, D. P. The Failing Heart Relies on Ketone Bodies as a Fuel. *Circulation* **2016**, *133* (8), 698–705. https://doi.org/10.1161/CIRCULATIONAHA.115.017355.

(12) Funada, J.; Betts, T. R.; Hodson, L.; Humphreys, S. M.; Timperley, J.; Frayn, K. N.; Karpe, F. Substrate Utilization by the Failing Human Heart by Direct Quantification Using Arterio-

Venous Blood Sampling. *PLoS ONE* **2009**, *4* (10), e7533. https://doi.org/10.1371/journal.pone.0007533.

(13) Sun, H.; Olson, K. C.; Gao, C.; Prosdocimo, D. A.; Zhou, M.; Wang, Z.; Jeyaraj, D.; Youn, J.-Y.; Ren, S.; Liu, Y.; Rau, C. D.; Shah, S.; Ilkayeva, O.; Gui, W.-J.; William, N. S.; Wynn, R. M.; Newgard, C. B.; Cai, H.; Xiao, X.; Chuang, D. T.; Schulze, P. C.; Lynch, C.; Jain, M. K.; Wang, Y. Catabolic Defect of Branched-Chain Amino Acids Promotes Heart Failure. *Circulation* **2016**, *133* (21), 2038–2049. https://doi.org/10.1161/CIRCULATIONAHA.115.020226.

(14) Fragasso, G.; Palloshi, A.; Puccetti, P.; Silipigni, C.; Rossodivita, A.; Pala, M.; Calori, G.; Alfieri, O.; Margonato, A. A Randomized Clinical Trial of Trimetazidine, a Partial Free Fatty Acid Oxidation Inhibitor, in Patients With Heart Failure. *J. Am. Coll. Cardiol.* **2006**, *48* (5), 992–998. https://doi.org/10.1016/j.jacc.2006.03.060.

(15) Cheitlin, M. D. Metabolic Modulation With Perhexiline in Chronic Heart Failure: A Randomized, Controlled Trial of Short-Term Use of a Novel Treatment. *Yearb. Cardiol.* **2007**, *2007*, 342–343. https://doi.org/10.1016/S0145-4145(08)70212-0.

(16) Gao, D.; Ning, N.; Niu, X.; Hao, G.; Meng, Z. Trimetazidine: A Meta-Analysis of Randomised Controlled Trials in Heart Failure. *Heart* **2011**, *97* (4), 278–286. https://doi.org/10.1136/hrt.2010.208751.

(17) Holubarsch, C. J. F.; Rohrbach, M.; Karrasch, M.; Boehm, E.; Polonski, L.; Ponikowski, P.; Rhein, S. A Double-Blind Randomized Multicentre Clinical Trial to Evaluate the Efficacy and Safety of Two Doses of Etomoxir in Comparison with Placebo in Patients with Moderate Congestive Heart Failure: The ERGO (Etomoxir for the Recovery of Glucose Oxidation) Study. *Clin. Sci.* **2007**, *113* (4), 205–212. https://doi.org/10.1042/CS20060307.

(18) Wang, W.; Zhang, L.; Battiprolu, P. K.; Fukushima, A.; Nguyen, K.; Milner, K.; Gupta, A.; Altamimi, T.; Byrne, N.; Mori, J.; Alrob, O. A.; Wagg, C.; Fillmore, N.; Wang, S.; Liu, D. M.; Fu, A.; Lu, J. Y.; Chaves, M.; Motani, A.; Ussher, J. R.; Reagan, J. D.; Dyck, J. R. B.; Lopaschuk, G. D. Malonyl CoA Decarboxylase Inhibition Improves Cardiac Function Post-Myocardial Infarction. *JACC Basic Transl. Sci.* **2019**, *4* (3), 385–400. https://doi.org/10.1016/j.jacbts.2019.02.003.

(19) Kolwicz, S. C.; Olson, D. P.; Marney, L. C.; Garcia-Menendez, L.; Synovec, R. E.; Tian, R. Cardiac-Specific Deletion of Acetyl CoA Carboxylase 2 Prevents Metabolic Remodeling During Pressure-Overload Hypertrophy. *Circ. Res.* **2012**, *111* (6), 728–738. https://doi.org/10.1161/CIRCRESAHA.112.268128.

(20) Shao, D.; Kolwicz, S. C.; Wang, P.; Roe, N. D.; Villet, O.; Nishi, K.; Hsu, Y.-W. A.; Flint, G. V.; Caudal, A.; Wang, W.; Regnier, M.; Tian, R. Increasing Fatty Acid Oxidation Prevents High-Fat Diet–Induced Cardiomyopathy Through Regulating Parkin-Mediated Mitophagy. *Circulation* **2020**, *142* (10), 983–997. https://doi.org/10.1161/CIRCULATIONAHA.119.043319.

(21) Lydell, C. Pyruvate Dehydrogenase and the Regulation of Glucose Oxidation in Hypertrophied Rat Hearts. *Cardiovasc. Res.* **2002**, *53* (4), 841–851. https://doi.org/10.1016/S0008-6363(01)00560-0.

(22) Karwi, Q. G.; Zhang, L.; Wagg, C. S.; Wang, W.; Ghandi, M.; Thai, D.; Yan, H.; Ussher, J. R.; Oudit, G. Y.; Lopaschuk, G. D. Targeting the Glucagon Receptor Improves Cardiac Function and Enhances Insulin Sensitivity Following a Myocardial Infarction. *Cardiovasc. Diabetol.* **2019**, *18* (1), 1. https://doi.org/10.1186/s12933-019-0806-4.

(23) Nielsen, R.; Møller, N.; Gormsen, L. C.; Tolbod, L. P.; Hansson, N. H.; Sorensen, J.; Harms, H. J.; Frøkiær, J.; Eiskjaer, H.; Jespersen, N. R.; Mellemkjaer, S.; Lassen, T. R.; Pryds, K.; Bøtker, H.

E.; Wiggers, H. Cardiovascular Effects of Treatment With the Ketone Body 3-Hydroxybutyrate in Chronic Heart Failure Patients. *Circulation* **2019**, *139* (18), 2129–2141. https://doi.org/10.1161/CIRCULATIONAHA.118.036459.

(24) Neinast, M. D.; Jang, C.; Hui, S.; Murashige, D. S.; Chu, Q.; Morscher, R. J.; Li, X.; Zhan, L.; White, E.; Anthony, T. G.; Rabinowitz, J. D.; Arany, Z. Quantitative Analysis of the Whole-Body Metabolic Fate of Branched-Chain Amino Acids. *Cell Metab.* **2019**, *29* (2), 417-429.e4. https://doi.org/10.1016/j.cmet.2018.10.013.

(25) Wang, T. J.; Larson, M. G.; Vasan, R. S.; Cheng, S.; Rhee, E. P.; McCabe, E.; Lewis, G. D.; Fox, C. S.; Jacques, P. F.; Fernandez, C.; O'Donnell, C. J.; Carr, S. A.; Mootha, V. K.; Florez, J. C.; Souza, A.; Melander, O.; Clish, C. B.; Gerszten, R. E. Metabolite Profiles and the Risk of Developing Diabetes. *Nat. Med.* **2011**, *17* (4), 448–453. https://doi.org/10.1038/nm.2307.

(26) Newgard, C. B. Interplay between Lipids and Branched-Chain Amino Acids in Development of Insulin Resistance. *Cell Metab.* **2012**, *15* (5), 606–614. https://doi.org/10.1016/j.cmet.2012.01.024.

(27) Newgard, C. B.; An, J.; Bain, J. R.; Muehlbauer, M. J.; Stevens, R. D.; Lien, L. F.; Haqq, A. M.; Shah, S. H.; Arlotto, M.; Slentz, C. A.; Rochon, J.; Gallup, D.; Ilkayeva, O.; Wenner, B. R.; Yancy, W. S.; Eisenson, H.; Musante, G.; Surwit, R. S.; Millington, D. S.; Butler, M. D.; Svetkey, L. P. A Branched-Chain Amino Acid-Related Metabolic Signature That Differentiates Obese and Lean Humans and Contributes to Insulin Resistance. *Cell Metab.* **2009**, *9* (4), 311–326. https://doi.org/10.1016/j.cmet.2009.02.002.

(28) Lian, K.; Du, C.; Liu, Y.; Zhu, D.; Yan, W.; Zhang, H.; Hong, Z.; Liu, P.; Zhang, L.; Pei, H.; Zhang, J.; Gao, C.; Xin, C.; Cheng, H.; Xiong, L.; Tao, L. Impaired Adiponectin Signaling

Contributes to Disturbed Catabolism of Branched-Chain Amino Acids in Diabetic Mice. *Diabetes* **2015**, *64* (1), 49–59. https://doi.org/10.2337/db14-0312.

(29) Harper, A. E.; Miller, R. H.; Block, K. P. Branched-Chain Amino Acid Metabolism. 46.

(30) Brosnan, J. T.; Brosnan, M. E. Branched-Chain Amino Acids: Enzyme and Substrate Regulation. *J. Nutr.* **2006**, *136* (1), 207S-211S. https://doi.org/10.1093/jn/136.1.207S.

(31) Noguchi, S.; Kondo, Y.; Ito, R.; Katayama, T.; Kazama, S.; Kadota, Y.; Kitaura, Y.; Harris, R. A.; Shimomura, Y. Ca2+-Dependent Inhibition of Branched-Chain α-Ketoacid Dehydrogenase Kinase by Thiamine Pyrophosphate. *Biochem. Biophys. Res. Commun.* **2018**, *504* (4), 916–920. https://doi.org/10.1016/j.bbrc.2018.09.038.

(32) Wynn, R. M.; Kato, M.; Machius, M.; Chuang, J. L.; Li, J.; Tomchick, D. R.; Chuang, D. T. Molecular Mechanism for Regulation of the Human Mitochondrial Branched-Chain α-Ketoacid Dehydrogenase Complex by Phosphorylation. *Structure* **2004**, *12* (12), 2185–2196. https://doi.org/10.1016/j.str.2004.09.013.

(33) Dolatabad, M. R.; Guo, L.; Xiao, P.; Zhu, Z.; He, Q.; Yang, D.; Qu, C.; Guo, S.; Fu, X.; Li, R.; Ge, L.; Hu, K.; Liu, H.; Shen, Y.; Yu, X.; Sun, J.; Zhang, P. Crystal Structure and Catalytic Activity of the PPM1K N94K Mutant. *J. Neurochem.* **2019**, *148* (4), 550–560. https://doi.org/10.1111/jnc.14631.

(34) Anthony, J. C.; Yoshizawa, F.; Anthony, T. G.; Vary, T. C.; Jefferson, L. S.; Kimball, S. R. Leucine Stimulates Translation Initiation in Skeletal Muscle of Postabsorptive Rats via a Rapamycin-Sensitive Pathway. *J. Nutr.* **2000**, *130* (10), 2413–2419. https://doi.org/10.1093/jn/130.10.2413.

(35) Jang, C.; Oh, S. F.; Wada, S.; Rowe, G. C.; Liu, L.; Chan, M. C.; Rhee, J.; Hoshino, A.; Kim, B.; Ibrahim, A.; Baca, L. G.; Kim, E.; Ghosh, C. C.; Parikh, S. M.; Jiang, A.; Chu, Q.; Forman, D. E.; Lecker, S. H.; Krishnaiah, S.; Rabinowitz, J. D.; Weljie, A. M.; Baur, J. A.; Kasper, D. L.; Arany, Z. A Branched-Chain Amino Acid Metabolite Drives Vascular Fatty Acid Transport and Causes Insulin Resistance. *Nat. Med.* **2016**, *22* (4), 421–426. https://doi.org/10.1038/nm.4057.

(36) Xue, P.; Zeng, F.; Duan, Q.; Xiao, J.; Liu, L.; Yuan, P.; Fan, L.; Sun, H.; Malyarenko, O. S.; Lu, H.; Xiu, R.; Liu, S.; Shao, C.; Zhang, J.; Yan, W.; Wang, Z.; Zheng, J.; Zhu, F. BCKDK of BCAA Catabolism Cross-Talking With the MAPK Pathway Promotes Tumorigenesis of Colorectal Cancer. *EBioMedicine* **2017**, *20*, 50–60. https://doi.org/10.1016/j.ebiom.2017.05.001.

(37) Tso, S.-C.; Gui, W.-J.; Wu, C.-Y.; Chuang, J. L.; Qi, X.; Skvorak, K. J.; Dorko, K.; Wallace, A. L.; Morlock, L. K.; Lee, B. H.; Hutson, S. M.; Strom, S. C.; Williams, N. S.; Tambar, U. K.; Wynn, R. M.; Chuang, D. T. Benzothiophene Carboxylate Derivatives as Novel Allosteric Inhibitors of Branched-Chain α-Ketoacid Dehydrogenase Kinase. *J. Biol. Chem.* **2014**, *289* (30), 20583–20593. https://doi.org/10.1074/jbc.M114.569251.

(38) Chen, M.; Gao, C.; Yu, J.; Ren, S.; Wang, M.; Wynn, R. M.; Chuang, D. T.; Wang, Y.; Sun, H. Therapeutic Effect of Targeting Branched-Chain Amino Acid Catabolic Flux in Pressure-Overload Induced Heart Failure. *J. Am. Heart Assoc.* **2019**, *8* (11), e011625. https://doi.org/10.1161/JAHA.118.011625.

(39) White, P. J.; McGarrah, R. W.; Grimsrud, P. A.; Tso, S.-C.; Yang, W.-H.; Haldeman, J. M.; Grenier-Larouche, T.; An, J.; Lapworth, A. L.; Astapova, I.; Hannou, S. A.; George, T.; Arlotto, M.; Olson, L. B.; Lai, M.; Zhang, G.-F.; Ilkayeva, O.; Herman, M. A.; Wynn, R. M.; Chuang, D. T.; Newgard, C. B. The BCKDH Kinase and Phosphatase Integrate BCAA and Lipid Metabolism via

Regulation of ATP-Citrate Lyase. *Cell Metab.* **2018**, *27* (6), 1281-1293.e7. https://doi.org/10.1016/j.cmet.2018.04.015.

(40) Bollinger, E.; Peloquin, M.; Libera, J.; Albuquerque, B.; Pashos, E.; Shipstone, A.; Hadjipanayis, A.; Sun, Z.; Xing, G.; Clasquin, M.; Stansfield, J. C.; Tierney, B.; Gernhardt, S.; Siddall, C. P.; Greizer, T.; Geoly, F. J.; Vargas, S. R.; Gao, L. C.; Williams, G.; Marshall, M.; Rosado, A.; Steppan, C.; Filipski, K. J.; Zhang, B. B.; Miller, R. A.; Roth Flach, R. J. BDK Inhibition Acts as a Catabolic Switch to Mimic Fasting and Improve Metabolism in Mice. *Mol. Metab.* **2022**, *66*, 101611. https://doi.org/10.1016/j.molmet.2022.101611.

(41) Murashige, D.; Jung, J. W.; Neinast, M. D.; Levin, M. G.; Chu, Q.; Lambert, J. P.; Garbincius, J. F.; Kim, B.; Hoshino, A.; Marti-Pamies, I.; McDaid, K. S.; Shewale, S. V.; Flam, E.; Yang, S.; Roberts, E.; Li, L.; Morley, M. P.; Bedi, K. C.; Hyman, M. C.; Frankel, D. S.; Margulies, K. B.; Assoian, R. K.; Elrod, J. W.; Jang, C.; Rabinowitz, J. D.; Arany, Z. Extra-Cardiac BCAA Catabolism Lowers Blood Pressure and Protects from Heart Failure. *Cell Metab.* **2022**, *34* (11), 1749-1764.e7. https://doi.org/10.1016/j.cmet.2022.09.008.

(42) Divakaruni, A. S.; Paradyse, A.; Ferrick, D. A.; Murphy, A. N.; Jastroch, M. Analysis and Interpretation of Microplate-Based Oxygen Consumption and PH Data. In *Methods in Enzymology*; Elsevier, 2014; Vol. 547, pp 309–354. https://doi.org/10.1016/B978-0-12-801415-8.00016-3.

(43) Divakaruni, A. S.; Rogers, G. W.; Murphy, A. N. Measuring Mitochondrial Function in Permeabilized Cells Using the Seahorse XF Analyzer or a Clark-Type Oxygen Electrode. *Curr. Protoc. Toxicol.* **2014**, *60* (1). https://doi.org/10.1002/0471140856.tx2502s60.

(44) Murashige, D.; Jang, C.; Neinast, M.; Edwards, J. J.; Cowan, A.; Hyman, M. C.; Rabinowitz, J. D.; Frankel, D. S.; Arany, Z. Comprehensive Quantification of Fuel Use by the Failing and Nonfailing Human Heart. *Science* **2020**, *370* (6514), 364–368. https://doi.org/10.1126/science.abc8861.

(45) Orr, A. L.; Ashok, D.; Sarantos, M. R.; Ng, R.; Shi, T.; Gerencser, A. A.; Hughes, R. E.; Brand, M. D. Novel Inhibitors of Mitochondrial Sn-Glycerol 3-Phosphate Dehydrogenase. *PLoS ONE* **2014**, *9* (2), e89938. https://doi.org/10.1371/journal.pone.0089938.

(46) *Mitochondrial Bioenergetics: Methods and Protocols*; Palmeira, C. M., Moreno, A. J., Eds.; Methods in Molecular Biology; Humana Press: Totowa, NJ, 2012; Vol. 810. https://doi.org/10.1007/978-1-61779-382-0.

(47) Bertholet, A. M.; Kirichok, Y. Patch-Clamp Analysis of the Mitochondrial H+ Leak in Brown and Beige Fat. *Front. Physiol.* **2020**, *11*, 326. https://doi.org/10.3389/fphys.2020.00326.

(48) Bertholet, A. M. The Use of the Patch-Clamp Technique to Study the Thermogenic Capacity of Mitochondria. *J. Vis. Exp.* **2021**, No. 171, 62618. https://doi.org/10.3791/62618.

(49) Bertholet, A. M.; Natale, A. M.; Bisignano, P.; Suzuki, J.; Fedorenko, A.; Hamilton, J.; Brustovetsky, T.; Kazak, L.; Garrity, R.; Chouchani, E. T.; Brustovetsky, N.; Grabe, M.; Kirichok, Y. Mitochondrial Uncouplers Induce Proton Leak by Activating AAC and UCP1. *Nature* **2022**, *606* (7912), 180–187. https://doi.org/10.1038/s41586-022-04747-5.

(50) Lou, P.-H.; Hansen, B. S.; Olsen, P. H.; Tullin, S.; Murphy, M. P.; Brand, M. D. Mitochondrial Uncouplers with an Extraordinary Dynamic Range. *Biochem. J.* **2007**, *407* (1), 129–140. https://doi.org/10.1042/BJ20070606.

(51) Pebay-Peyroula, E. Structure of Mitochondrial ADP/ATP Carrier in Complex with Carboxyatractyloside. **2003**, *426*.

(52) Goedeke, L.; Perry, R. J.; Shulman, G. I. Emerging Pharmacological Targets for the Treatment of Nonalcoholic Fatty Liver Disease, Insulin Resistance, and Type 2 Diabetes. *Annu. Rev. Pharmacol. Toxicol.* **2019**, *59* (1), 65–87. https://doi.org/10.1146/annurev-pharmtox-010716-104727.

(53) Kajimura, S.; Saito, M. A New Era in Brown Adipose Tissue Biology: Molecular Control of Brown Fat Development and Energy Homeostasis. *Annu. Rev. Physiol.* **2014**, *76* (1), 225–249. https://doi.org/10.1146/annurev-physiol-021113-170252.

(54) Murphy, M. P. How Mitochondria Produce Reactive Oxygen Species. *Biochem. J.* **2009**, *417* (1), 1–13. https://doi.org/10.1042/BJ20081386.

(55) Korshunov, S. S.; Skulachev, V. P.; Starkov, A. A. High Protonic Potential Actuates a Mechanism of Production of Reactive Oxygen Species in Mitochondria. *FEBS Lett.* **1997**, *416* (1), 15–18. https://doi.org/10.1016/S0014-5793(97)01159-9.

(56) Pell, V. R.; Chouchani, E. T.; Frezza, C.; Murphy, M. P.; Krieg, T. Succinate Metabolism: A New Therapeutic Target for Myocardial Reperfusion Injury. *Cardiovasc. Res.* **2016**, *111* (2), 134–141. https://doi.org/10.1093/cvr/cvw100.

(57) Nickel, A. G.; von Hardenberg, A.; Hohl, M.; Löffler, J. R.; Kohlhaas, M.; Becker, J.; Reil, J.-C.; Kazakov, A.; Bonnekoh, J.; Stadelmaier, M.; Puhl, S.-L.; Wagner, M.; Bogeski, I.; Cortassa, S.; Kappl, R.; Pasieka, B.; Lafontaine, M.; Lancaster, C. R. D.; Blacker, T. S.; Hall, A. R.; Duchen, M. R.; Kästner, L.; Lipp, P.; Zeller, T.; Müller, C.; Knopp, A.; Laufs, U.; Böhm, M.; Hoth, M.; Maack, C.

Reversal of Mitochondrial Transhydrogenase Causes Oxidative Stress in Heart Failure. *Cell Metab.* **2015**, *22* (3), 472–484. https://doi.org/10.1016/j.cmet.2015.07.008.

(58) Chouchani, E. T.; Pell, V. R.; James, A. M.; Work, L. M.; Saeb-Parsy, K.; Frezza, C.; Krieg, T.; Murphy, M. P. A Unifying Mechanism for Mitochondrial Superoxide Production during Ischemia-Reperfusion Injury. *Cell Metab.* **2016**, *23* (2), 254–263. https://doi.org/10.1016/j.cmet.2015.12.009.

(59) Peoples, J. N.; Saraf, A.; Ghazal, N.; Pham, T. T.; Kwong, J. Q. Mitochondrial Dysfunction and Oxidative Stress in Heart Disease. *Exp. Mol. Med.* **2019**, *51* (12), 1–13. https://doi.org/10.1038/s12276-019-0355-7.

(60) Brennan, J.; Southworth, R.; Medina, R.; Davidson, S.; Duchen, M.; Shattock, M. Mitochondrial Uncoupling, with Low Concentration FCCP, Induces ROS-Dependent Cardioprotection Independent of KATP Channel Activation. *Cardiovasc. Res.* **2006**, *72* (2), 313–321. https://doi.org/10.1016/j.cardiores.2006.07.019.

(61) Brennan, J.; Berry, R.; Baghai, M.; Duchen, M.; Shattock, M. FCCP Is Cardioprotective at Concentrations That Cause Mitochondrial Oxidation without Detectable Depolarisation. *Cardiovasc. Res.* **2006**, *72* (2), 322–330. https://doi.org/10.1016/j.cardiores.2006.08.006.

(62) Minners, J. Dinitrophenol, Cyclosporin A, and Trimetazidine Modulate Preconditioning in the Isolated Rat Heart: Support for a Mitochondrial Role in Cardioprotection. *Cardiovasc. Res.* **2000**, *47* (1), 68–73. https://doi.org/10.1016/S0008-6363(00)00069-9.

(63) Hoerter, J.; Gonzalez-Barroso, M.-M.; Couplan, E.; Mateo, P.; Gelly, C.; Cassard-Doulcier, A.-M.; Diolez, P.; Bouillaud, F. Mitochondrial Uncoupling Protein 1 Expressed in the Heart of

Transgenic Mice Protects Against Ischemic-Reperfusion Damage. *Circulation* **2004**, *110* (5), 528–533. https://doi.org/10.1161/01.CIR.0000137824.30476.0E.

(64) Murphy, E.; Steenbergen, C. Regulation of Mitochondrial Ca $^{2+}$ Uptake. *Annu. Rev. Physiol.* **2021**, *83* (1), 107–126. https://doi.org/10.1146/annurev-physiol-031920-092419.

(65) Bernardi, P. The Mitochondrial Permeability Transition Pore: A Mystery Solved? *Front. Physiol.* **2013**, *4*. https://doi.org/10.3389/fphys.2013.00095.

(66) Finkel, T.; Menazza, S.; Holmström, K. M.; Parks, R. J.; Liu, J.; Sun, J.; Liu, J.; Pan, X.; Murphy, E. The Ins and Outs of Mitochondrial Calcium. *Circ. Res.* **2015**, *116* (11), 1810–1819. https://doi.org/10.1161/CIRCRESAHA.116.305484.

(67) Perry, R. J.; Zhang, D.; Zhang, X.-M.; Boyer, J. L.; Shulman, G. I. Controlled-Release Mitochondrial Protonophore Reverses Diabetes and Steatohepatitis in Rats. *Science* **2015**, *347* (6227), 1253–1256. https://doi.org/10.1126/science.aaa0672.

(68) Alexopoulos, S. J.; Chen, S.-Y.; Brandon, A. E.; Salamoun, J. M.; Byrne, F. L.; Garcia, C. J.; Beretta, M.; Olzomer, E. M.; Shah, D. P.; Philp, A. M.; Hargett, S. R.; Lawrence, R. T.; Lee, B.; Sligar, J.; Carrive, P.; Tucker, S. P.; Philp, A.; Lackner, C.; Turner, N.; Cooney, G. J.; Santos, W. L.; Hoehn, K. L. Mitochondrial Uncoupler BAM15 Reverses Diet-Induced Obesity and Insulin Resistance in Mice. *Nat. Commun.* **2020**, *11* (1), 2397. https://doi.org/10.1038/s41467-020-16298-2.

(69) Zhou, M.; Shao, J.; Wu, C.-Y.; Shu, L.; Dong, W.; Liu, Y.; Chen, M.; Wynn, R. M.; Wang, J.; Wang, J.; Gui, W.-J.; Qi, X.; Lusis, A. J.; Li, Z.; Wang, W.; Ning, G.; Yang, X.; Chuang, D. T.; Wang, Y.; Sun, H. Targeting BCAA Catabolism to Treat Obesity-Associated Insulin Resistance. *Diabetes* **2019**, *68* (9), 1730–1746. https://doi.org/10.2337/db18-0927.

(70) Voronova, V.; Sokolov, V.; Morias, Y.; Boezelman, M. J.; Wågberg, M.; Henricsson, M.; Hansson, K.; Goltsov, A.; Peskov, K.; Sundqvist, M. Evaluation of Therapeutic Strategies Targeting BCAA Catabolism Using a Systems Pharmacology Model. *Front. Pharmacol.* **2022**, *13*, 993422. https://doi.org/10.3389/fphar.2022.993422.

(71) Roth Flach, R. J.; Bollinger, E.; Reyes, A. R.; Laforest, B.; Kormos, B. L.; Liu, S.; Reese, M. R.; Martinez Alsina, L. A.; Buzon, L.; Zhang, Y.; Bechle, B.; Rosado, A.; Sahasrabudhe, P. V.; Knafels, J.; Bhattacharya, S. K.; Omoto, K.; Stansfield, J. C.; Hurley, L. D.; Song, L.; Luo, L.; Breitkopf, S. B.; Monetti, M.; Cunio, T.; Tierney, B.; Geoly, F. J.; Delmore, J.; Siddall, C. P.; Xue, L.; Yip, K. N.; Kalgutkar, A. S.; Miller, R. A.; Zhang, B. B.; Filipski, K. J. Small Molecule Branched-Chain Ketoacid Dehydrogenase Kinase (BDK) Inhibitors with Opposing Effects on BDK Protein Levels. *Nat. Commun.* **2023**, *14* (1), 4812. https://doi.org/10.1038/s41467-023-40536-y.

(72) Liu, S.; Kormos, B. L.; Knafels, J. D.; Sahasrabudhe, P. V.; Rosado, A.; Sommese, R. F.; Reyes, A. R.; Ward, J.; Roth Flach, R. J.; Wang, X.; Buzon, L. M.; Reese, M. R.; Bhattacharya, S. K.; Omoto, K.; Filipski, K. J. Structural Studies Identify Angiotensin II Receptor Blocker-like Compounds as Branched-Chain Ketoacid Dehydrogenase Kinase Inhibitors. *J. Biol. Chem.* **2023**, *299* (3), 102959. https://doi.org/10.1016/j.jbc.2023.102959.

(73) Chen, M. J.; Dixon, J. E.; Manning, G. Genomics and Evolution of Protein Phosphatases. *Sci. Signal.* **2017**, *10* (474), eaag1796. https://doi.org/10.1126/scisignal.aag1796.

(74) Rubio, M.; Avitabile, D.; Fischer, K.; Emmanuel, G.; Gude, N.; Miyamoto, S.; Mishra, S.; Schaefer, E. M.; Brown, J. H.; Sussman, M. A. Cardioprotective Stimuli Mediate Phosphoinositide 3-Kinase and Phosphoinositide Dependent Kinase 1 Nuclear Accumulation in

Cardiomyocytes. *J. Mol. Cell. Cardiol.* **2009**, *47* (1), 96–103. https://doi.org/10.1016/j.yjmcc.2009.02.022.

(75) Li, S.; Yokota, T.; Wang, P.; Ten Hoeve, J.; Ma, F.; Le, T. M.; Abt, E. R.; Zhou, Y.; Wu, R.; Nanthavongdouangsy, M.; Rodriguez, A.; Wang, Y.; Lin, Y.-J.; Muranaka, H.; Sharpley, M.; Braddock, D. T.; MacRae, V. E.; Banerjee, U.; Chiou, P.-Y.; Seldin, M.; Huang, D.; Teitell, M.; Gertsman, I.; Jung, M.; Bensinger, S. J.; Damoiseaux, R.; Faull, K.; Pellegrini, M.; Lusis, A. J.; Graeber, T. G.; Radu, C. G.; Deb, A. Cardiomyocytes Disrupt Pyrimidine Biosynthesis in Nonmyocytes to Regulate Heart Repair. *J. Clin. Invest.* **2022**, *132* (2), e149711. https://doi.org/10.1172/JCI149711.

(76) Green, C. R.; Wallace, M.; Divakaruni, A. S.; Phillips, S. A.; Murphy, A. N.; Ciaraldi, T. P.; Metallo, C. M. Branched-Chain Amino Acid Catabolism Fuels Adipocyte Differentiation and Lipogenesis. *Nat. Chem. Biol.* **2016**, *12* (1), 15–21. https://doi.org/10.1038/nchembio.1961.

(77) Yang, K.; Doan, M. T.; Stiles, L.; Divakaruni, A. S. Measuring CPT-1-Mediated Respiration in Permeabilized Cells and Isolated Mitochondria. *STAR Protoc.* **2021**, *2* (3), 100687. https://doi.org/10.1016/j.xpro.2021.100687.

(78) Divakaruni, A. S.; Jastroch, M. A Practical Guide for the Analysis, Standardization and Interpretation of Oxygen Consumption Measurements. *Nat. Metab.* **2022**, *4* (8), 978–994. https://doi.org/10.1038/s42255-022-00619-4.

(79) Rogers, G. W.; Brand, M. D.; Petrosyan, S.; Ashok, D.; Elorza, A. A.; Ferrick, D. A.; Murphy, A. N. High Throughput Microplate Respiratory Measurements Using Minimal Quantities Of Isolated Mitochondria. *PLoS ONE* **2011**, *6* (7), e21746. https://doi.org/10.1371/journal.pone.0021746.

(80) Vacanti, N. M.; Divakaruni, A. S.; Green, C. R.; Parker, S. J.; Henry, R. R.; Ciaraldi, T. P.; Murphy, A. N.; Metallo, C. M. Regulation of Substrate Utilization by the Mitochondrial Pyruvate Carrier. *Mol. Cell* **2014**, *56* (3), 425–435. https://doi.org/10.1016/j.molcel.2014.09.024.

(81) Trefely, S.; Ashwell, P.; Snyder, N. W. FluxFix: Automatic Isotopologue Normalization for Metabolic Tracer Analysis. *BMC Bioinformatics* **2016**, *17* (1), 485. https://doi.org/10.1186/s12859-016-1360-7.